2010

# A Generalized Inverter Control Method for a Variable Speed Wind Power System Under Unbalanced Operating Conditions

Shuang Wu
*Cleveland State University*

# A GENERALIZED INVERTER CONTROL METHOD FOR A VARIABLE SPEED WIND POWER SYSTEM UNDER UNBALANCED OPERATING CONDITIONS

SHUANG WU

Bachelor of Science in Electrical Engineering

North China University of Technology

July 2006

submitted in partial fulfillment of requirements for the degree

MASTER OF SCIENCE IN ELECTRICAL ENGINEERING

at the

CLEVELAND STATE UNIVERSITY

April, 2010

This thesis has been approved

for the Department of Electrical and Computer Engineering

and the College of Graduate Studies by

_____

Dissertation Committee Chairperson, Dr. Ana V Stankovic

_____

Department/Date

_____

Committee Member, Dr. Lili Dong

_____

Department/Date

_____

Committee Member, Dr. Jerzy T. Sawicki

_____

Department/Date

## ACKNOWLEDGEMENTS

First of all, I would like to thank my advisor Dr. Ana V. Stankovic. Without her encouragement and guidance, I can not finish the thesis. I still remember when I began the wind power research and had no background at machines; she encouraged me and patiently showed me how to do research by doing the literature survey for useful information. She is easygoing but she sets high standard on study and research. Her enthusiasm on the topic helps me to concentrate on the research and mature intellectually.

I would also like to thank Ke Chen who shares his research results on the control of rectifier with me and this gives me a lot of information so I can finish the simulation of the inverter in a short time. His professional skills and characteristic merits make him a real model for me.

At last but not least, I would like to thank my family for their endless love and supports! They give me the strength to pursue the degree.

# A GENERALIZED INVERTER CONTROL METHOD FOR A VARIABLE SPEED WIND POWER SYSTEM UNDER UNBALANCED OPERATING CONDITIONS

**SHUANG WU**

## ABSTRACT

This thesis presents a generalized control method for complete harmonic elimination and adjustable power factor of a grid side inverter under unbalanced operating conditions used in variable speed wind power systems. The theoretical analysis of the proposed control method is described and verified by simulation in Simulink ®. Two types of traditional control methods are also explained and applied in the wind power system for comparison, which are the indirect current control in a-b-c reference frame and the active and reactive power control in d-q synchronous frame. This method is verified for the gird fault right-through operation as well.

# TABLE OF CONTENTS

# NOMENCLATURE

PWM: Pulse width modulation

d-q: Direct and quadrature axes

IG: Induction generator

PM: Permanent-magnet

IGBT: Insulated-gate bipolar transistor

FFT: Fast Fourier transform

DC: Direct current

AC: Alternating current

# LIST OF TABLES

# LIST OF FIGURES

# CHAPTER I

# INTRODUCTION AND LITERATURE SURVEY

## 1.1 Introduction

Wind power energy is a free, renewable and clean energy source. The United States has more than 8000 GW available in wind power resources. In 2008, the Department of Energy's report concluded that "the U.S. possesses sufficient and affordable wind resources to obtain at least 20% of its electricity from the wind by 2030. [1]" The economic stimulus bill passed in February 2009 contains various provisions to benefit the wind industry.

Significant wind power capacity is beginning to be connected to the grid so that wind can be fully utilized as a power source. However, there are still technical challenges in interfacing wind power to the electricity grid [2], [3], [4]. The power grid is with constant frequency. If the wind turbine is directly connected to the grid, the generator has to run with a constant rotating speed. Traditionally, variable pitch constant speed turbines and gear boxes are coupled to the generator so that with the changing of the wind speed, the generator can still run at a constant speed. But the

gear box brings a lot of noise, which does harm to the environment, and the physical abrasion means the degradation of the turbine and generator. Another option is the frequency conversion between the grid and the generator, and this is achieved by two power electronics converters, which are also called the back-to-back PWM converters. With the decreasing price of silicon and the increasing power rating ability, the power converter using the insulated gate bipolar transistors (IGBT) is able to handle the power in the range of 1 MVA with a switching frequency about 1KHz to 100 KHz [5], which makes it a possible solution for the wind power application. Figure 1.1 shows the variable-speed wind turbine with fully rated converter configuration and a permanent-magnet generator.

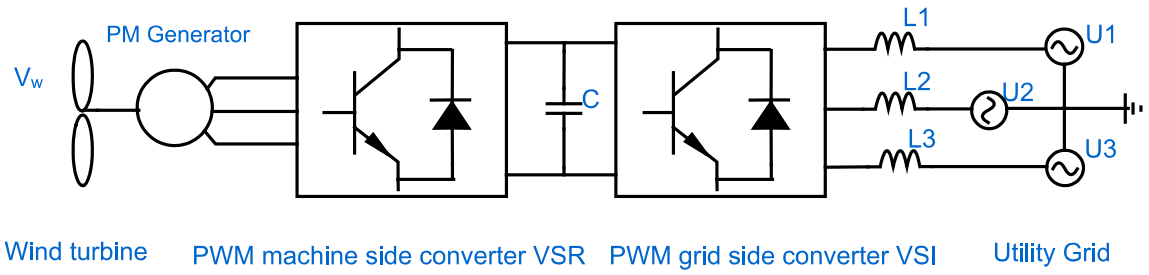


Figure 1. 1: The variable-speed wind power system with fully rated converters and a permanent-magnet generator

The machine side converter, which is a rectifier, sets the torque demand according to the speed to achieve maximum turbine power and transfer the variable frequency power to a DC link. The grid side converter, which is an inverter, transfers the DC link power to the power grid with the grid frequency and voltage. At the same time, the grid side converter is controlled to maintain the DC link voltage at a constant value.

The features of the power converter are attractive, but it has its own drawbacks, especially for the grid side converter. It is very sensitive to grid disturbance; when the

grid side voltage is unbalanced. Under unbalanced operating conditions there is a deterioration of the inverter input DC voltage and output currents. It has been shown in reference [6], [7] that unbalanced voltages contain a significant negative-phase-sequence component, causing the derived current reference to be time variant, which will result in a huge second order harmonic in the DC link voltage. This will in turn bring a third-order harmonic for the AC side currents. In wind power industrial application, the harmonic caused by the unbalance grid side voltage has been shown to not be easily absorbed by the limited DC-link capacitor, which is normally located in the nacelle on the top of the turbine tower. And with the unbalance which may occur frequently especially in weak system, the harmonic should be eliminated by the control of the gird side inverter.

In this thesis, the wind power systems with the variable wind speed under the unbalanced grid operation are proposed.

This research method is based on the harmonic elimination control, which was originally proposed for a PWM rectifier [8]. The method proposed in [8] has been modified and used for the wind power application.

In Chapter 2, the general solution for harmonic elimination of a grid side inverter under unbalanced operating conditions is presented in detail. An analytical solution for complete harmonic elimination with adjustable power factor is obtained.

In Chapter 3, the models of the systems using the permanent-magnet generator and induction generator are presented in the Simulink® with SimPowerSystems™ tool box. The simulation results for the optimal wind power acquisition and the low order harmonic elimination under unbalanced grid operation are given and compared with the simulation results, which are obtained by using the typical methods for the control of the grid side converter.

In Chapter 4, the conclusion is given and the future works are proposed.

## 1.2 Literature survey

This chapter presents a review of significant previous work related to this research. The following five general areas provide information relevant to this study.

1. Variable-speed wind energy system and the characteristics of wind turbine.

2. Permanent-magnet generator in wind power application and the corresponding machine side rectifier control.

3. Squirrel cage induction generator in wind power application and the corresponding machine side rectifier control.

4. Traditional grid side inverter control.

5. The recent studies on unbalance harmonic elimination for the wind power application.

### 1.2.1 Variable-speed wind-energy system and the characteristics of wind turbine

Variable power generation enables the operation of the turbine at its optimal power coefficient over a wide range of wind speeds. The output power of a wind turbine is given by.

$$P_m = \frac{1}{2}\rho A V_w^3 C_p(\beta,\lambda) \tag{1.1}$$

Where $\rho$ is the density of air. $A$ is the wind turbine swept area. $V_w$ is the wind speed. $C_p$ is the power coefficient and it is the function of the pitch angle $\beta$ and the tip speed ratio $\lambda$.

$$\lambda = R\frac{\omega_w}{V_w} \tag{1.2}$$

$R$ is the wind turbine radius, and $\omega_w$ is the wind turbine angular speed [9].

It can be seen in (1.1) that wind energy can be utilized most efficiently when the power coefficient of the turbine is highest. The tip speed ratio $\lambda_{opt}$, meeting this condition is determined by the inherent characteristic of the turbine. So the wind turbine angular speed has to change in correspondence to the change of the wind speed in order to collect the maximum power.

With the change of the wind speed and the rotor speed of the generator, in mechanical aspect, the electromagnetic torque has to be controlled.

The optimum torque and optimum power corresponding to the wind speed are:

$$T_{opt} = K_{opt}\omega_{opt}^2 \tag{1.3}$$

$$P_{opt} = K_{opt}\omega_{opt}^3 \tag{1.4}$$

where $K_{opt}$ is optimum coefficient.

In electrical aspect, the electromagnetic torque of the generator can be controlled by the current of the stator windings, and this is the main purpose of the machine side converter, which is a PWM voltage source rectifier (VSR).

### 1.2.2 Permanent-magnet generator in wind power application and the machine side rectifier control

The permanent-magnet synchronous generator has numerous advantages over other machines. The stator currents of an induction generator contain not only the torque-producing currents, but also the magnetizing components. With the use of the permanent-magnet in the rotor, the stator currents need only be toque-producing. It

means the permanent-magnet synchronous generator will operate at higher power factor because of the absence of magnetizing currents. So the permanent-magnet synchronous generator will be more efficient than the induction generator. As the wound-rotor synchronous generator, there must be a dc excitation for the rotor supplied by brush and slip rings, which means rotor losses and brush maintenance [10]. By using the permanent-magnet rotor, the other excitation parts can be gotten rid of. Moreover, permanent-magnet synchronous generator can have a high number of poles, so they do not need any gear box if used in the wind power application. Because of the reduction of magnet price and magnetic characteristic improvement [11], permanent-magnet synchronous generators have recently received an increase in attention, especially for wind power energy.

Figure 1.1 has shown the permanent-magnet synchronous generator connected to the grid by two PWM converters for the variable speed wind power system.

Figure 1.2 shows the per-phase equivalent circuit of a permanent-magnet synchronous generator.

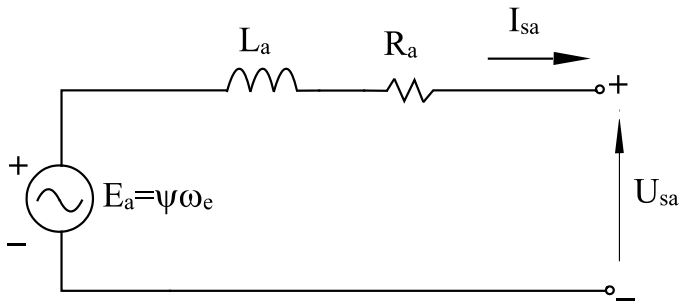


Figure 1. 2: The per-phase equivalent circuit of a permanent-magnet synchronous generator.

The mathematical model of a permanent-magnet synchronous generator is derived in the following assumption:

- Saturation is neglected.
- Induced EMF is sinusoidal.
- Eddy currents and hysteresis losses are negligible.

Based on the assumption, according to the KVL, the circuit of the generator can be defined as:

$$U_{sa} = \Psi \omega_e - j\omega_e L_a I_{sa} - R_a I_{sa}$$

$$U_{xb} = \Psi \omega_e - j\omega_e L_b I_{sb} - R_b I_{sb} \quad (1.5)$$

$$U_{sc} = \Psi \omega_e - j\omega_e L_c I_{sc} - R_c I_{sc}$$

Where $U_{sa}$ is the phase A voltage, $I_{sa}$ is phase A current, $L_a$ is phase A inductance and $R_a$ is phase A resistance, $\Psi$ is the magnet flux , $\omega_e$ The stator voltage rotor speed. Since the parameters in three phases are the same and balance, phase B and phase C are with the same denoting method.

The stator voltage electrical speed is related to the rotor mechanical speed as follows:

$$\omega_e = p\omega_r \quad (1.6)$$

where $p$ is the pole pair number.

To control the permanent-magnet synchronous generator in a simply and generously used method, the equations (1.5) of the generator in a, b, c, coordinate are projected on a reference d-q coordinate system rotating synchronously with the magnet flux [12]. The d, q variable are obtained from a, b, c variable through the Park transformation.

Voltage $U_{sa}$ , $U_{sb}$ , $U_{sc}$ can be measured and transformed to $U_\alpha$ and $U_\beta$ by multiplying the matrix $M_{abc\_\alpha\beta o}$.

$$M_{abc\_\alpha\beta o} = \frac{2}{3}\begin{bmatrix} 1 & -\frac{1}{2} & -\frac{1}{2} \\ 0 & -\frac{\sqrt{3}}{2} & \frac{\sqrt{3}}{2} \\ \frac{1}{2} & \frac{1}{2} & \frac{1}{2} \end{bmatrix} \tag{1.7}$$

The corresponding rotating space vector $U_d$ and $U_q$ are calculated by multiplying $U_\alpha$ and $U_\beta$ with the matrix $M_{\alpha\beta\_dqo}$.

$$M_{\alpha\beta\_dqo} = \begin{bmatrix} \cos\theta_e & \sin\theta_e & 0 \\ -\sin\theta_e & \cos\theta_e & 0 \\ 0 & 0 & 1 \end{bmatrix} \tag{1.8}$$

The angular position $\theta_e$ of the stator voltage is calculated by using the equation:

$$\theta_e = \int \omega_e dt = \tan^{-1}\frac{U_\alpha}{U_\beta} \tag{1.9}$$

The three phase grid currents $i_{sa}$, $i_{sb}$, $i_{sc}$ are measured and transferred to $i_d$ and $i_q$ using the same matrices above.

The dynamic model in the magnet flux reference system is as follow:

$$u_{Sd} = -R_s i_{Sd} - L_s\frac{di_{Sd}}{dt} + L_s\omega_e i_{Sq} \tag{1.10}$$

$$u_{Sq} = -R_s i_{Sq} - L_s\frac{di_{Sq}}{dt} + L_s\omega_e i_{Sd} + \omega_e\Psi \tag{1.11}$$

Where $u_{sd}$, $u_{sq}$ are the stator phase voltages in d-q frame, $L_s$ is the generator inductance and $R_s$ is the generator resistance.

$$L_s = L_a = L_b = L_c \tag{1.12}$$

$$R_s = R_a = R_b = R_c \tag{1.13}$$

The electromagnetic toque in d-q frame is given by,

$$T_e = \frac{3}{2} p \Psi i_{Sq} \tag{1.14}$$

The purpose of the control of the permanent-magnet generator is to achieve optimal performance. The optimum torque corresponding to the wind speed is given in equation (1.3). With knowing the wind speed and the corresponding rotor speed, the generator should be controlled to get the optimal torque.

Equation (1.14) shows the relationship between the q-axis current and electromagnetic toque. Since the pole pairs and the magnetic flux linkage are constant, the electromagnetic torque is directly proportional to $i_{sq}$.

$$T_e = K i_{Sq} \tag{1.15}$$

$$K = \frac{3}{2} p \Psi \tag{1.16}$$

So the desired $T_e^*$ is obtained by setting the desired $i_{sq}^*$. The direct-axis current $i_{sd}^*$ component can be set to zero to minimize current for a given toque and therefore minimize resistive losses. [12] This control by using the vectors in d-q frame is also called vector control.

Figure 1.3 shows the control loops of the machine side converter connected to the permanent-magnet generator.

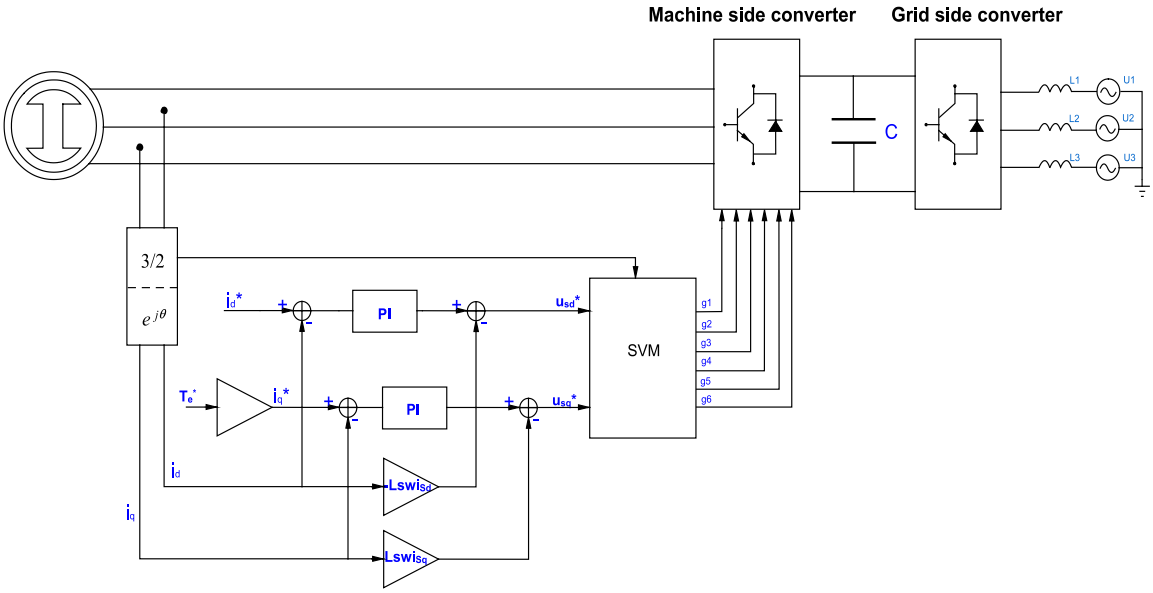


Figure 1. 3: The vector control of the machine side converter connected to the permanent-magnet generator.

The required d-q components of the rectifier voltage vector are derived from two proportional and integral current controllers. One is controlling the d-axis current and the other is controlling the q-axis current.

According to the linear system theory, from the state equations (1.10) and (1.11) of the circuit, the transfer functions between the currents and voltages can be expressed as

$$T(s) = \frac{i_{sd}}{u_{sd}'} = \frac{i_{sq}}{u_{sq}'} = \frac{1}{L_s s + R} \tag{1.17}$$

Where $u_{sd}'$, $u_{sq}'$ are the voltage components in the d-q axes that control the corresponding current components, and s is the Laplace operator.

### 1.2.3 Squirrel cage induction generator in wind power application and the machine side rectifier control

Induction generators have their advantages over the synchronous generator: they are brushless and are rugged constructions, which means low cost and minimum maintenance required; self-protection against sever overloads and short-circuits, good dynamic response, which means simple and reliable operation. However, with many distinct advantages listed above, there are obstacles for the machine to be operated as a generator. There are three prerequisites for the IG to generator AC current:

(1) The rotor speed $\omega_m$ of the induction machine must be higher than the synchronous speed $\omega_{sync}$ or the slip speed has to be negative value so the induction machine can run in generation mode.

The synchronous speed is defined as

$$\omega_{sync} = \frac{120 f_e}{p} \tag{1.18}$$

The Slip speed s is defined as

$$s = \frac{\omega_{sync} - \omega_m}{\omega_{sync}} \times 100\% \tag{1.19}$$

(2) Residual magnetism in the iron of the magnetic circuits is needed to set up a small alternating voltage in the stator.

(3) Besides the residual magnetism, the excitation currents are needed to magnetize the core. An isolated induction generator without magnetizing currents won't generate any power. The excitation currents for grid connected induction generator are supplied from the grid, which draws the reactive power from the grid. For a stand-alone induction generator self excitation is possible with the capacitor banks connected to the stator [13]. For an induction generator which is connected to

the grid by two back-to-back PWM converters, the reactive power can either be provided by the machine side rectifier or by an external capacitor bank [14]. In this thesis, the main purpose of the machine side rectifier is to achieve the optimal power acquisition, so a fixed capacitor bank is chosen for the excitation. Figure 1.4 shows the SEIG generator connected by two PWM converters to the grid for the variable speed wind power application.

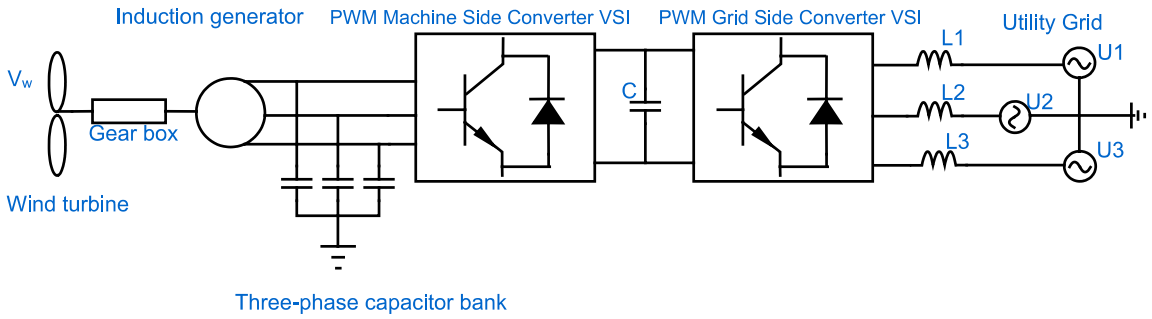


Figure 1. 4: The variable-speed wind power system with fully rated converter and a squirrel cage induction generator

There are different control techniques for induction machine, scalar control, vector and field-oriented control. For the scalar control, it includes the open loop Volts/Hz control and torque and flux control. In this thesis, the purpose of the control is to get the desired torque value with different rotor speeds for the optimal power acquiring. The direct torque and flux control is applied. Scalar control only controls the magnitude of the variable. The voltage of the machine can be controlled to control the flux, and frequency or slip can be controlled to control the torque [15].

The control scheme of the induction generator is shown in figure 1.5.

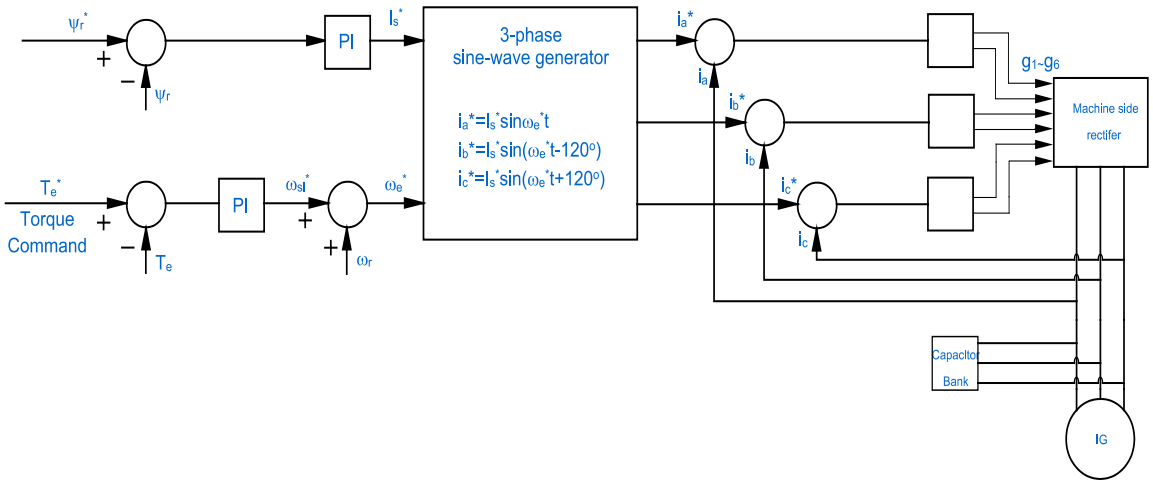


Figure 1. 5: The scalar control of the induction generator.

Instead of controlling the input voltage of the machine side rectifier, the stator current which is the input current of the rectifier can be controlled since the torque and flux of the machine are related to the current. For the torque control loop, the actual value of the torque is fed back to the PI controller and compared with the reference. The error signal is used to update the stator slip speed. The angular frequency of the stator current is obtained by adding the slip speed and the rotor electrical speed.

The relationship between the rotor electrical speed and mechanical speed is defended as:

$$\omega_r = (\frac{p}{2}) \times \omega_m \qquad (1.20)$$

For the flux control loop, the actual value of the flux is fed back to the PI controller and compared with the reference. The error signal is used to update the stator current magnitude.

The hysteresis controller is used to make the machine stator currents track the reference currents so the torque can be controlled to follow the optimal value when the wind speed changes and the rotor flux is kept constant.

### 1.3 Control of a grid-side PWM inverter

The configuration of the grid side inverter is basically the same as a rectifier, Figure 1.6 shows the grid side inverter, while the power flows in an opposite direction, from the DC side to the AC side.

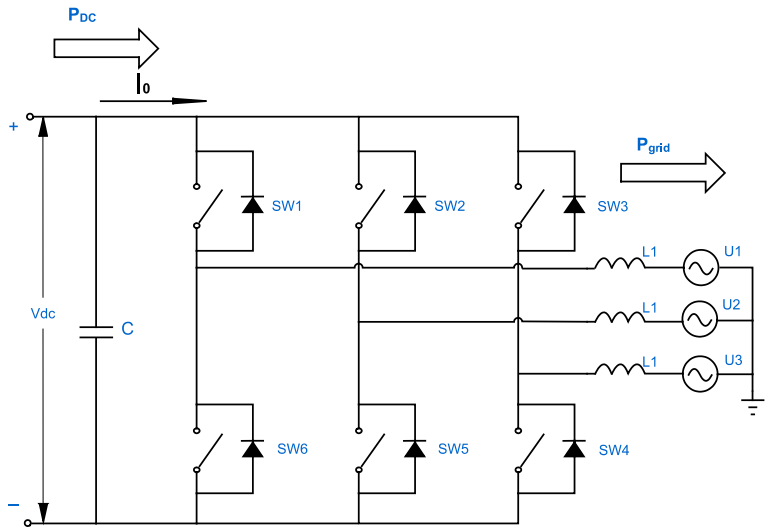


Figure 1. 6: Grid side converter transfers the power from DC link to grid.

According to KVL and KCL, the circuit can be defined with the equation:

$$\begin{bmatrix} u_a \\ u_b \\ u_c \end{bmatrix} = \begin{bmatrix} u_{sa} \\ u_{sb} \\ u_{sc} \end{bmatrix} - R \begin{bmatrix} i_a \\ i_b \\ i_c \end{bmatrix} - L \frac{d}{dt} \begin{bmatrix} i_a \\ i_b \\ i_c \end{bmatrix} \tag{1.21}$$

Where L and R are the grid inductance and resistance. $u_a$, $u_b$, $u_c$ are the three phase line-neutral voltages. $u_{sa}, u_{sb}, u_{sc}$ are the three phase output voltages of the bridge. $i_a, i_b$, $i_c$ are three phase grid currents.

Figure 1.7 shows the per-phase equivalent circuit. Figure 1.8 shows the phase diagrams.

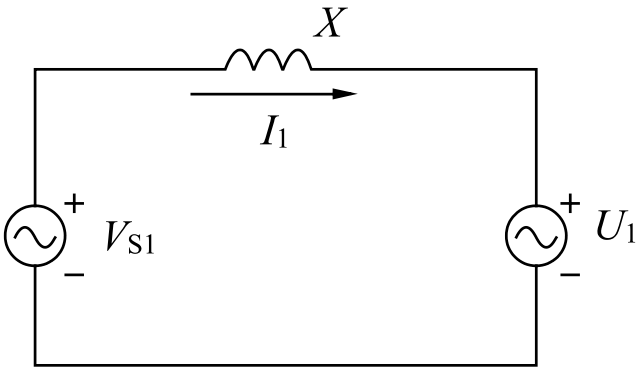


Figure 1. 7: The per-phase equivalent circuit

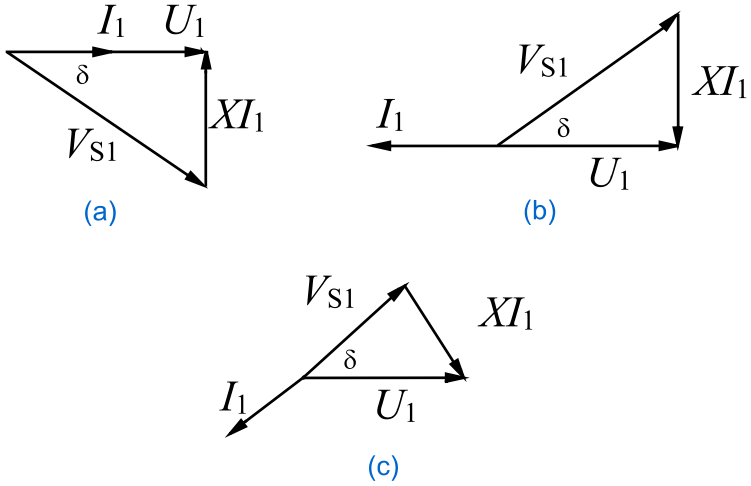


Figure 1. 8: The phase diagrams

Power flow in the PWM converter is controlled by adjusting the phase shift angle $\delta$ between the source voltage $U_1$ and the respective converter reflected input voltage $V_{s1}$ [8]. In Figure 1.8 (a), when $U_1$ leads $V_{s1,}$ the real power flows from AC source to DC, the converter operates as a rectifier. In Figure 1.8 (b), when $U_1$ lags $V_{s1}$, power flows from DC side to AC， the converter operates as an inverter.

The real power transferred is given as

$$P = \frac{U_1 V_{s1}}{X_1} \sin \delta \tag{1.22}$$

The ac power factor is adjusted by controlling the amplitude of $V_{s1}$, shown as Figure 1.8 (c).

The purpose of the grid-side inverter control is to balance the power between the AC grid and the DC link. The power transferred via the DC link should be fed to the grid immediately. And the dc-link voltage needs to be controlled to assure a constant value within the dc-link. The active and reactive power control for the inverter has been shown in references [12], [16], and [17].

The dynamic model of the grid side inverter, when selecting a reference frame rotating synchronously with the grid voltage is given by,

$$u_d = u_{sd} - Ri_d - L\frac{di_d}{dt} + \omega_e L i_q \tag{1.23}$$

$$u_q = u_{sq} - Ri_q - L\frac{di_q}{dt} - \omega_e L i_d \tag{1.24}$$

Since the three-phase grid voltages are with constant amplitude and with constant frequency, $u_d$ and $u_q$ are constant. In a balanced three-phase system, active and reactive powers in the d-q reference frame can be expressed as:

$$P = \frac{3}{2}(u_d i_d + u_q i_q) \tag{1.25}$$

$$Q = \frac{3}{2}(u_d i_q + u_q i_d) \tag{1.26}$$

Since the rotating reference frame is aligned with the d-axis, $u_q$ is zero, equation (1.25) and (1.26) can be expressed as,

$$P = \frac{3}{2}u_d i_d \tag{1.27}$$

$$Q = \frac{3}{2}u_d i_q \tag{1.28}$$

The active power transmitted by the DC link can be expressed as

$$P_{dc} = V_{dc} I_{dc} \tag{1.29}$$

The power transferred via the DC link should be equal to the power fed into the grid:

$$P_{dc} = P_{ac}. \tag{1.30}$$

$$\frac{3}{2} u_d i_d = V_{dc} I_{dc}. \tag{1.31}$$

From Equation (1.27) and (1.31), it can be seen that the active power control can be achieved by controlling direct axis current $i_d$.

An outer DC voltage control loop is used to keep the DC link voltage constant. The error $V_{dc}$*-$V_{dc}$ and a PI controller can be used to update the active power so the direct axis current reference $i_d$* is obtained.

The reactive power is also implemented in the control, $i_q$* is set according to the reactive power Q and $u_d$. Because the reactive power can not be determined from the dc grid, the amount of reactive power will be given as an external nominal value according to the need of the grid. Figure 1.9 shows the grid side inverter control scheme.

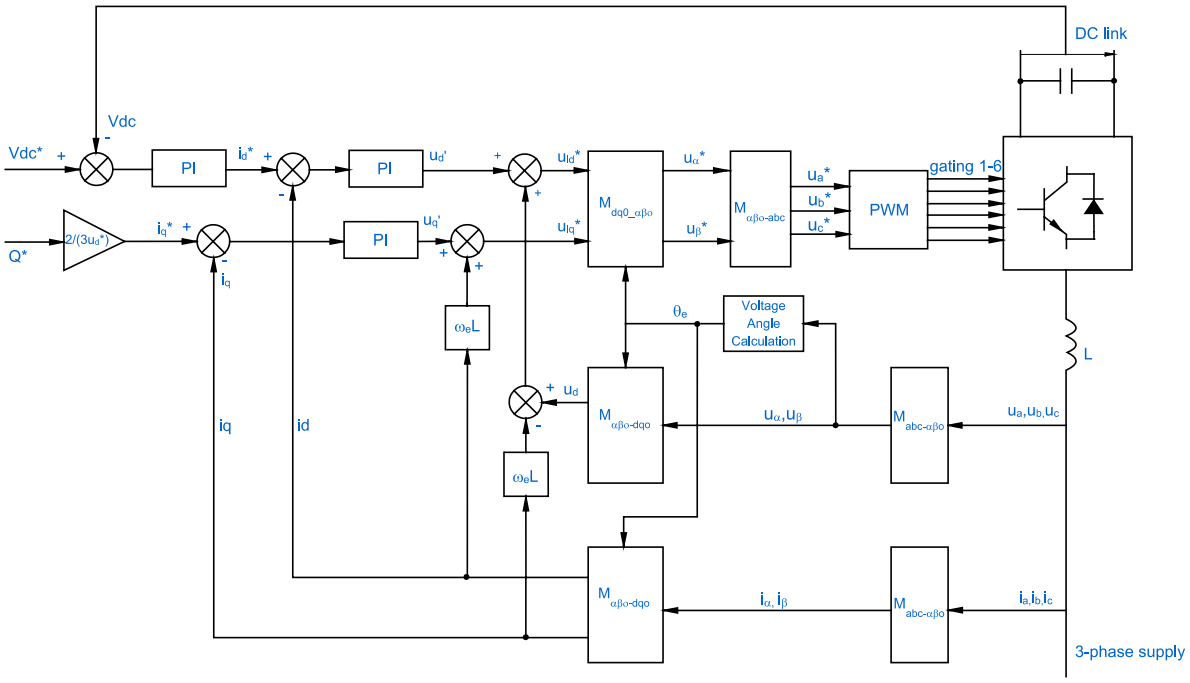


Figure 1. 9: Active and reactive power control for the grid-side inverter.

According to the state equation (1.23) and (1.24), Let

$$Ri_d + L\frac{di_d}{dt} = u_d' \tag{1.32}$$

$$Ri_q + L\frac{di_q}{dt} = u_q' \tag{1.33}$$

The transfer function between voltage and current is given by

$$T(s) = \frac{i_d}{u_d'} = \frac{i_q}{u_q'} = \frac{1}{Ls + R} \tag{1.34}$$

And equation (1.23) and (1.24) can be expressed as

$$u_{sd}^* = u_d' + (-\omega_e L i_q + u_d) \tag{1.35}$$

$$u_{sq}^* = u_q' + (\omega_e L i_d + u_q) \tag{1.36}$$

Where $u_{sd}^*, u_{sq}^*$ are the reference output voltages for the grid-side inverter. $u_{sd}^*, u_{sq}^*$ are then transformed to $u_\alpha^*, u_\beta^*$ by multiplying it with the inverse matrix given by (1.8).

Finally, $u_a^*, u_b^*, u_c^*$ are calculated by multiplying the inverse matrix of matrix (1.7) and are used as the input signal for the PWM generator.

The PWM generator uses the three sinusoidal voltage reference signals and compares them with a saw wave signal separately to generate six gating signals to control 6 switches.

Besides the reactive and active power control using the space vector in d-q frame, the indirect current control for the boost rectifier in a-b-c frame [18] can also be applied in the control for the inverter. Figure 1.10 shows the indirect current control scheme.

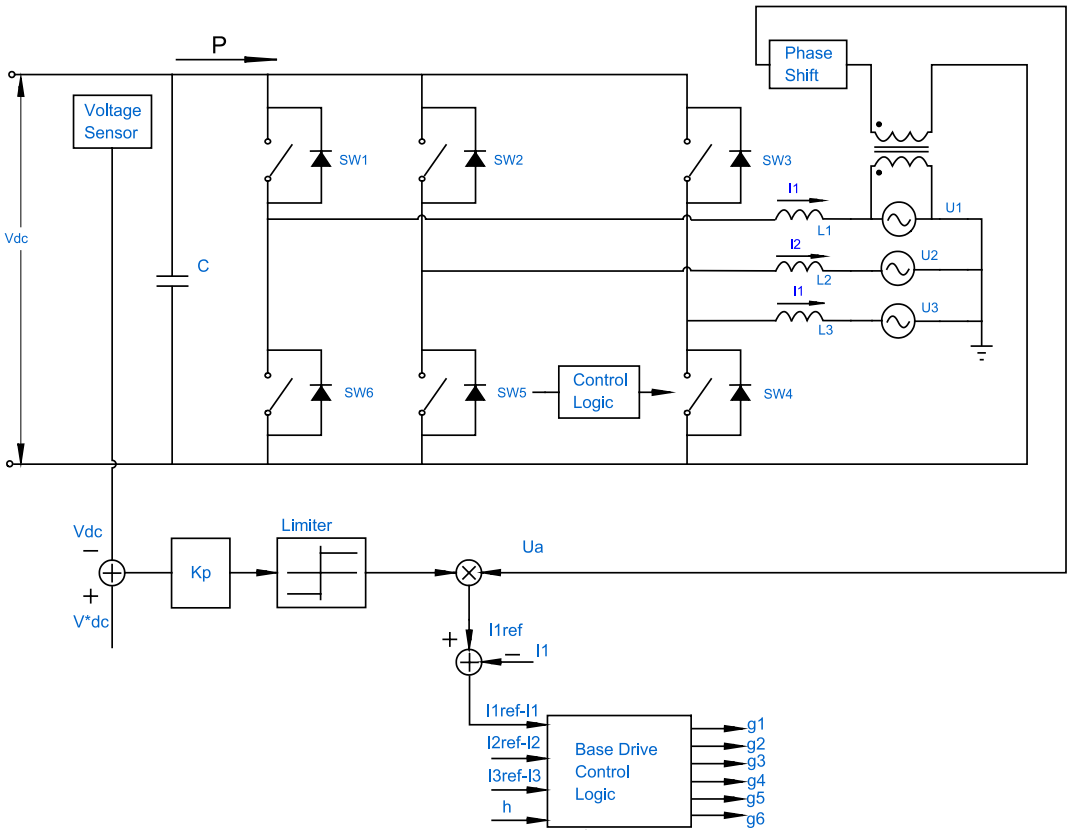


Figure 1. 10: Indirect current control of the grid inverter.

The line current reference is derived through the multiplication of a term proportional to the bus voltage error by a template sinusoidal waveform. The sinusoidal template is directly proportional to the grid voltage (phase to ground) with a phase shift. By varying the phase shift degree between the sinusoidal template and grid voltage, variable power factor can be achieved. The line current is then controlled to track this current reference. Current regulation is accomplished by using the hysteresis controller.

### 1.4 The recent study on unbalanced grid operation in wind power application

The studies [2], [7], [8], [19] have detailed explanations about the causes and effects of the unbalanced grid operations. In a weak power system network, an

unbalanced load at the distribution lines can cause unbalanced voltage condition. This is particularly true for rural electricity power systems where the wind turbines are normally connected. An unbalanced condition can also be caused by unsymmetrical transformer windings or unbalanced transmission-line impedances, open wye, and open delta.

Muljadi *et al* [19] summarized the problems caused by unbalanced voltage in a wind power system connected directly to an induction generator. The unbalanced grid will cause the stator currents of the induction generator to be unbalanced. The unbalanced currents create unequal heating on the stator winding which will degrade the insulation of the winding and short the life expectancy of the winding. Unbalanced stator currents also create torque pulsation on the shaft, resulting in audible noise and extra mechanical stress.

For the variable-speed wind power system with two back-to-back PWM converters, the impacts to the generator might decrease because the converter decouples the generator from the grid. But due to the inherent drawbacks of the PWM VSI, the unbalanced grid brings other problems to the system. There is a deterioration of the inverter input DC voltage and output currents. It has been shown in references [7], [8] that unbalanced voltage contains a significant negative-phase-sequence component, causing the derived current reference to vary in time, which will lead the DC voltage of the inverter with significant second-order harmonics. This will in turn bring third-order harmonics to the AC side. The DC link voltage pulsation will increase. The damaging risk of the DC-link capacitor and the AC current pulsation will seriously pollute the grid.

Hansen *et al*. [20] proposed the control method for the wind power system which is connected with the PM generator via the frequency converter during the grid

fault. However, the fault ride-through control is based on the control of the generator rectifier. A damping controller, which is to use the DC capacitor as short-term energy storage is implemented to counteract the torque and speed oscillations and ensure a stable operation of the wind turbine under the grid fault.

Abedini *et al*. [21] proposed a control method by adding a limiter to limit the grid currents at inverter and decrease the power generated from the machine during the grid fault.

Y. Zhang *et al*. [22] proposed the inverter control strategy for the wind power system with a permanent-magnet generator under unbalanced three-phase voltage. The negative sequence current is decomposed and added to the current template which is calculated based on the phase lock loop (PLL). The control method guaranteed the sinusoidal and three-phase balance grid side current. However, no information is provided for the DC link voltage.

Lazarov *et al*. [23] applied the control method for the grid inverter based on [24], to control the positive and negative sequence current control in d-q rotating frame. The input and output harmonics is eliminated by eliminating the second order reactive and active power. The input power of the inverter is defined as

$$\frac{2}{3}\begin{bmatrix} P_0 \\ Q_0 \\ P_{s2} \\ P_{c2} \end{bmatrix} = \begin{bmatrix} P_0 \\ Q_0 \\ 0 \\ 0 \end{bmatrix} = \begin{bmatrix} E_d^p & E_q^p & E_d^n & E_q^n \\ E_q^p & -E_d^p & E_q^n & E_d^n \\ E_q^n & -E_d^n & -E_q^p & E_d^p \\ E_d^n & E_q^n & E_d^p & E_q^p \end{bmatrix} \begin{bmatrix} I_d^p \\ I_q^p \\ I_d^n \\ I_q^p \end{bmatrix} \tag{1.37}$$

The references for positive and negative dq components of the currents in synchronous frames are determined in

$$\left[I_{dq}\right] = \left[E_{dq}\right]^{-1}\left[S\right] \tag{1.38}$$

Chong *et al*. [7] applied the control method based on [23], [24] and the control scheme is shown in Figure 1.11

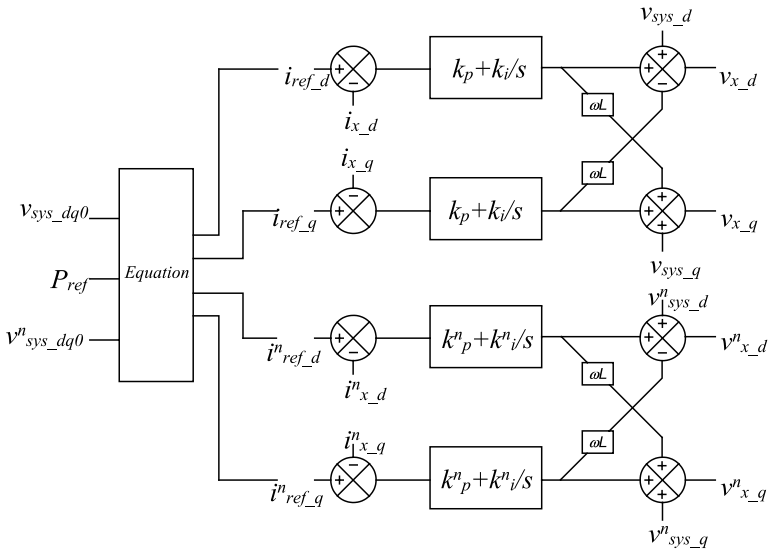

Figure 1. 11: Grid-side inverter control scheme in ref. [7]

However, the model proposed in [7] and [24] ignores the power exchange with the inductors. So under extremely unbalanced case or for a system with large inductance value, the method is not effective.

Yazdami *et al*. [25] proposed a control strategy with two modes to control the positive and negative sequence separately. One mode is to balance the grid side currents. The other mode is to mitigate the DC link voltage ripples under unbalanced grid conditions. For the second mode to mitigate the DC link voltage ripple, the instantaneous active power at the ac terminals of the VSC is directly regulated based on [26], [27] so the harmonics are eliminated more effectively even for extremely unbalance case.

Hu *et al*. [28] proposed the control scheme based on [25], [26], [27]. The four input current references can be calculated as

$$\begin{bmatrix} I^*_{d+} \\ I^*_{q+} \\ I^*_{d-} \\ I^*_{q-} \end{bmatrix} = \frac{2}{3D} \begin{bmatrix} D_1 & D_2 \\ D_2 & -D_1 \\ -D_3 & D_4 \\ -D_4 & D_3 \end{bmatrix} \begin{bmatrix} p_o^{in*} \\ q_o^{in*} \end{bmatrix} \tag{1.39}$$

Where $D_1$, $D_2$, $D_3$, $D_4$, are all nonlinear expression, with $E$, $V$ and $E^2, V^2$

expressed in positive and negative sequence rotating frame. Figure 1.12 shows the control scheme.

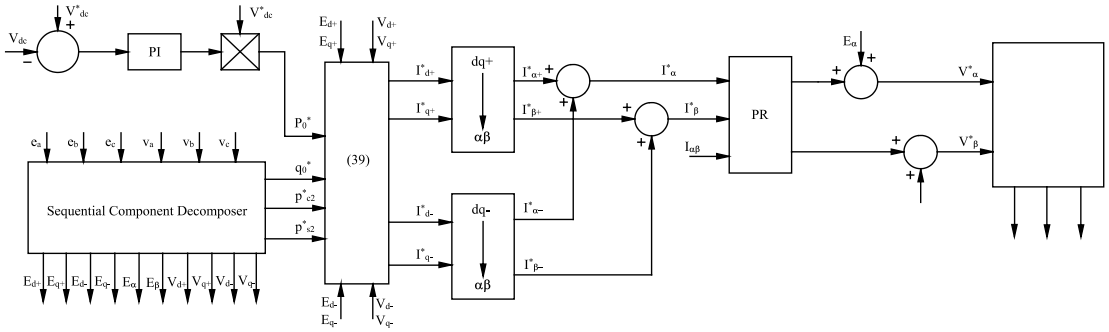


Figure 1. 12: Grid-side inverter control scheme [28]

The reference current is obtained under rotating frame and then is transformed back to α β frame to eliminate the filter which is required for dual current control. The controller is employed in the stationary frame and it is proved that the method is effective under generalized unbalanced operation conditions.

Rodriguez *et al*. [29] [30] separately presented and compared five reactive and active power control strategies developed for the inverter operating under unbalance grid conditions. However, the active power and reactive power are controlled without considering each other.

## 1.5 Comparison of this thesis and recent studies

In this thesis, a generalized method of input-output harmonic elimination for a grid side VSI is proposed based on [14]; the proposed method is general and can be used for all levels of unbalanced grid operation.

In contrast to the studies in [20], [21], the proposed method controls the inverter to eliminate input and output harmonic under unbalanced grid operation so to

eliminate the power pulsation. The wind power system can still work and the generator does not need to be disconnected from the grid even under extremely unbalanced cases. Moreover, the generator can still work under the optimal power tracking and transfer the power to the grid under the extremely unbalanced case.

In contrast to the studies about the control of the voltage source inverter under unbalanced grid operation or during the grid fault [7],[22]-[25], [29]-[30], the method is proposed in a-b-c frame without any frame or sequence transformation and decomposition. In the analysis and calculations, all variable are using phasor representation. Furthermore, only three hysteresis controllers are needed to make the actual currents track the reference currents. No filter or complicated controller design are needed. This saves a lot of time for the online calculation and minimizes the errors which may accumulate during transformation. These make the physical implementation easier and require less hardware.

However, the hysteresis current controller has a variable switching frequency, and this frequency may become very high under some particular circumstances, while the voltage space vector PWM controller has a constant switching frequency.

More importantly, the proposed control method is general because it applies for all levels of unbalance in grid voltages and line impedances with adjustable power factor, while such information is not provided in the previous studies.

Table 1.1 provides a summary of the features of the proposed method in this thesis and control schemes in [7], [22], [23], [25], [28].

Table 1. 1: Comparison between the proposed method and control schemes in [7], [22], [23], [25], [28].

| | **Method in this thesis** | **Method in [22]** | **Methods in [23],[7]** | **Methods in [25],[28]** |
|---|---|---|---|---|
| **Frame and sequence transformation** | a-b-c frame; No transformation required | d-q transformation and sequence decompositions | d-q transformation and sequence decompositions | d-q transformation and sequence decompositions. $\alpha\ \beta$ is required in [28] |
| **Current Regulation** | Current reference calculated in a-b-c frame; actual currents directly track the references | Reference currents are obtained by adding negative sequence component to the output current from three-phase PLL | Reference currents are positive and negative dq components | Reference currents are positive and negative dq components |
| **PWM controller** | Hysteresis current controller | Hysteresis current controller | Space Vector PWM | Space Vector PWM |
| **Unbalance degree** | Extremely unbalanced | Slightly unbalance | Slightly unbalance | Extremely unbalanced |
| **Filter required** | No | No | Notch and low pass filter | Notch and low pass filter in [25], No in [28], but a MF PR resonant current regulator is proposed |

# CHAPTER II

# THEORETICAL ANALYSIS

## 2.1 The wind power system connected to an unbalanced grid

The variable speed wind power system consists of a wind turbine, a generator and two back to back PWM converters. The machine side converter rectifies the variable-magnitude and variable-frequency voltage to a DC voltage. The grid side converter inverts the DC voltage to the AC voltage with the same magnitude and frequency as the grid. The grid side PWM converter has many advantages with typical controls such as the indirect current control and direct active and reactive control under balanced operation. However, under unbalanced grid voltage operation, the grid side current will contain the negative-sequence components and cause the low order harmonics to flow. This low order harmonics in grid currents will cause the DC link voltage and the electromagnetic torque pulsations at the twice the grid frequency.

## 2.2 Harmonic elimination methods

In this chapter, the method for input-output harmonic elimination of the PWM VSI under severe fault conditions in the wind power system is proposed.

Dr. Ana V. Stankovic [8] proposed a generalized method of input-output harmonic elimination for PWM boost type rectifiers under severe fault conditions in the power systems. Ke Chen [8], [31] implemented the method on a 250W a prototype and validated the method in extremely unbalanced case. This thesis derives the solutions for the current references of the grid side inverter for the harmonic elimination under the unbalanced grid operation.

Figure 2.1 shows the circuit of the grid side inverter and Figure 2.2 shows the equivalent circuits.

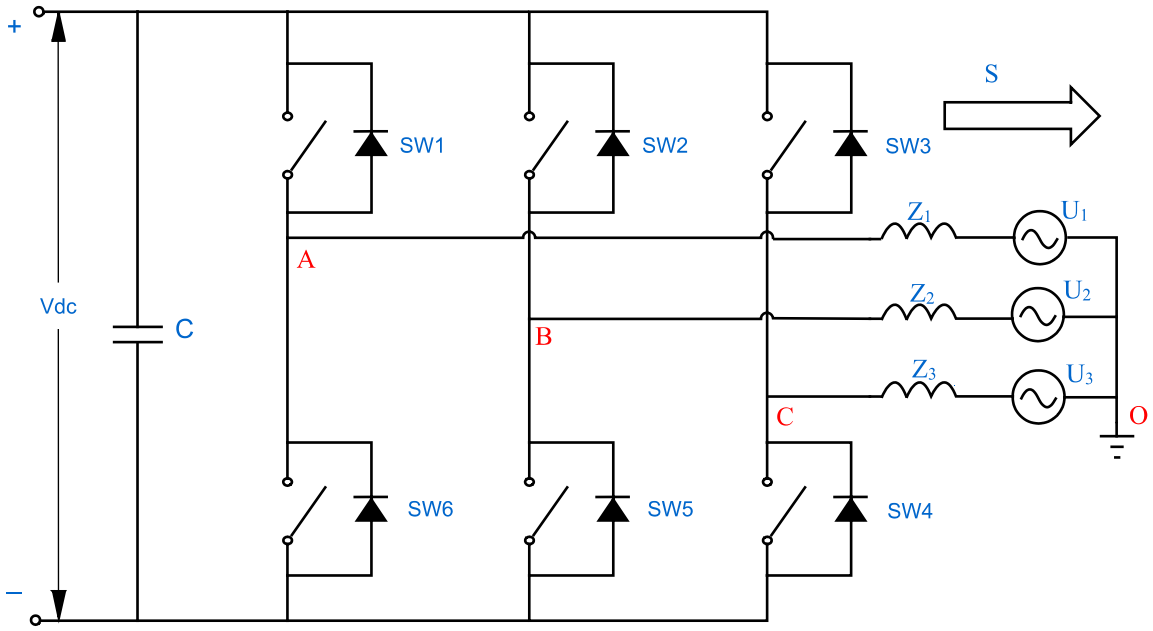


Figure 2. 1: The circuit of grid side inverter connoted to the grid with line impedances

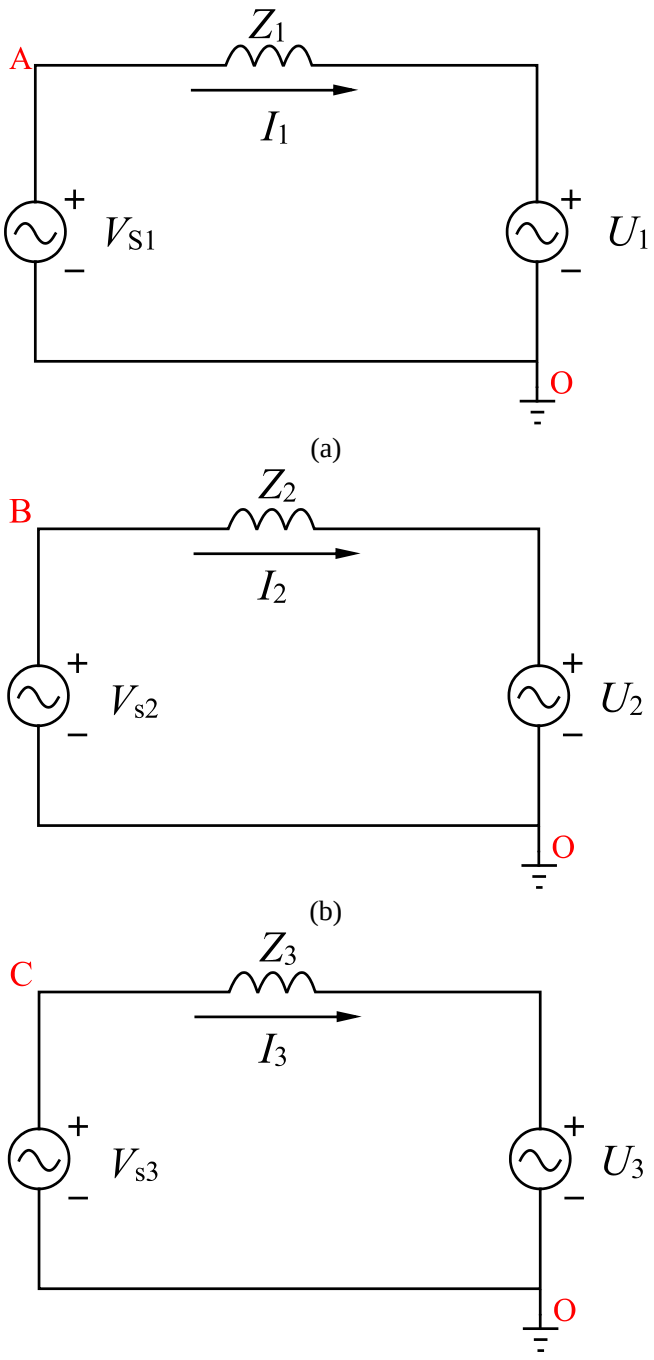


Figure 2. 2: The equivalent circuits of phase A, phase B and phase C

Harmonic elimination is achieved by generating unbalanced reference commands for the three grid side currents under unbalanced input voltages.

According to the Kirchhoff's voltage law (KVL),

$$U_1 = -z_1 I_1 + V_{s1} \tag{2.1}$$

$$U_2 = -z_2 I_2 + V_{s2} \tag{2.2}$$

$$U_3 = -z_3 I_3 + V_{s3} \tag{2.3}$$

Where $U_1, U_2, U_3$ are grid side voltages, $z_1, z_2, z_3$ are line side impedance, $I_1, I_2, I_3$ are grid side currents. $V_{s1}, V_{s2}, V_{s3}$ are synthesized voltages at the input of the rectifier.

$V_{s1}, V_{s2}, V_{s3}$ can also be expressed as:

$$V_{s1} = SW_1 \frac{V_{dc}}{2\sqrt{2}} \tag{2.4}$$

$$V_{s2} = SW_2 \frac{V_{dc}}{2\sqrt{2}} \tag{2.5}$$

$$V_{s3} = SW_3 \frac{V_{dc}}{2\sqrt{2}} \tag{2.6}$$

Where $V_{dc}$ is the DC link voltage and $SW_1, SW_2, SW_3,$ are the switching functions. By substituting equation (2.4), (2.5), (2.6) in to (2.1), (2.2), (2.3) the following equations are obtained.

$$U_1 = -z_1 I_1 + SW_1 \frac{V_{dc}}{2\sqrt{2}} \tag{2.7}$$

$$U_2 = -z_2 I_2 + SW_2 \frac{V_{dc}}{2\sqrt{2}} \tag{2.8}$$

$$U_3 = -z_3 I_3 + SW_3 \frac{V_{dc}}{2\sqrt{2}} \tag{2.9}$$

By multiplying equation (2.7), (2.8), (2.9) by $I_1, I_2, I_3$ respectively and adding them together, the following equation is obtained:

$$U_1 I_1 + U_2 I_2 + U_3 I_3 = -z_1 {I_1}^2 - z_2 {I_2}^2 - z_3 {I_3}^2 + \frac{V_{dc}}{2\sqrt{2}} V_{s1}(SW_1 I_1 + SW_2 I_2 + SW_3 I_3) \tag{2.10}$$

Equation (2.11) represents the condition for the second harmonic elimination [8]

$$SW_1 I_1 + SW_2 I_2 + SW_3 I_3 = 0 \tag{2.11}$$

By substituting equation (2.11) into (2.10), the following equation is obtained:

$$U_1 I_1 + U_2 I_2 + U_3 I_3 = -z_1 I_1^{\,2} - z_2 I_2^{\,2} - z_3 I_3^{\,2} \tag{2.12}$$

The conjugate of the complex power for a Y connection three-phase voltage source is:

$$S^* = -U_1^* I_1 - U_2^* I_2 - U_3^* I_3 \tag{2.13}$$

According to Kirchhoff's current law (KCL),

$$I_1 = -I_2 - I_3 \tag{2.14}$$

By substituting equation (2.14) into (2.13) and (2.12) the following equations are obtained.

$$S^* = -U_1^*(-I_2 - I_3) - U_2^* I_2 - U_3^* I_3 \tag{2.15}$$

$$I_2(-U_1 + U_2) + I_3(U_3 - U_1) = -(z_1 + z_2) I_1^{\,2} - (z_1 + z_3) I_3^{\,2} - 2 z_1 I_2 I_3 \tag{2.16}$$

Equation (2.15) can be rearranged as:

$$I_2 = \frac{S^* + (U_3^* - U_1^*) I_3}{(U_1^* - U_2^*)} \tag{2.17}$$

By substituting equation (2.17) into (2.16), the following equation can be obtained:

$$\begin{aligned} &\frac{S^* + (U_3^* - U_1^*) I_3}{(U_1^* - U_2^*)}(-U_1 + U_2) + (U_3 - U_1) I_3 = \\ &-(z_1 + z_2)\left(\frac{S^* + (U_3^* - U_1^*) I_3}{(U_1^* - U_2^*)}\right)^2 - (z_1 + z_3) I_3^{\,2} - 2 z_1 I_3 \left(\frac{S^* + (U_3^* - U_1^*) I_3}{(U_1^* - U_2^*)}\right) \end{aligned} \tag{2.18}$$

Equation (2.18) can be rearranged as:

$$\left(-(z_1+z_3)-\frac{2z_1(U_3^*-U_1^*)}{(U_1^*-U_2^*)}-(z_1+z_2)\frac{(U_3^*-U_1^*)^2}{(U_1^*-U_2^*)^2}\right)I_3^2$$
$$\left(-(U_3-U_1)-\frac{(U_3^*-U_1^*)(U_2-U_1)}{(U_1^*-U_2^*)}-2(z_1+z_2)\frac{(U_3^*-U_1^*)S^*}{(U_1^*-U_2^*)^2}-2z_1\frac{S^*}{U_1^*-U_2^*}\right)I_3 \qquad (2.19)$$
$$\left(-\frac{S^*(U_2-U_1)}{(U_1^*-U_2^*)}-\frac{(z_1+z_2)S^{*2}}{(U_1^*-U_2^*)^2}\right)=0$$

Current $I_3$ can be obtained from the above quadratic equation by using the quadratic formula:

$$I_3=\frac{-b\pm\sqrt{b^2-4ac}}{2a} \qquad (2.20)$$

Where

$$a=-(z_1+z_3)-\frac{2z_1(U_3^*-U_1^*)}{(U_1^*-U_2^*)}-(z_1+z_2)\frac{(U_3^*-U_1^*)^2}{(U_1^*-U_2^*)^2} \qquad (2.21)$$

$$b=-(U_3-U_1)-\frac{(U_3^*-U_1^*)(U_2-U_1)}{(U_1^*-U_2^*)}-2(z_1+z_2)\frac{(U_3^*-U_1^*)S^*}{(U_1^*-U_2^*)^2}-2z_1\frac{S^*}{U_1^*-U_2^*} \qquad (2.22)$$

$$c=-\frac{S^*(U_2-U_1)}{(U_1^*-U_2^*)}-\frac{(z_1+z_2)S^{*2}}{(U_1^*-U_2^*)^2} \qquad (2.23)$$

Chen [31] provided the constraints of the solutions. The three-phase switching functions $SW_1, SW_2, SW_3,$ must be less than or equal to one to ensure that the analytical solution is valid for the PWM bridge.

Equations (2.14), (2.17), (2.19) represent the steady-state solution for input and output harmonic elimination under unbalanced grid voltages.

# CHAPTER III

# SIMULATION RESULTS

A harmonic elimination method used for the grid side inverter under unbalanced operations is derived in the previous chapter. A closed-loop control method for keeping the constant DC link voltage is proposed based on the open loop configuration analysis.

The controls of the voltage-fed rectifier of the wind power system with a permanent magnet generator and the system with a squirrel cage induction generator for optimal power acquisition are explained separately in the first chapter. For a specific wind speed, there is only one rotating speed and torque corresponding to the optimal wind power acquisition. The reference torques with different wind speeds operations are derived according to the wind turbine characteristics. In this thesis, vector control with the torque control is applied for the permanent magnet generator. Scalar control with the torque and flux control is applied for the squirrel cage induction generator.

In this chapter, the wind power system is simulated in MATLAB Simulink using the SimPowerSystem tool box. The control for harmonic elimination under

unbalanced grid operation and the control for optimal wind power acquisition are examined. Five different cases, from balance to extremely unbalanced grid operation are selected for the simulation. The simulation results of traditional indirect current control in a-b-c frame and the traditional vector control in d-q rotating frame for the for the grid side inverter are also included in this chapter for comparison.

## 3.1 Control Strategy for the wind power system connected with a permanent-magnet generator.

The operation of the proposed wind power system with the permanent-magnet generator with the schemes of optimal wind power acquisition and harmonic elimination control is simulated using the MATLAB Simulink SimPowerSystem tool box.

The overall systems circuit diagram is shown in figure 3.1. It can be seen that the grid is composed of three single-phase sources. The machine side rectifier is shown in Figure 3.2 and the grid side inverter is shown in Figure 3.3. Each of them is a three-phase bridge which consists of six IGBTs and six anti-parallel diodes. The six IGBTs are controlled by six gating signals. The grid side inverter is connected to the grid with three coupling inductors

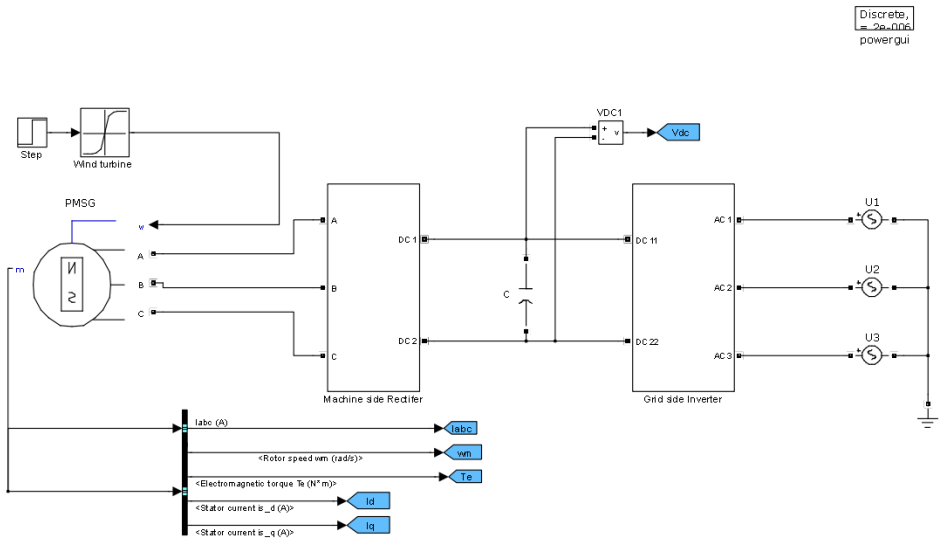


Figure 3. 1: Diagram of a permanent-magnet synchronous generator connected by back-to-back PWM converters to the grid for variable wind speed application.

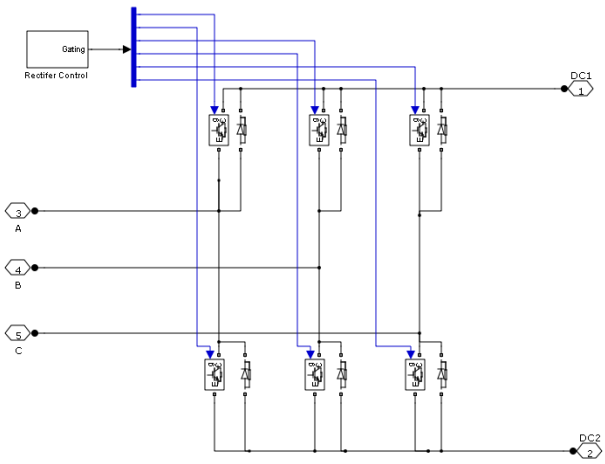


Figure 3. 2: Diagram of the machine side rectifier connected to a permanent-magnet generator

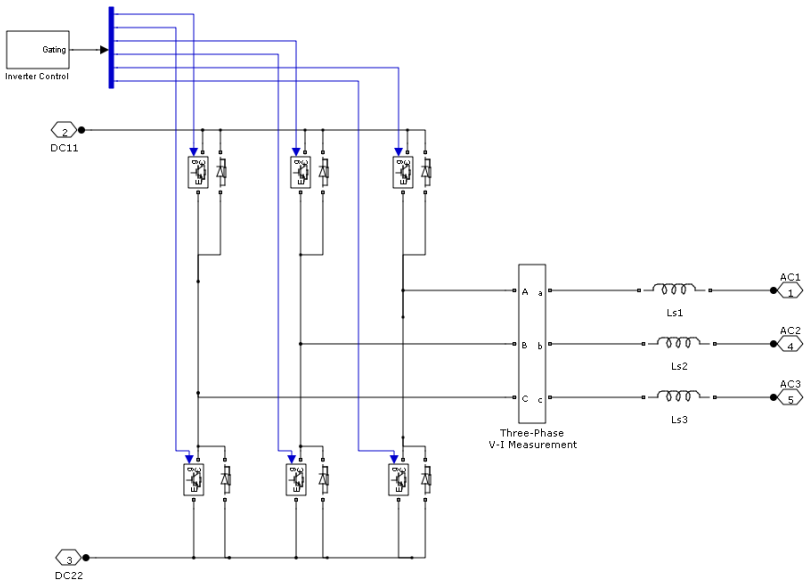


Figure 3. 3: Diagram of the grid side inverter

### 3.1.1 Control of the machine side rectifier for the permanent-magnet generator

The purpose of the control of the permanent magnet generator is to achieve the optimal performance. The optimal torque is stored in a lookup table with the wind speed and generator rotor speed as the indexes. The desired $i_{sd}$* current is set to be zero and the desired $i_{sq}$* current is calculated by using the equation:

$$T_e = \frac{3}{2} p \Psi i_{sq} \tag{3.1}$$

The desired $i_{sq}$* and $i_{sd}$* currents and the measured $i_{sq}$ and $i_{sd}$ currents are transformed to $i_{s\alpha}$*, $i_{s\beta}$* and $i_{s\alpha}$, $i_{s\beta}$ in the $\alpha$ $\beta$ stationary coordinate. The errors of the currents are used to form the required $u_\alpha$ and $u_\beta$ voltage components of the rectifier vector by two separate PI current controllers. Space vector is used to generate six switching signals for six IGBTs. The diagram of the control system for the machine side is shown in figure 3.4.

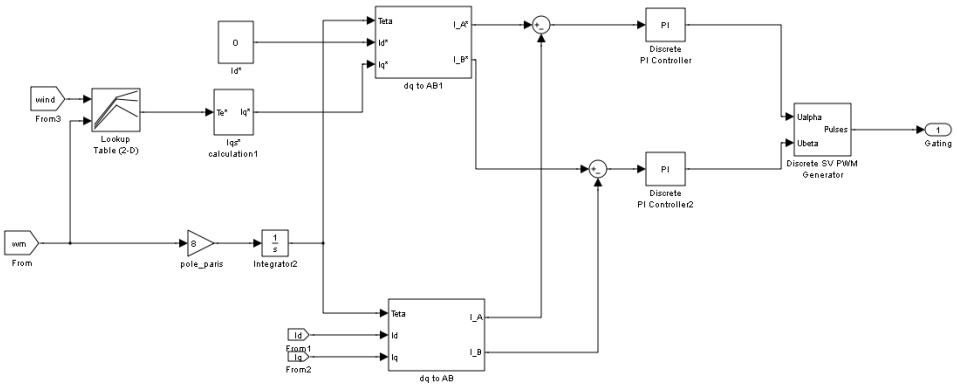


Figure 3. 4: Diagram of the machine side rectifier control system

### 3.1.2 Control of the grid side voltage-fed inverter for the wind power system connected with a permanent-magnet generator

Closed-loop operation of the voltage-fed boost type inverter keeps the DC link voltage constant. The output of the DC link voltage controller sets a reference for the three phase currents. The control loop is shown in the figure 3.5.

The DC link voltage is fed back to the controller and compared with the reference DC voltage. The error signal is used to update the setting of the active power P, added by the reactive power Q, obtained the complex power S, which is for the calculations of the reference currents. Three-phase reference currents are generated in real time. A hysteresis controller is used to make the line side currents track the reference currents so the DC link voltage is controlled and the low order harmonics are eliminated in grid side and the DC link under unbalanced grid operation. By controlling the DC link voltage, the instant power transmission from the machine to the grid is achieved.

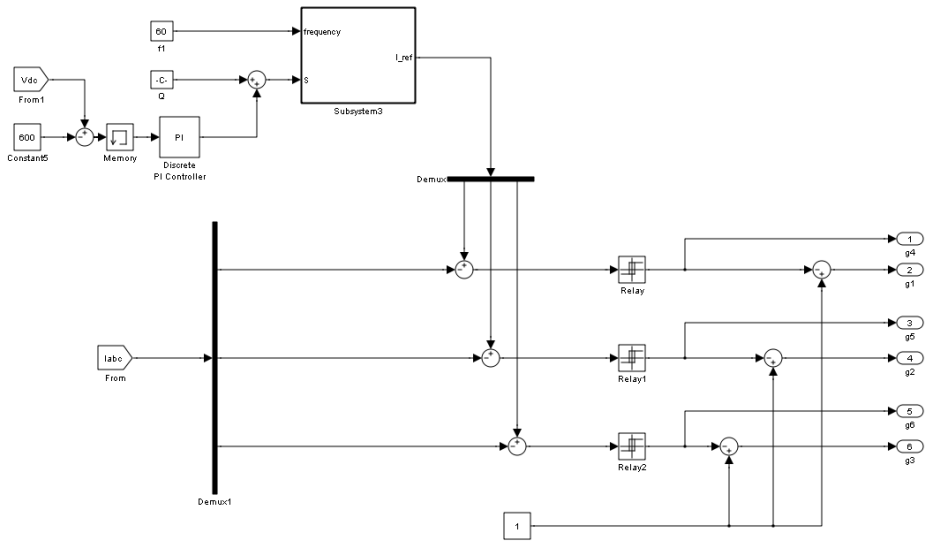


Figure 3. 5: Diagram of the grid side inverter control system

## 3.2 Simulation results of the wind power system with the permanent magnet generator

Five different simulation cases are selected to verify the optimal power acquisition in the machine side and the harmonic elimination of the gird side inverter under unbalanced grid voltage operation. Comparison cases are provided with standard indirect current control in a-b-c frame and traditional vector control in d-q rotating frame. Table 3.1 lists the parameters of the permanent-magnet generator used in the simulation; Table 3.2 lists the parameters of the DC link and the converters. Table 3.3 lists the simulation cases.

Table 3. 1: Parameters used for the permanent-magnet generator used in the simulation

| | |
|---|---|
| **Stator phase resistance Rs** | 2.8750 ohm |
| **Inductances in d,q axis** | Ld(H)=51 mL; Lq(H)=51mL |
| **Poles** | 16 |
| **Torque Constant** | 6 N.m/A_peak |
| **Voltage constant** | 725.5197 V_peak L-L/krpm |
| **Power Rating** | 3 kW |
| **Rated Voltage** | 480 V (wye three-phase stator winding) |
| **Speed** | 800 rpm |
| **NdFeB magnets provide proper flux density in the air gap** | |

Table 3. 2: Parameters of the DC link and converters for the wind power system with permanent-magnet generator

| **Parameter** | **Value** | **Parameter** | **Value** |
|---|---|---|---|
| $f_{grid}$ | 60 Hz | Hysteresis band | 0.02A |
| $C_{dclink}$ | 300 μ F | Switch on resistance | 0.5 Ω |
| IGBT forward voltage | 1V | Diode forward voltage | 1.5V |
| Sampling time | 0.02ms | | |

Table 3. 3: Simulation cases for the wind power system with permanent-magnet generator

| **Case** | **Grid side voltage** | **Line impedance** | **Power factor** |
|---|---|---|---|
| 1 | $U_a$=220∠0, $U_b$ =220∠-120, $U_c$ =220∠120. | $L_1 = L_2 = L_3 =$ 5mL | 1 |
| 2 | $U_a$=110∠0, $U_b$ =160∠-120, $U_c$ =220∠120. | $L_1 = L_2 = L_3 =$ 5mL | 1 |
| 3 | $U_a$=0∠0, $U_b$ =110∠-120, $U_c$ =220∠120. | $L_1 = L_2 = L_3 =$ 5mL | 1 |
| 4 | $U_a$=0∠0, $U_b$ =110∠-120, $U_c$ =220∠120. | $L_1 = L_3$ = 5mL ; $L_2$ =0 mL | 1 |
| 5 | $U_a$=0∠0, $U_b$ =110∠-120, $U_c$ =220∠120. | $L_1 = L_3$ = 5mL ; $L_2$ =0 mL | 0.7 lagging |

In the simulation, a look-up table is used with the wind speed as the index and the rotor speed as the output. Figure 3.6 shows the simulation results of the wind turbine characteristics. The wind speeds are 8 m/s, 9 m/s, 10 m/s, 11 m/s, 12 m/s. The x axis indicates the rotor speed, and the y axis indicates the mechanical torque.

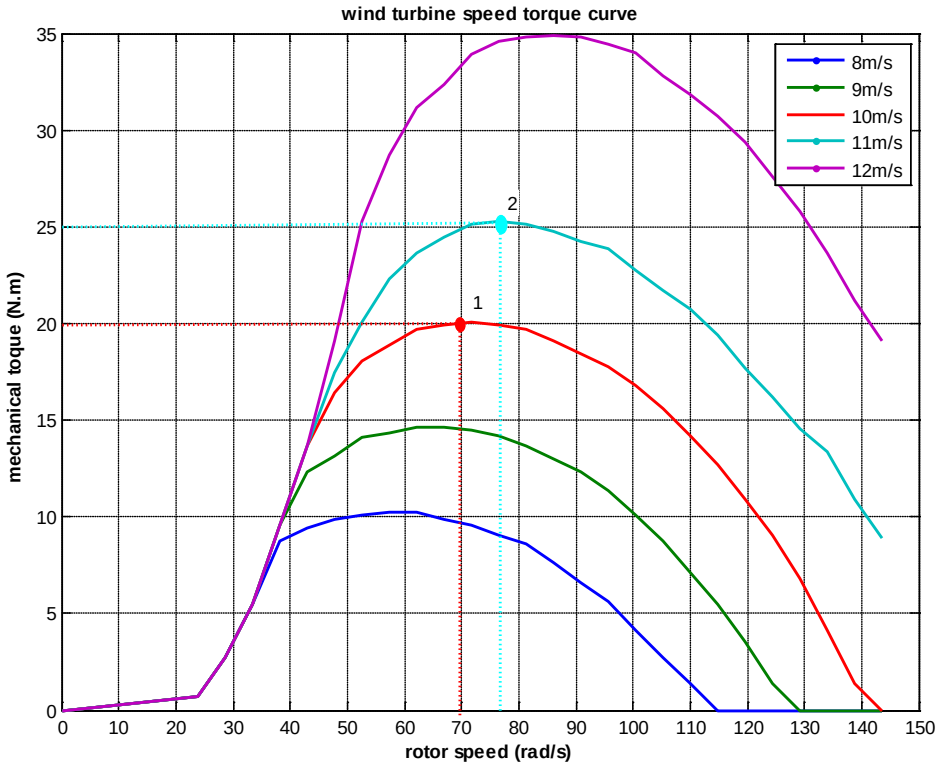


Figure 3. 6: The simulation result of the wind turbine characteristics.

In figure 3.6, Point 1 and Point 2 indicate the optimal power acquired from the wind turbine with the wind speed of 10m/s and 11m/s.

Between 0s-1.0s, the wind speed is 10m/s, the rotor mechanical speed $\omega_{m1} = 70$ rad/s, $n_{m1} = 668.45$ r/min.

Between 1.9s-2.0, the wind speed is 11m/s, the rotor mechanical speed $\omega_{m2} = 78$ rad/s, $n_{m2} = 744.85$ r/min.

According to the equation

$$f_e = \frac{n_m P}{120} \tag{3.2}$$

Where P is poles number, which is 16 in this case.

In the steady state, the corresponding electrical frequency is

$$f_{e1} = \frac{668.45 \text{ r/min} \times 16}{120} = 89 \text{ Hz} \tag{3.3}$$

$$f_{e2} = \frac{744.85 \text{ r/min} \times 16}{120} = 99 \text{ Hz} \quad (3.4)$$

The simulation results of stator currents with different rotor speeds are shown in figure 3.7 (a), (b).

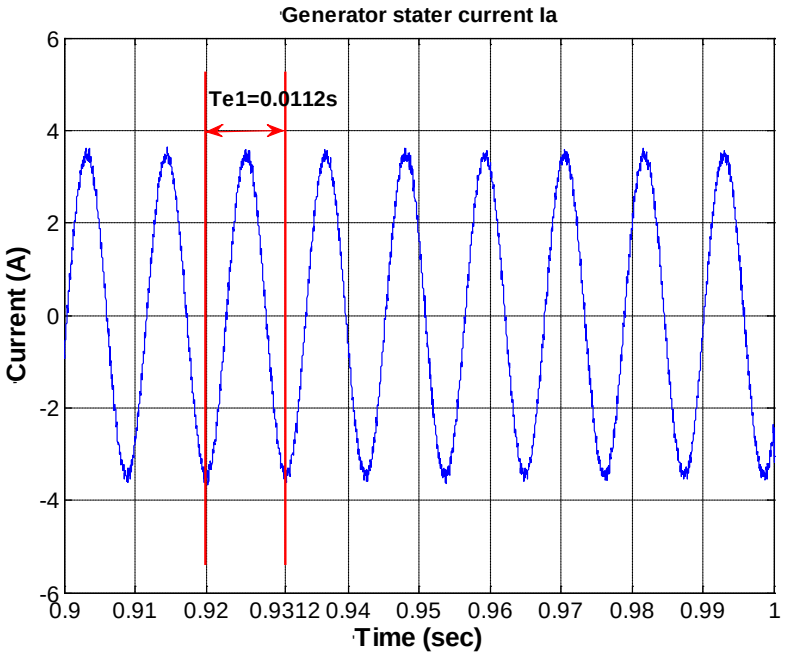


(a)

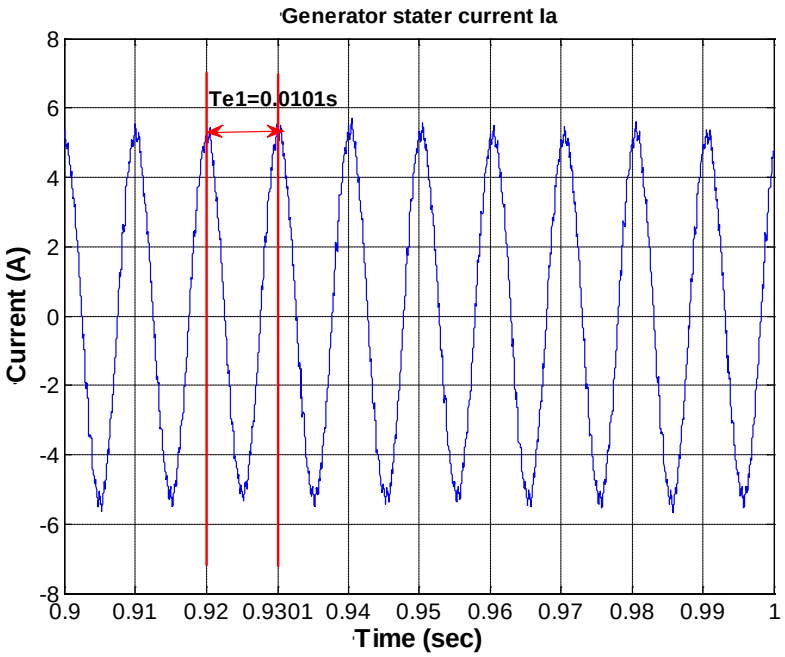


(b)

Figure 3. 7: PM generator stator currents with different rotor speeds.

In the steady state, the electromagnetic torque is equal to the mechanical torque: $T_e = T_m$.

The electrical power the generator transformed from the mechanical power is

$$P_G = T_e \omega_m \quad (3.5).$$

Between 0-1.0 s, the optimal power is

$$P_{G1} = -20(N.m) \times 70(rad/s) = -1400(W) \quad (3.6)$$

Between 1.0-2.0 s, the optimal power is

$$P_{G2} = -25(N.m) \times 78(rad/s) = -1950(W) \quad (3.7)$$

At 1.0s the wind speed changes and the rotor speed changes. The corresponding optimal torque needed to be changed, which is achieved by the change of the three phase stator currents. It can be seen in figure 3.8, the magnitude of the stator currents change at 1.0 second.

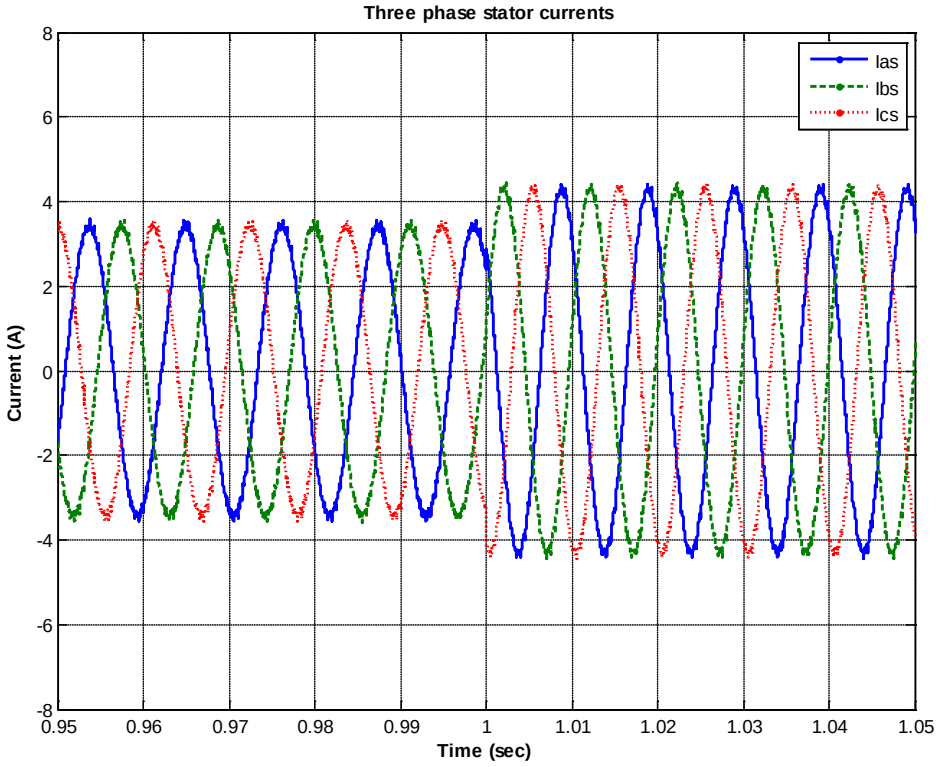


Figure 3. 8: The three phase stator currents of the PM generator.

In case 1, the operation of the three-phase grid side converter is simulated under the balanced grid voltages. Under unbalanced voltage operation, from case 2 to case 3, and under unbalanced line impedance case 4 and case 5, with indirect current control and vector control, three-phase output currents are distorted with three time harmonics and the DC link voltage is with second order ripples due to the unbalance grid voltage. Furthermore, under the unbalanced grid operation, it can be seen from the simulation result that with the indirect current control, variable power factor control can not be achieved at the grid side inverter. .

The simulation results of the grid side voltage, the grid side currents, average active and reactive power at grid, the DC link voltage, the DC link current, the electromagnetic torque of the generator, and the spectrum of the grid side currents are shown below with three difference methods for 6 cases. The stator currents and the generator output voltages are provided for Case 6 to show the effect of unbalanced grid operation on the generator and for the comparison among the different methods for the grid side inverter.

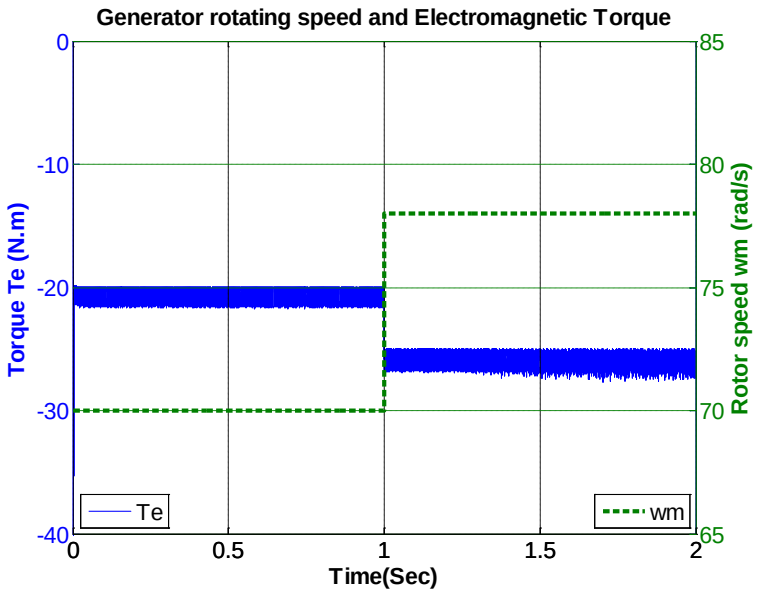


Figure 3. 9: Torque and rotor speed of PM generator connected to the grid for

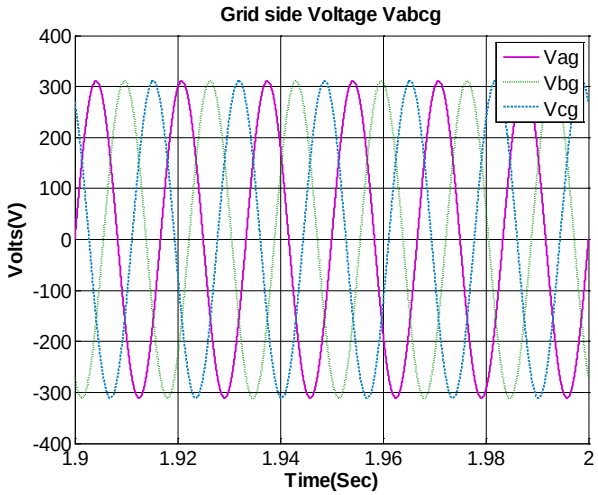


Figure 3. 10: Three-phase grid voltage (phase to ground) for Case 1

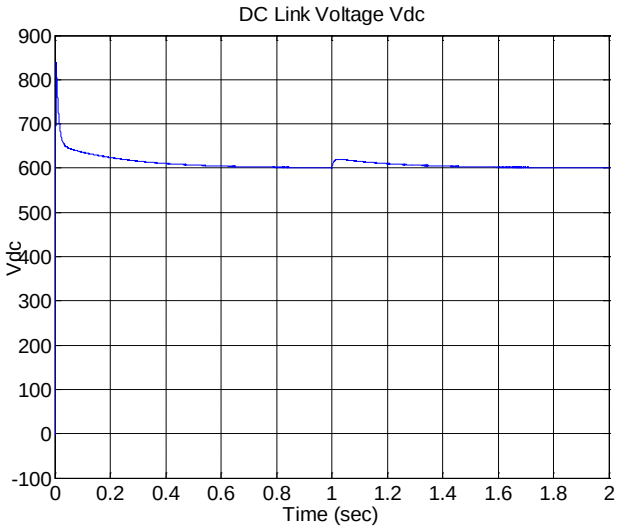


Figure 3. 11: DC link voltage for Case 1

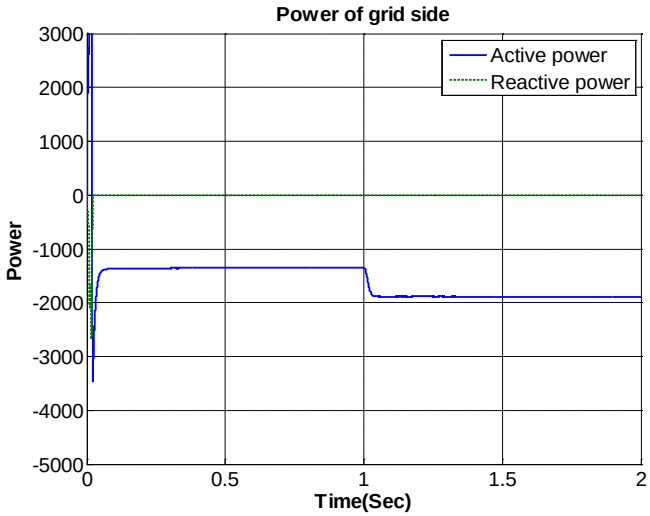


Figure 3. 12: Active and reactive power of the grid for Case 1

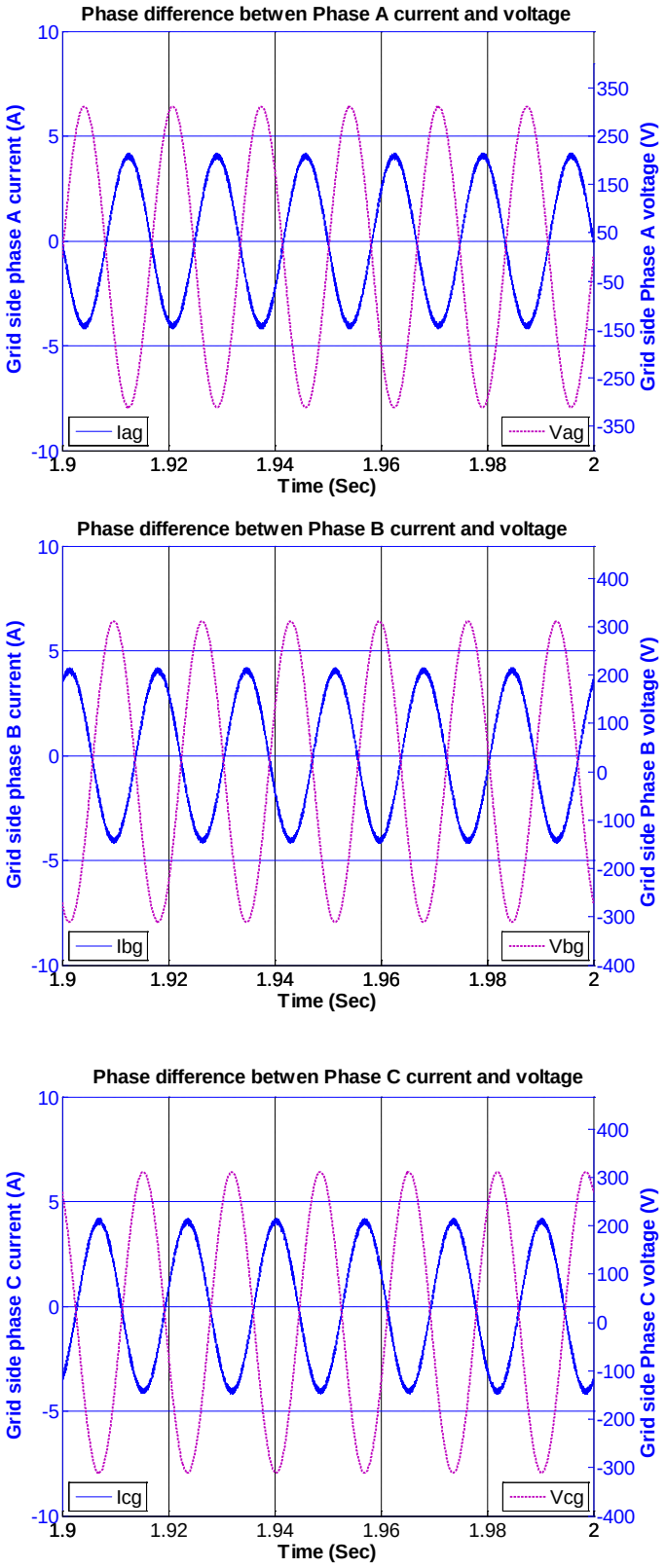


Figure 3. 13: Phase currents with voltages for Case 1

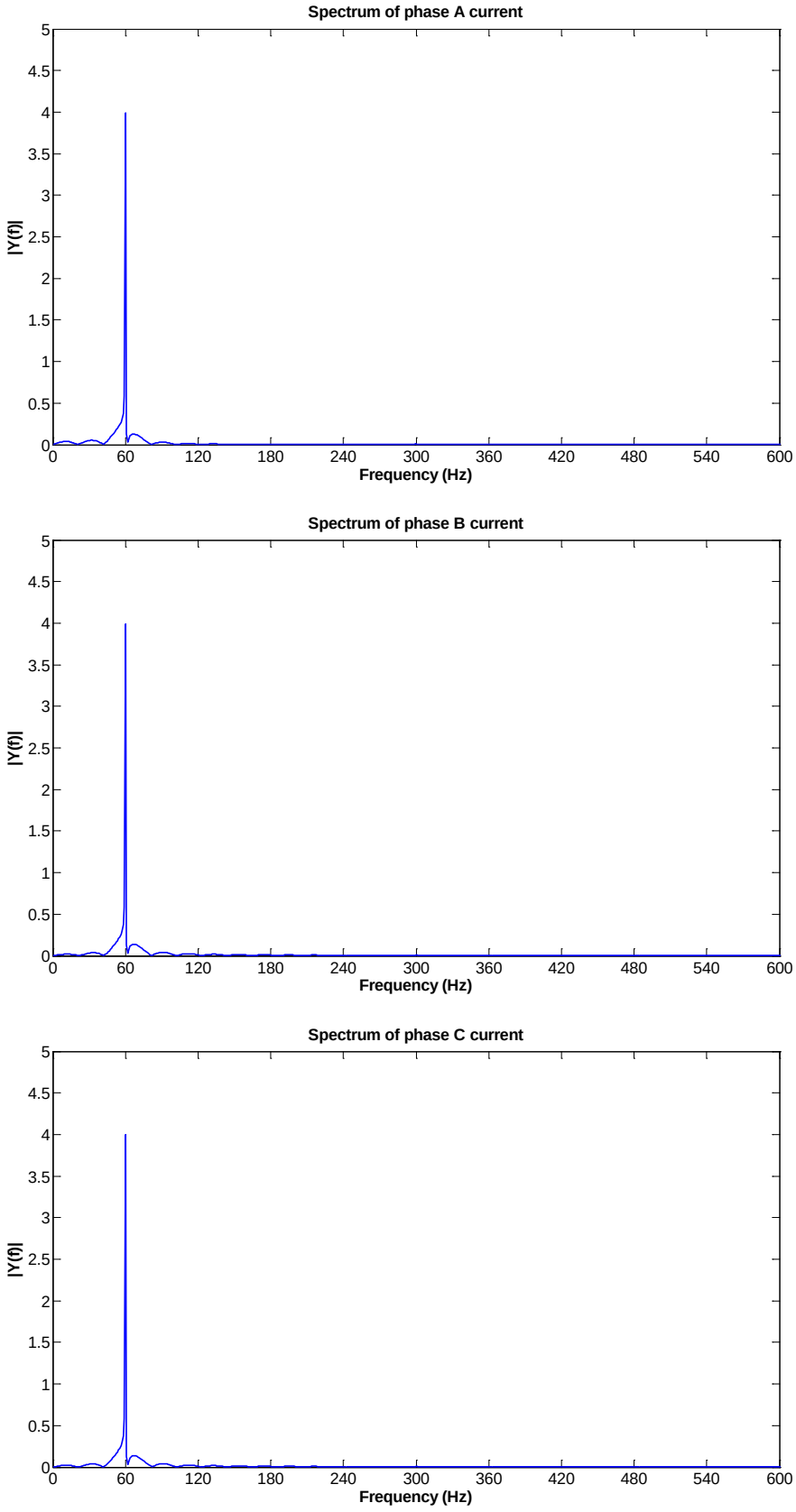


Figure 3. 14: Spectrum of currents for Case 1

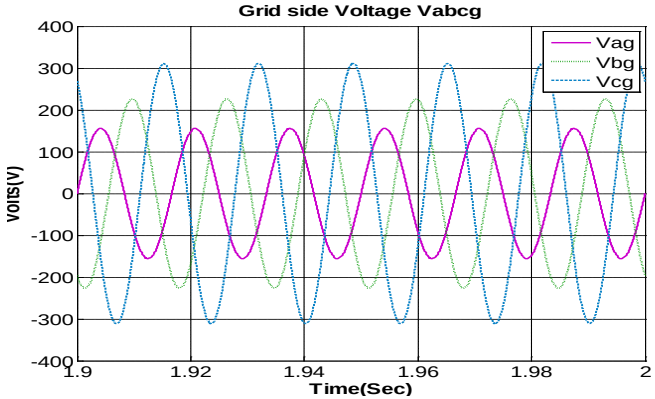


Figure 3. 15: Three-phase grid voltage of Case 2

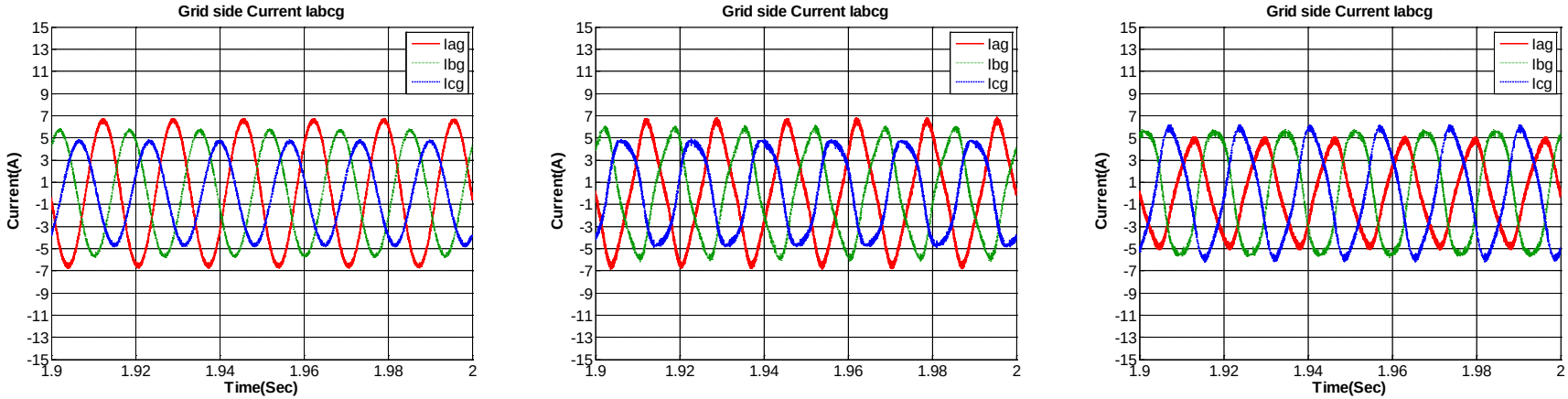


(a) (b) (c)

Figure 3. 16: Three-phase grid currents and of Case 2

(a) Proposed control; (b) Standard d-q method; (c) Standard indirect current method.

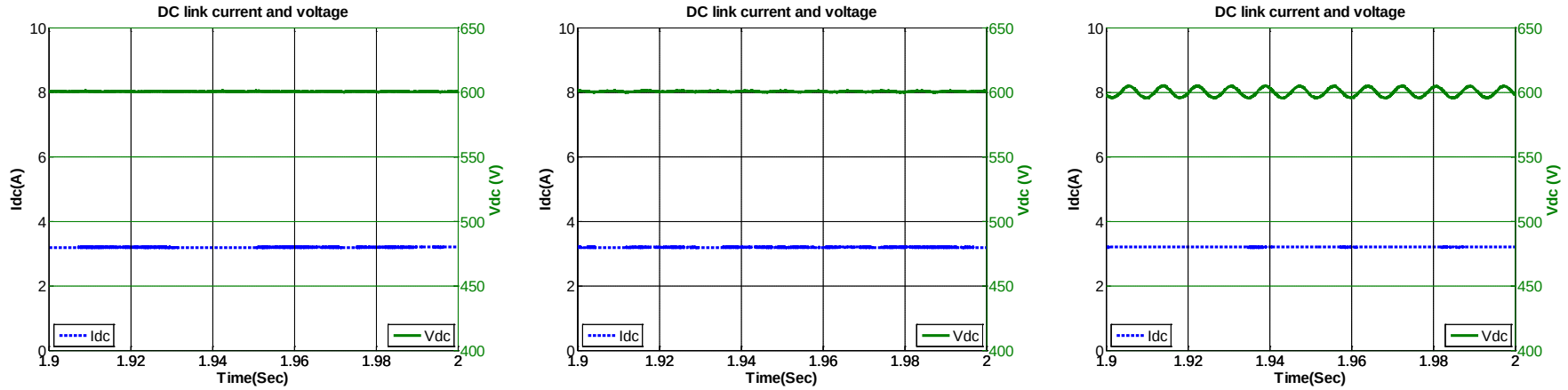


(a) (b) (c)

Figure 3. 17: DC link current and voltage of Case 2

(a) Proposed control; (b) Standard d-q method; (c) Standard indirect current method.

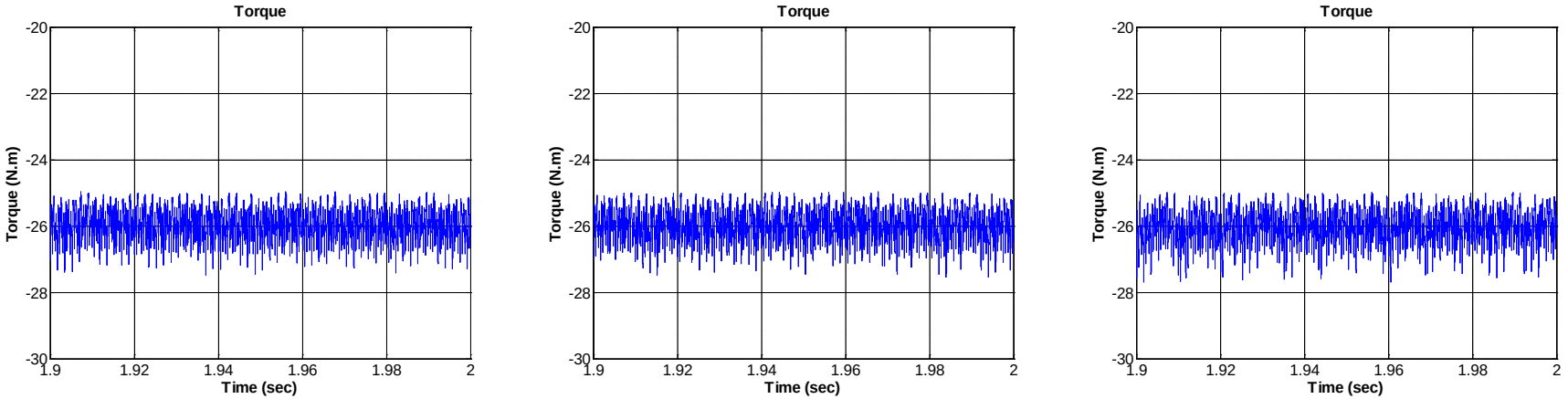


(a) (b) (c)

Figure 3. 18: Electromagnetic torque of PM generator of Case 2:

(a) Proposed control; (b) Standard d-q method; (c) Standard indirect current method

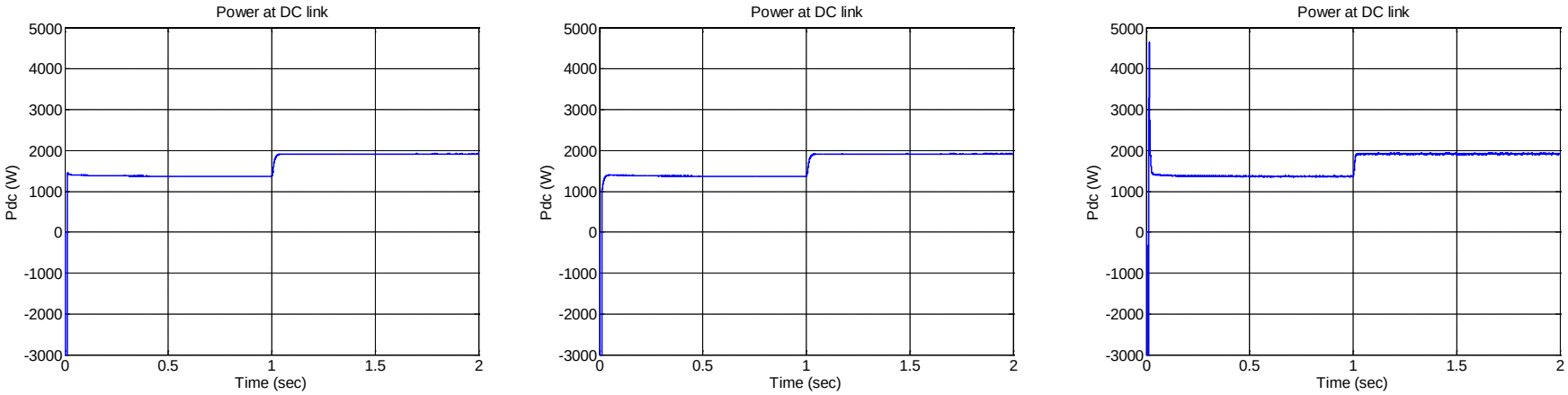


(a) (b) (c)

Figure 3. 19: DC link power of Case 2

(a) Proposed control; (b) Standard d-q method; (c) Standard indirect current method

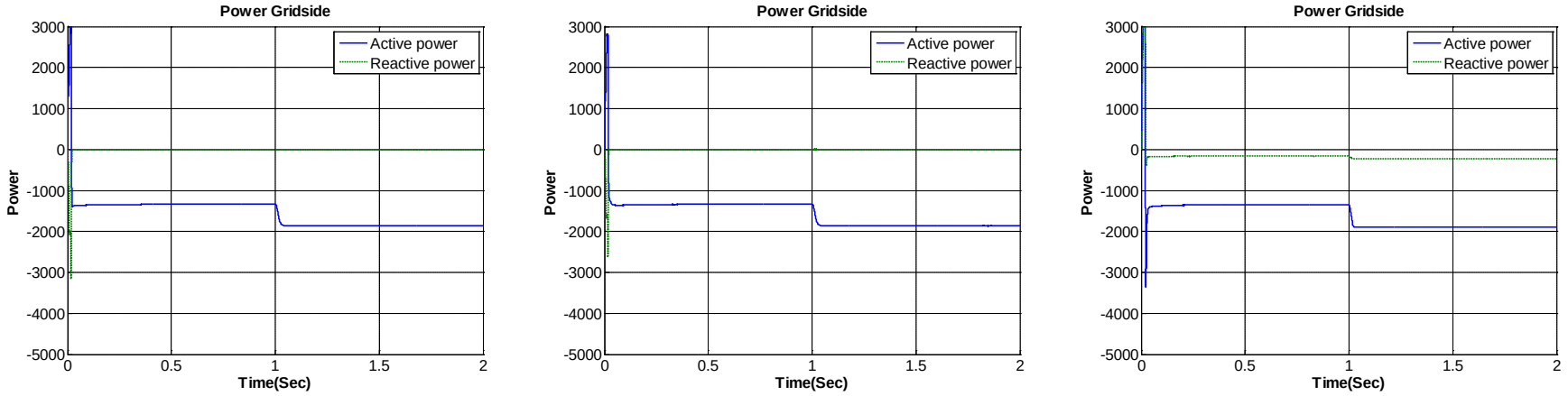


(a) (b) (c)

Figure 3. 20: Average output active and reactive power of Case 2:

(a) Proposed control; (b) Standard d-q method; (c) Standard indirect current method

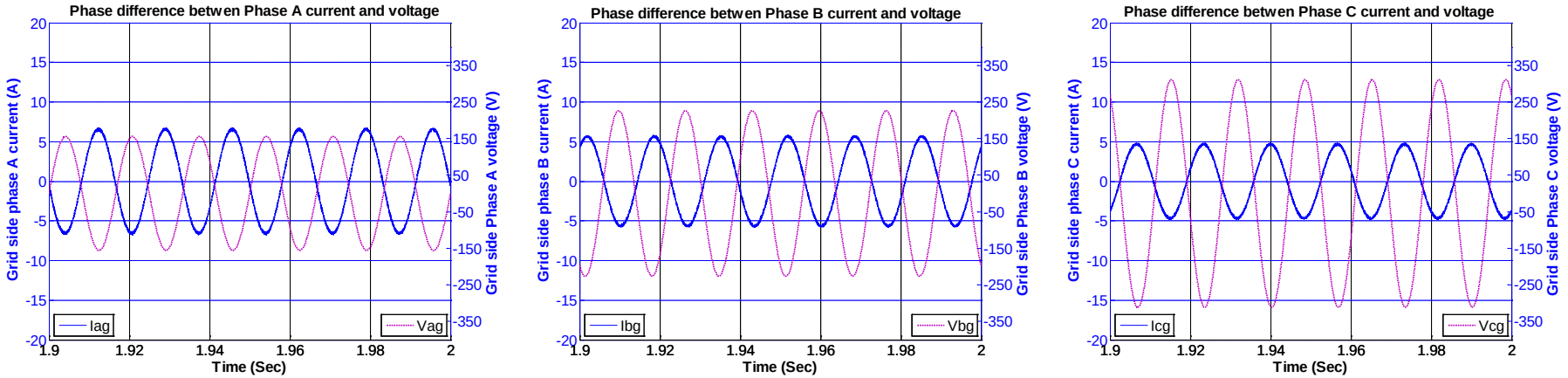


(a) (b) (c)

Figure 3. 21: Phase-currents with voltages for Case 2
(a) Phase A; (b) Phase B; (c) Phase C

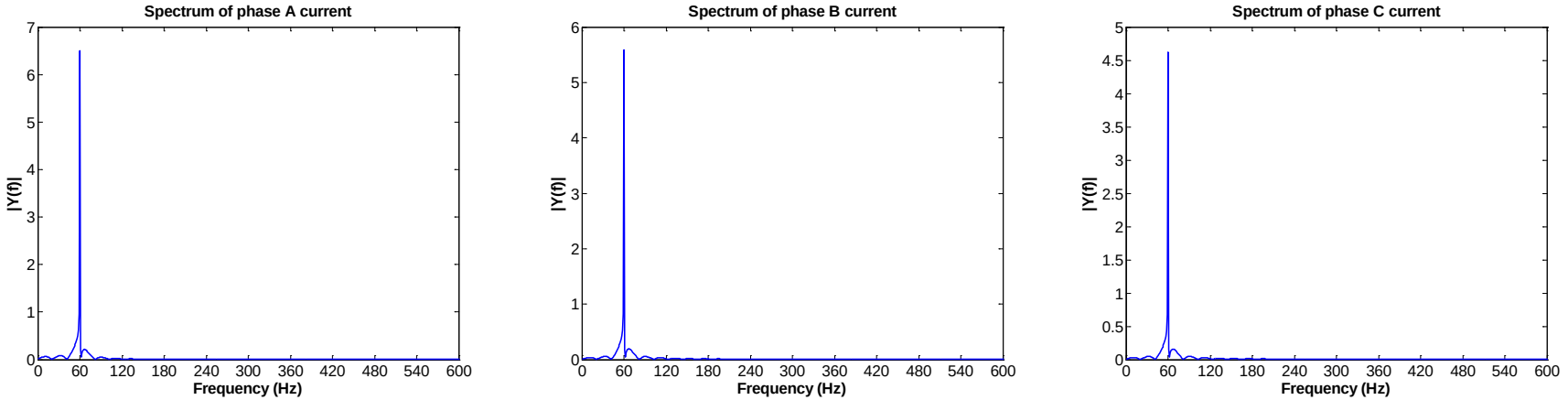


(a) (b) (c)

Figure 3. 22: Spectrums of grid currents for Case 2 with proposed method
(a) Phase A; (b) Phase B; (c) Phase C

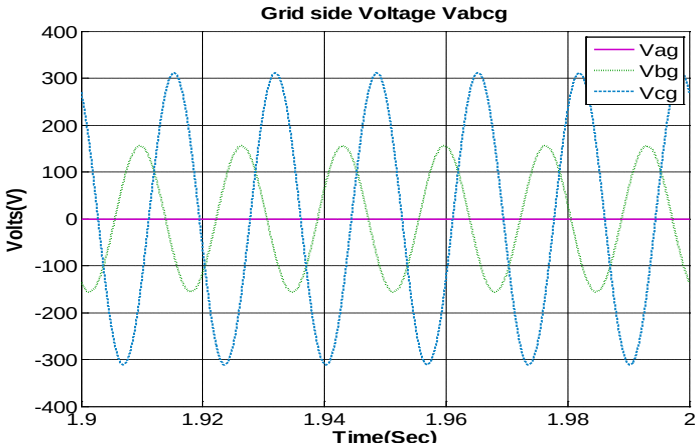


Figure 3. 23: Three-phase grid voltage of Case 3



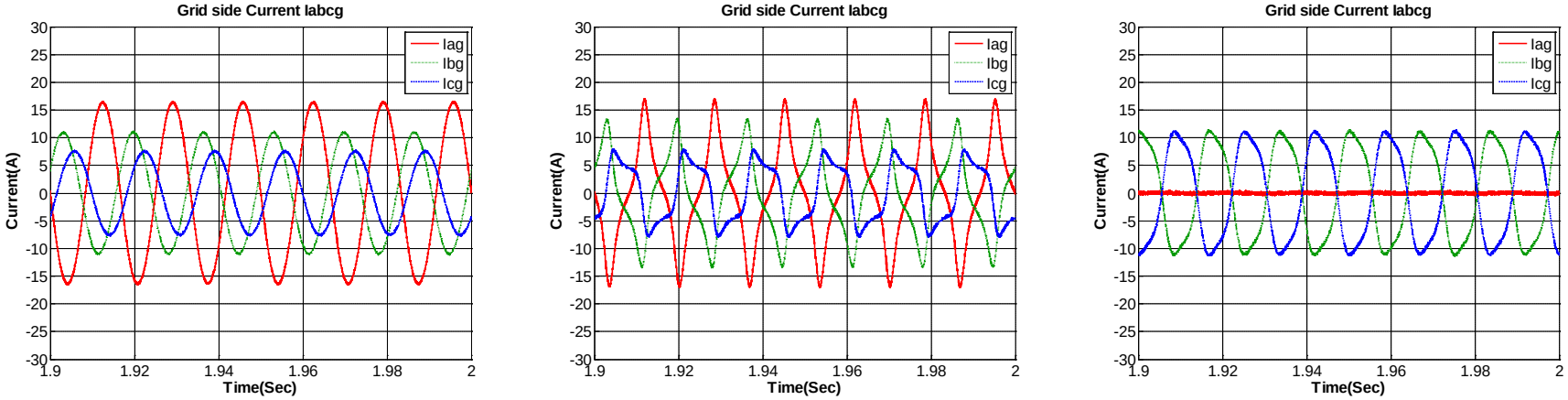


(a) (b) (c)

Figure 3. 24: Three-phase grid currents of Case 3

(b) Proposed control; (b) Standard d-q method; (c) Standard indirect current method.

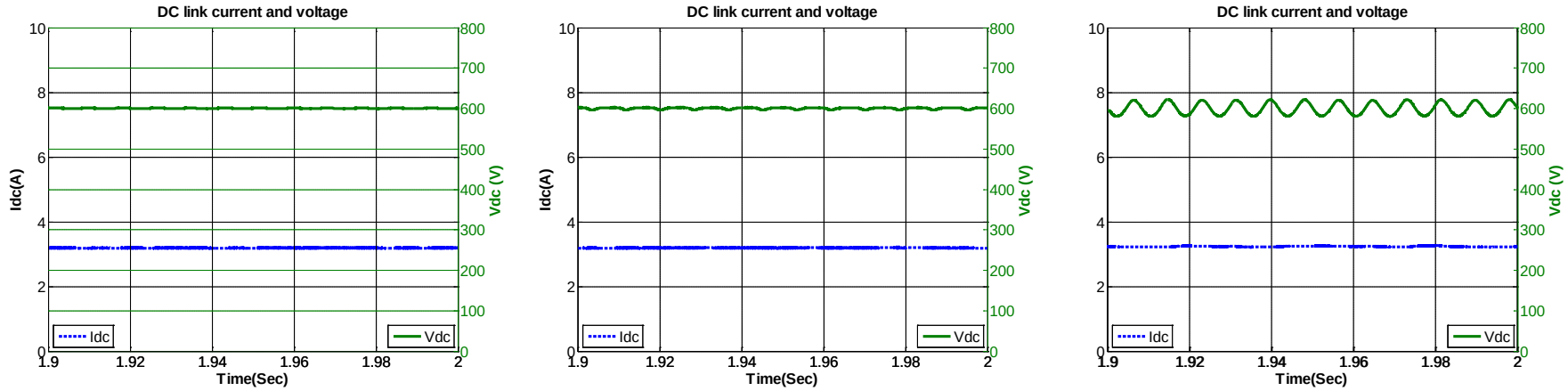


(a) (b) (c)

Figure 3. 25: DC link current and voltage of Case 3

(c) Proposed control; (b) Standard d-q method; (c) Standard indirect current method.

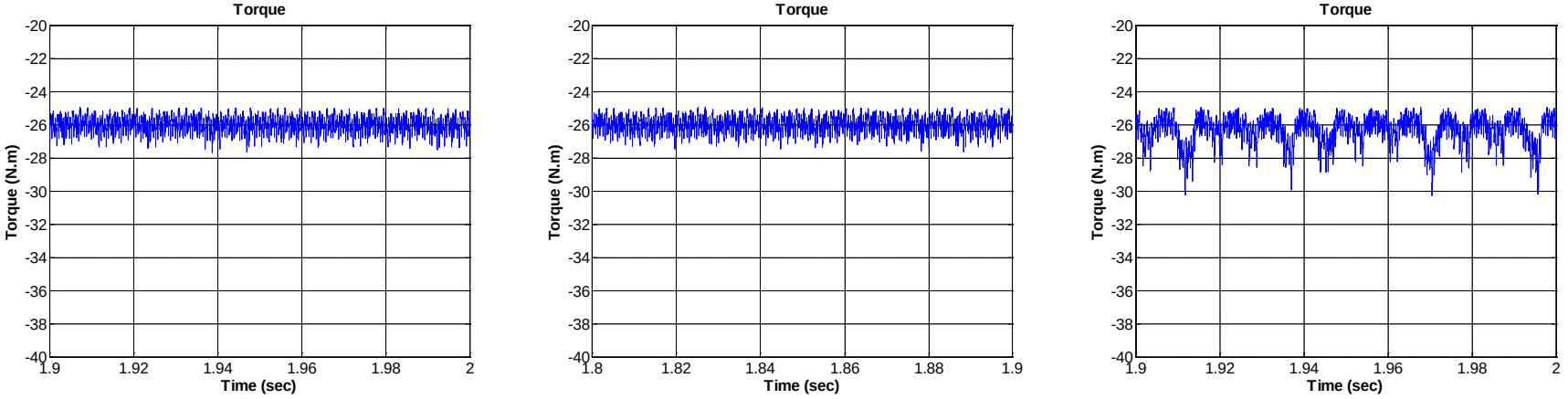


(a) (b) (c)

Figure 3. 26: Electromagnetic torque of PM generator of Case 3

(a) with proposed control ; (b) with standard d-q method; (c) with standard indirect current method.

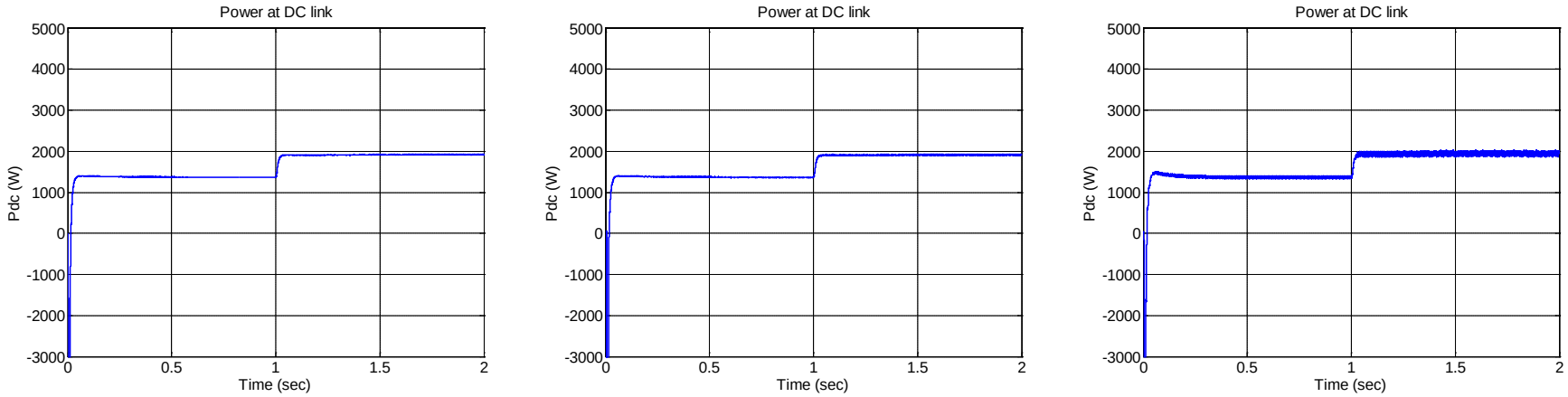


(a) (b) (c)

Figure 3. 27: DC link power of Case 3:
(a) with proposed control; (b) with standard d-q method; (c) with standard indirect current method.



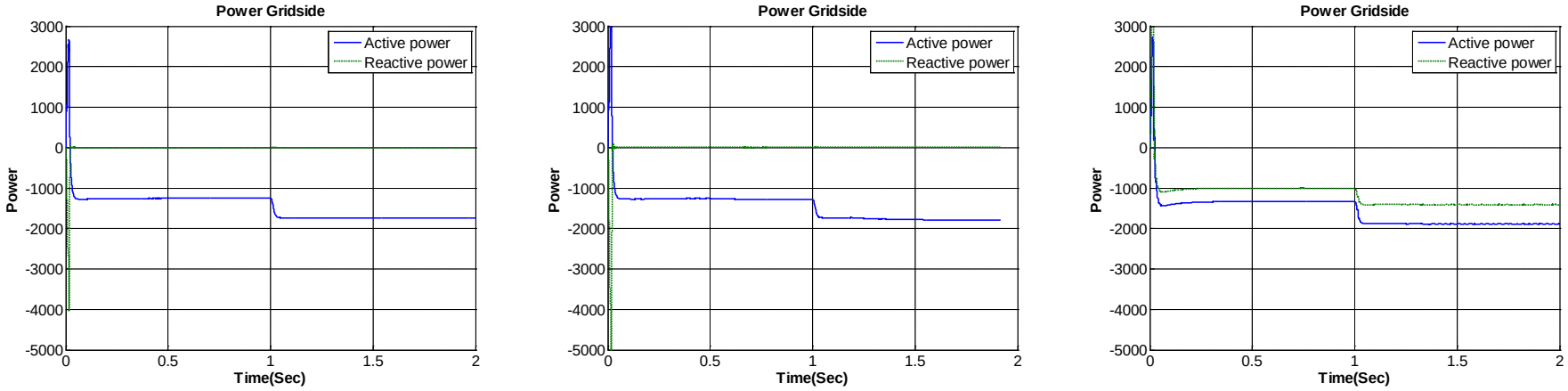


(a) (b) (c)

Figure 3. 28: Average output active and reactive power of Case 3:
(a) with proposed control; (b) with standard d-q method; (c) with standard indirect current method.

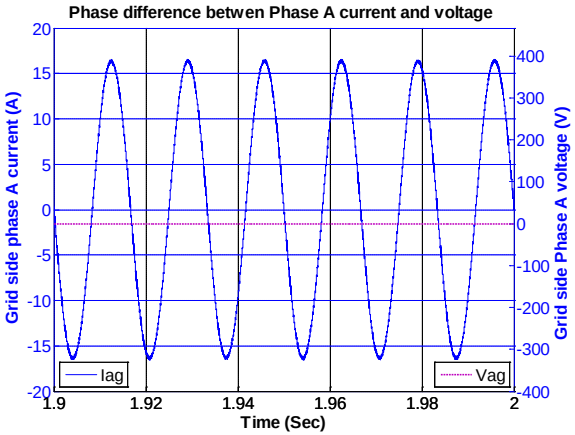


(a)

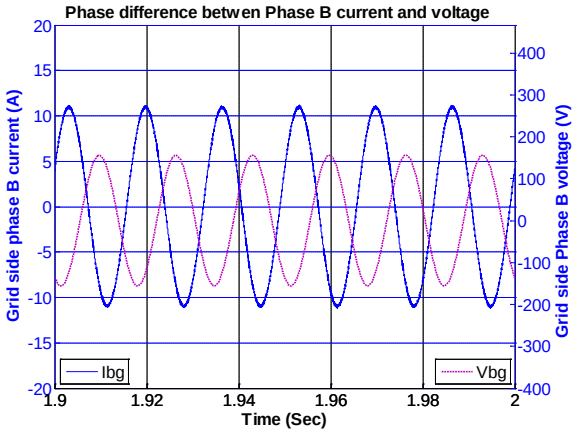


(b)

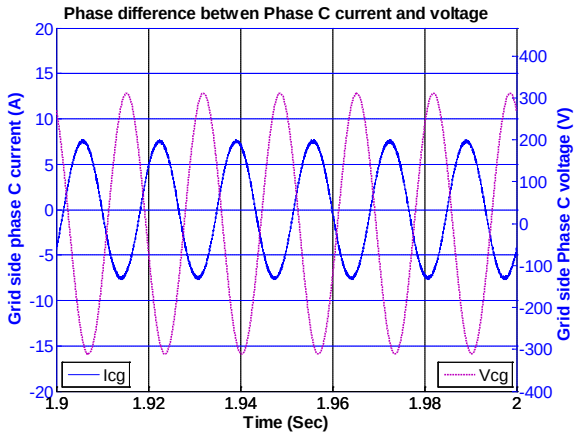


(c)

Figure 3. 29: Phase-currents with voltages for Case 3 with proposed method
(a) Phase A; (b) Phase B; (c) Phase C

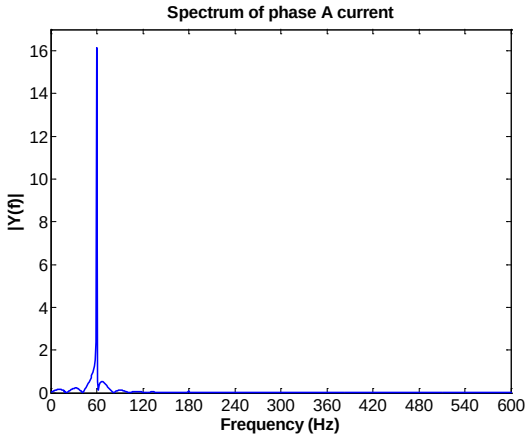


(a)

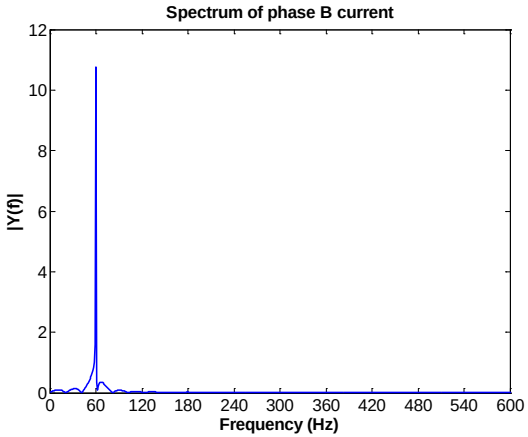


(b)

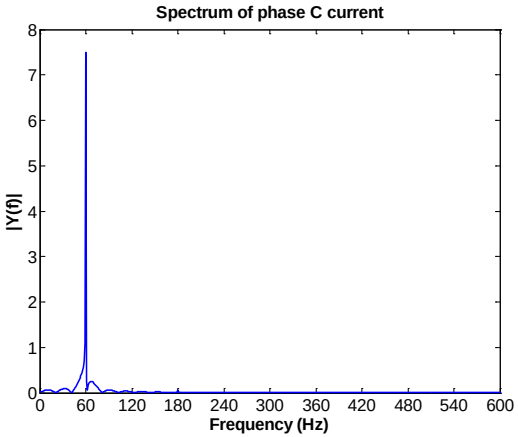


(c)

Figure 3. 30: Spectrums of grid currents for Case 3 with proposed method
(b) Phase A; (b) Phase B; (c) Phase C

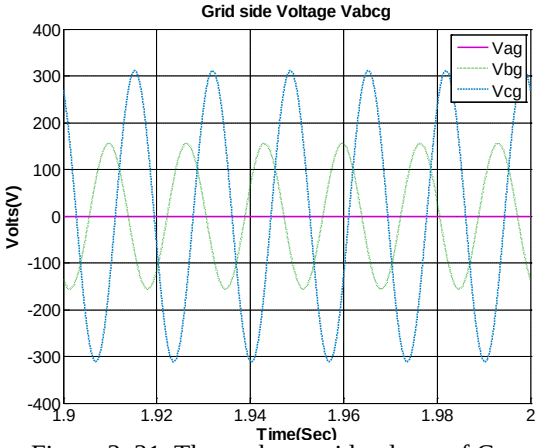


Figure 3. 31: Three-phase grid voltage of Case 4



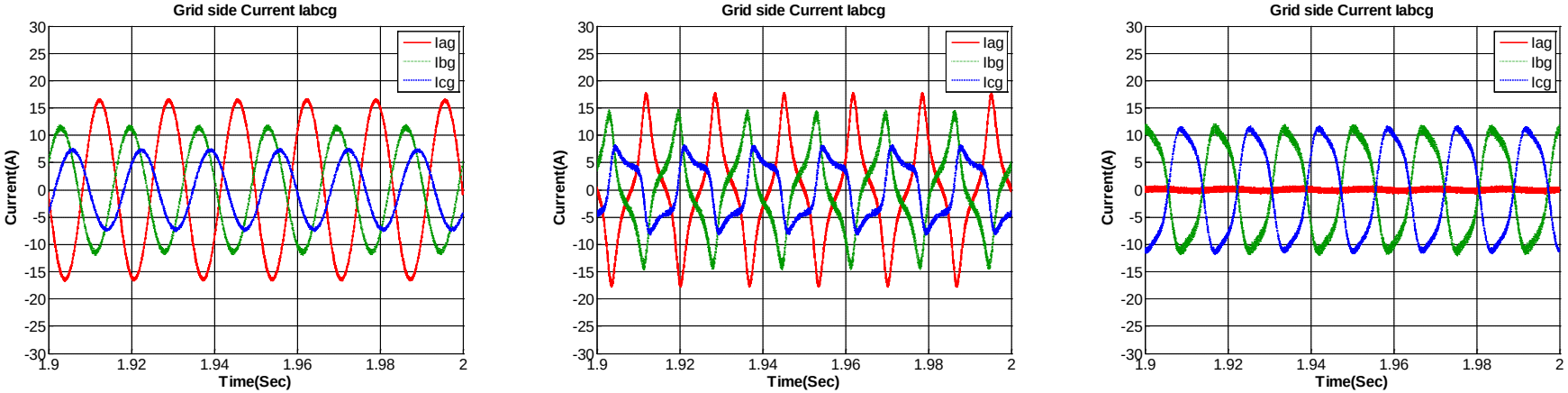


(a) (b) (c)

Figure 3. 32: Three-phase grid currents of Case 4
(a)Proposed control; (b) Standard d-q method; (c) Standard indirect current method

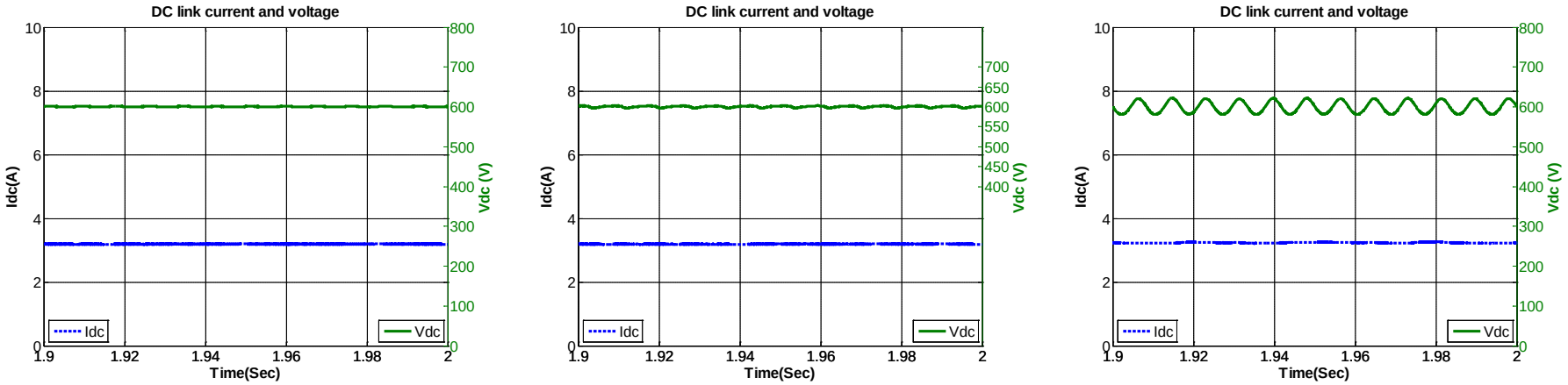


(a) (b) (c)

Figure 3. 33: DC link current and voltage of Case 4

(a) Proposed control; (b) Standard d-q method; (c) Standard indirect current method.



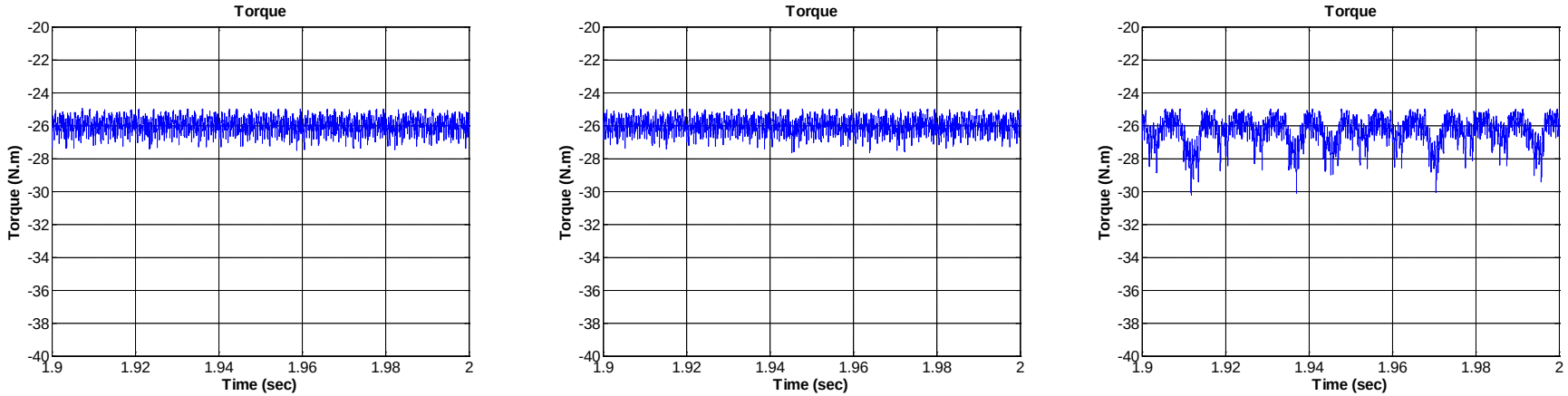


(a) (b) (c)

Figure 3. 34: Electromagnetic torque of PM generator of Case 4

(a) Proposed control; (b) Standard d-q method; (c) Standard indirect current method

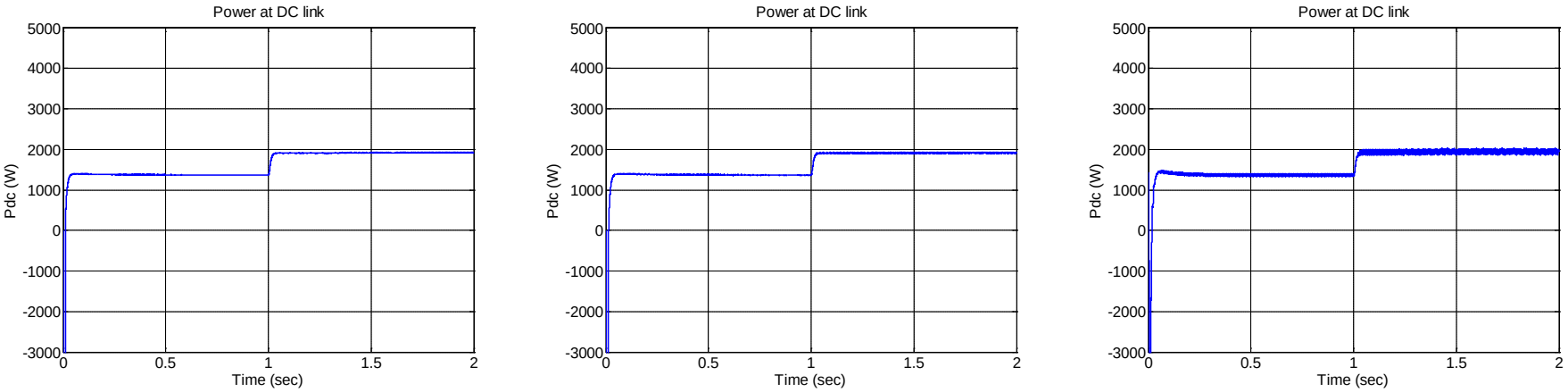


(a) (b) (c)

Figure 3. 35: DC link power of Case 4
(a) Proposed control; (b) Standard d-q method; (c) Standard indirect current method



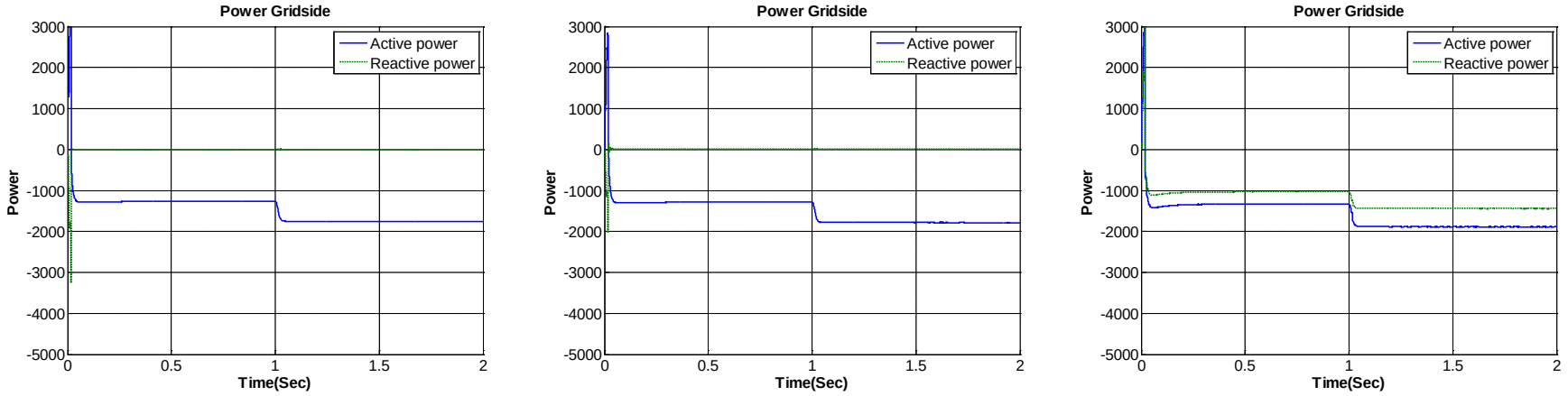


(a) (b) (c)

Figure 3. 36: Average output active and reactive power of Case 4
(a) Proposed control; (b) Standard d-q method; (c) Standard indirect current method

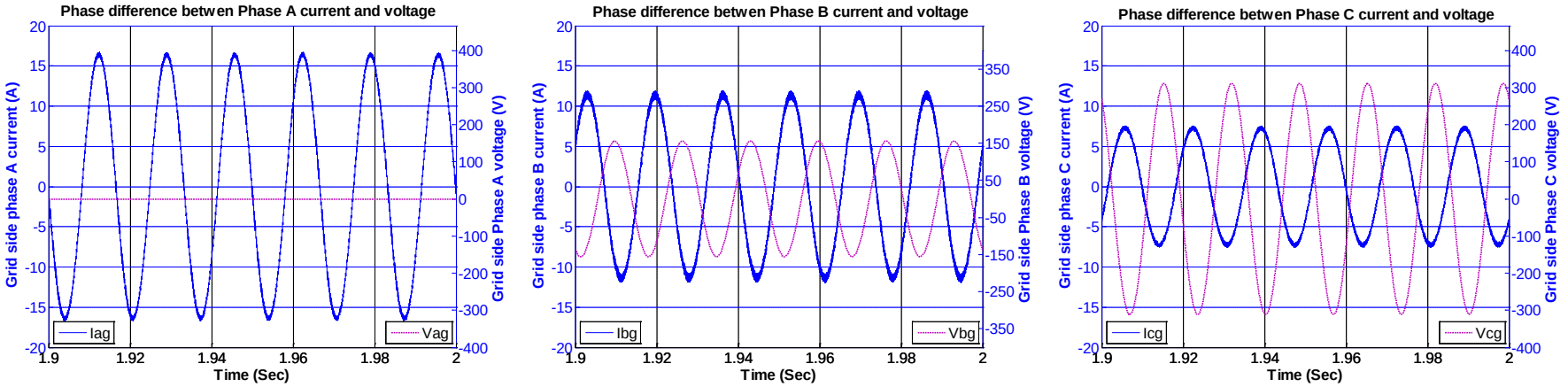


(a) (b) (c)

Figure 3. 37: Phase-currents with voltages for Case 4 with proposed method
(a) Phase A ; (b) Phase B; (c) Phase C



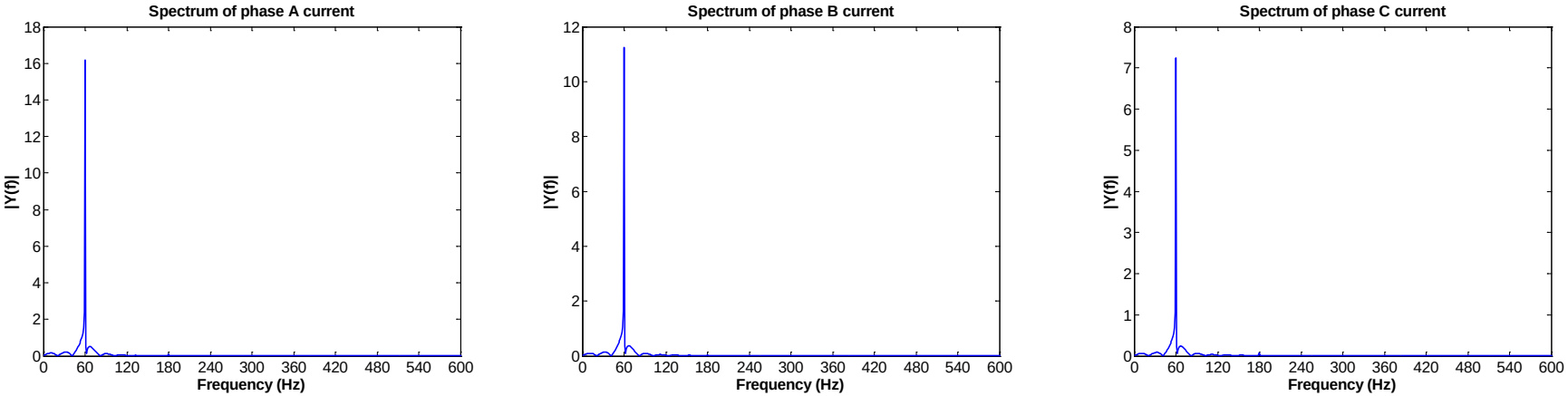


(a) (b) (c)

Figure 3. 38: Spectrums of grid currents for Case 4 with proposed method
(a) Phase A; (b) Phase B; (c) Phase C

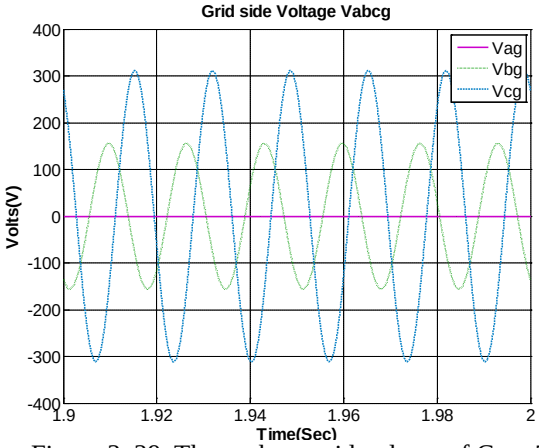


Figure 3. 39: Three-phase grid voltage of Case 5

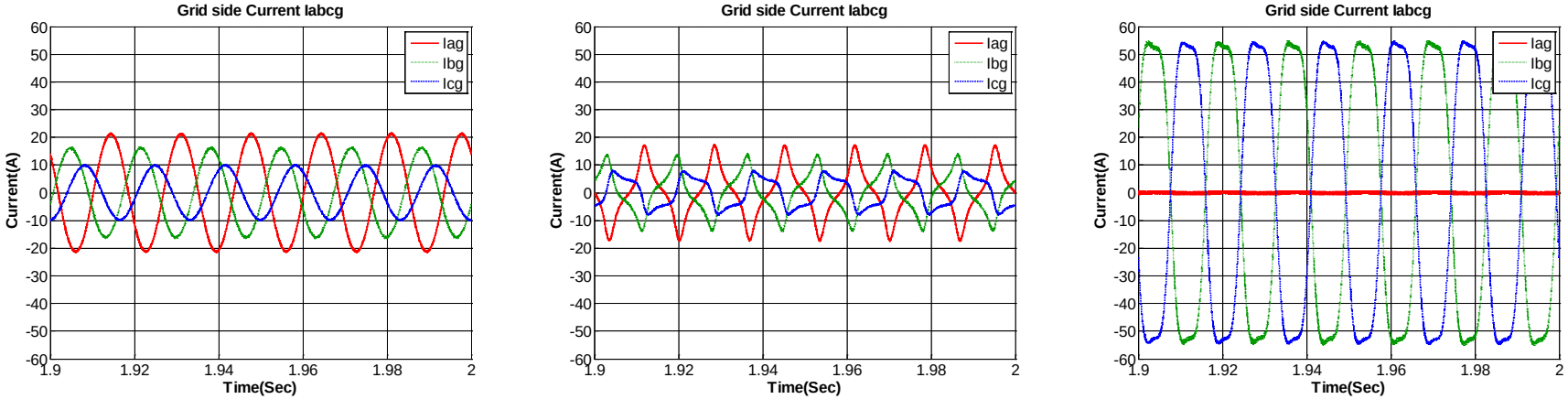


(a) (b) (c)

Figure 3. 40: Three-phase grid currents of Case 5
(a) Proposed control; (b) Standard d-q method; (c) Standard indirect current method

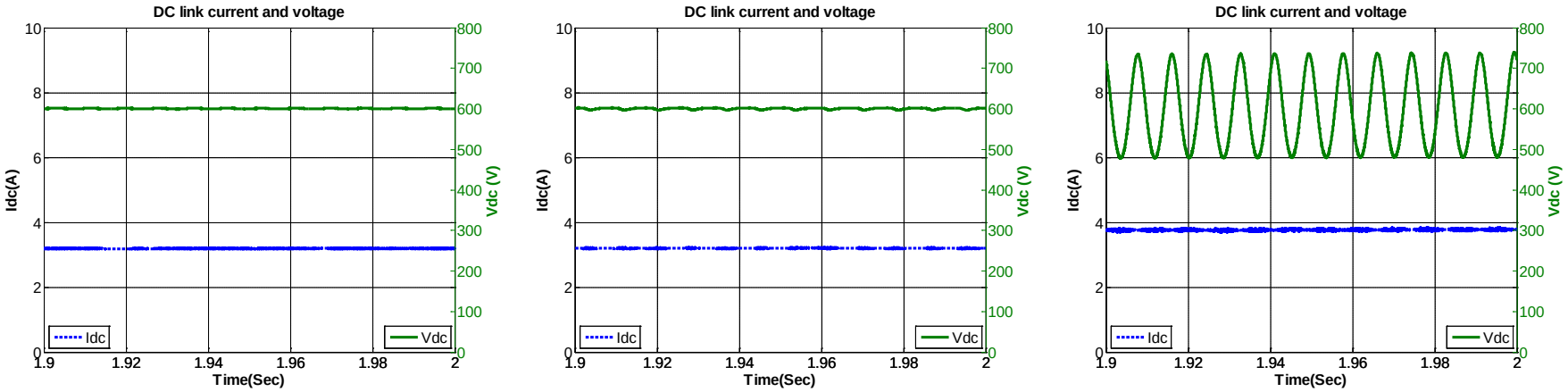


(a) (b) (c)

Figure 3. 41: DC link current and voltage of Case 5
(a) Proposed control; (b) Standard d-q method; (c) Standard indirect current method

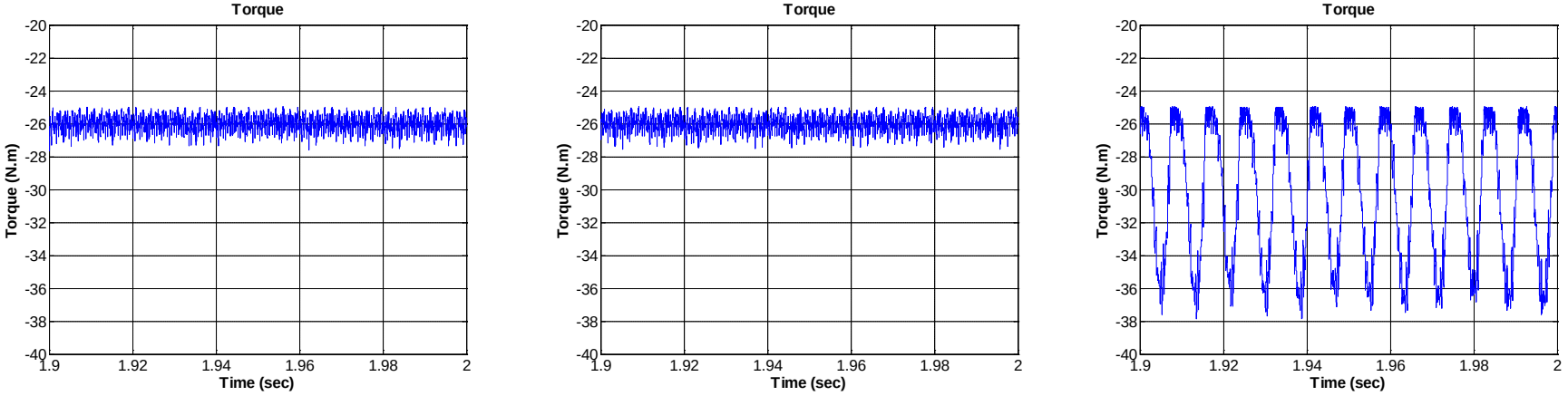


(a) (b) (c)

Figure 3. 42: Electromagnetic torque of PM generator of Case 5
(a) Proposed control; (b) Standard d-q method; (c) Standard indirect current method

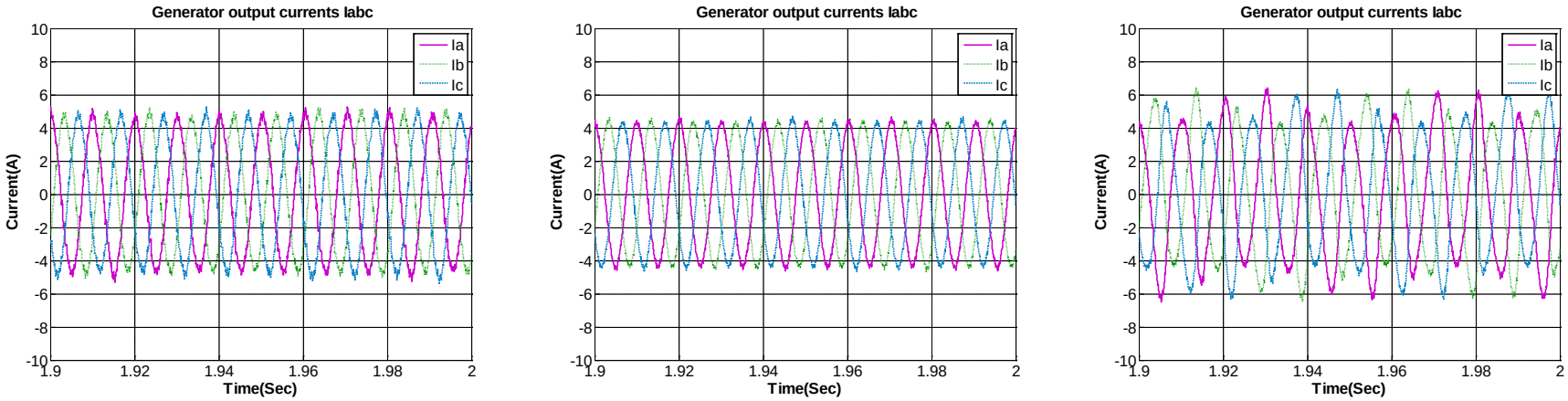


(a) (b) (c)

Figure 3. 43: Generator stator current of Case 5
(a) Proposed control; (b) Standard d-q method; (c) Standard indirect current method

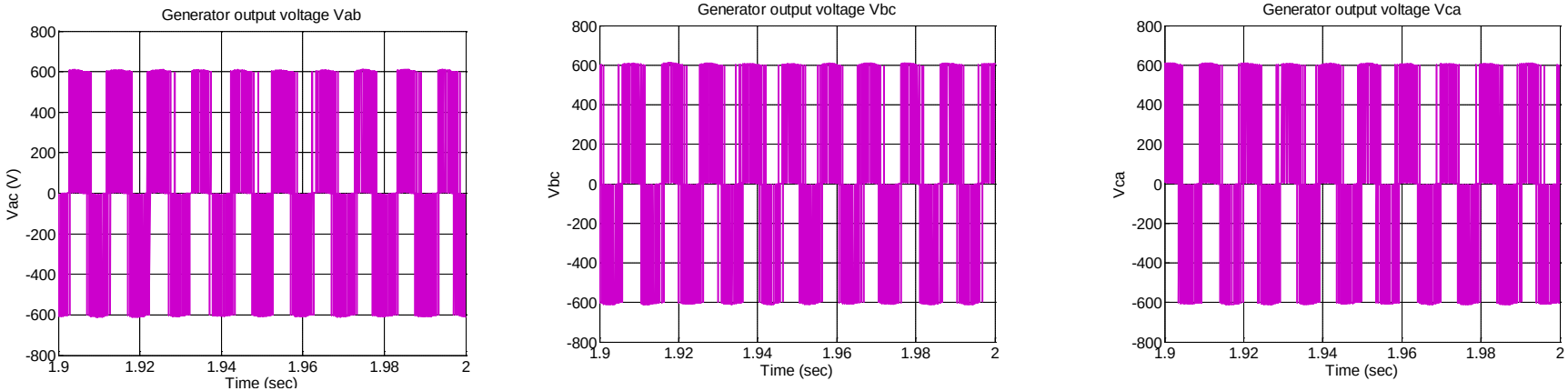


(a) (b) (c)

Figure 3. 44: Generator output voltages for Case 5 with proposed method
(a) Vab; (b) Vbc; (c) Vca

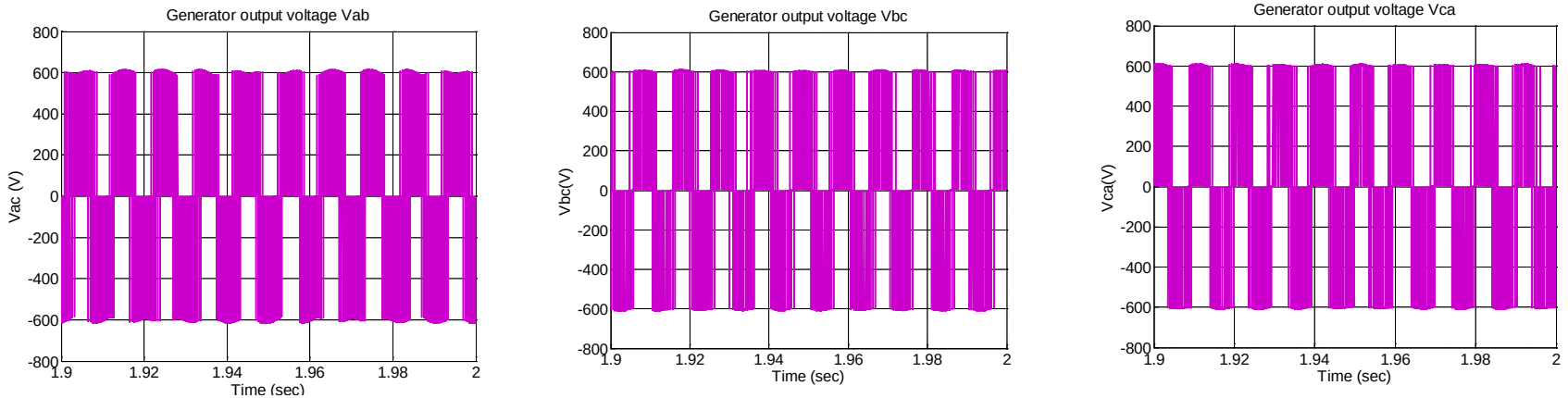


(a) (b) (c)

Figure 3. 45: Generator output voltages for Case 5 with standard d-q method
(a) Vab; (b) Vbc; (c) Vca



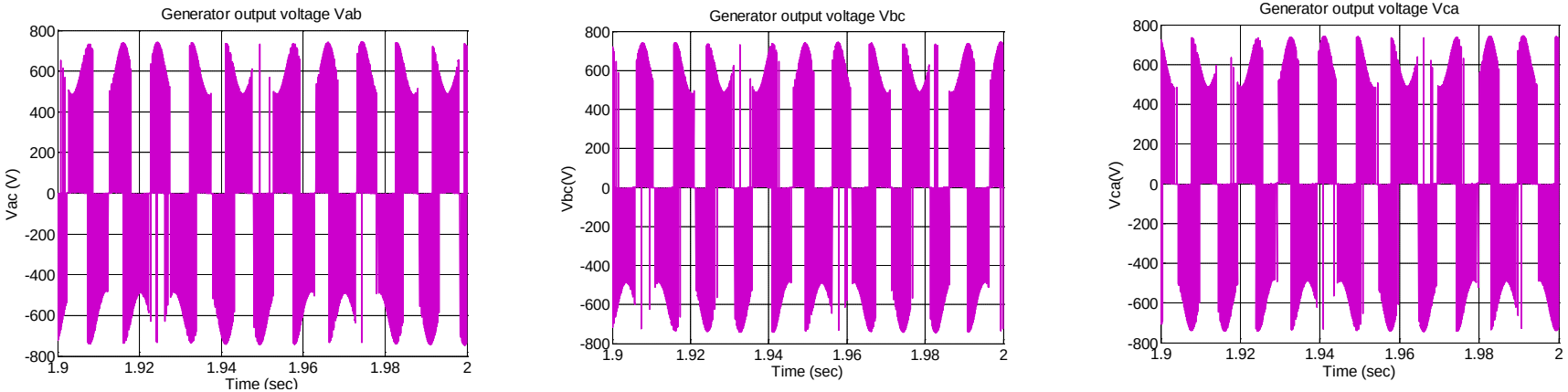


(a) (b) (c)

Figure 3. 46: Generator output voltages for Case 5 with standard indirect current method
(a) Vab; (b) Vbc; (c) Vca

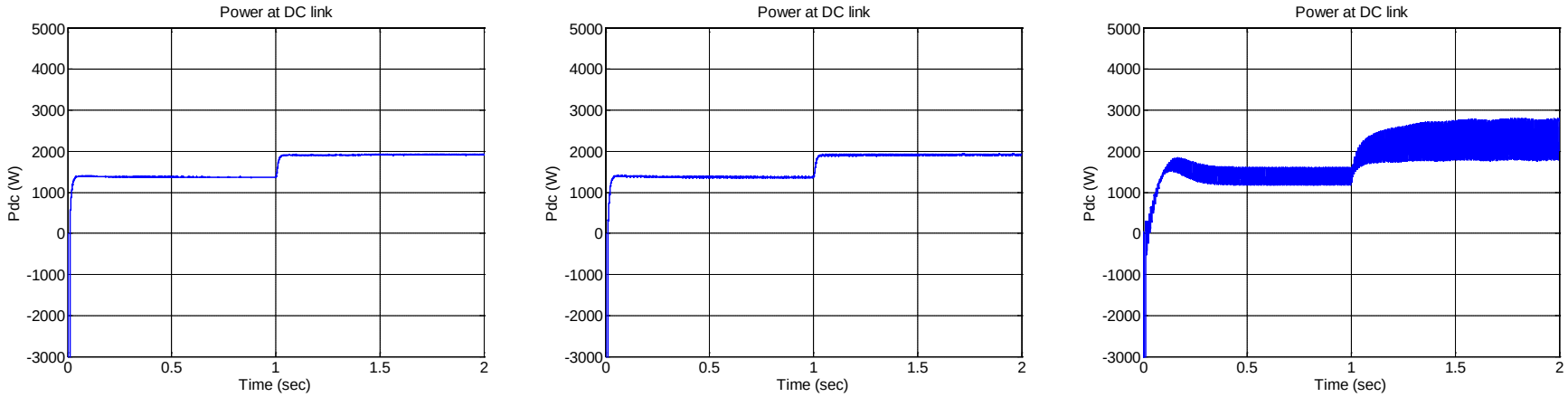


Figure 3. 47: DC link power of Case 5

(a) Proposed control; (b) Standard d-q method; (c) Standard indirect current method



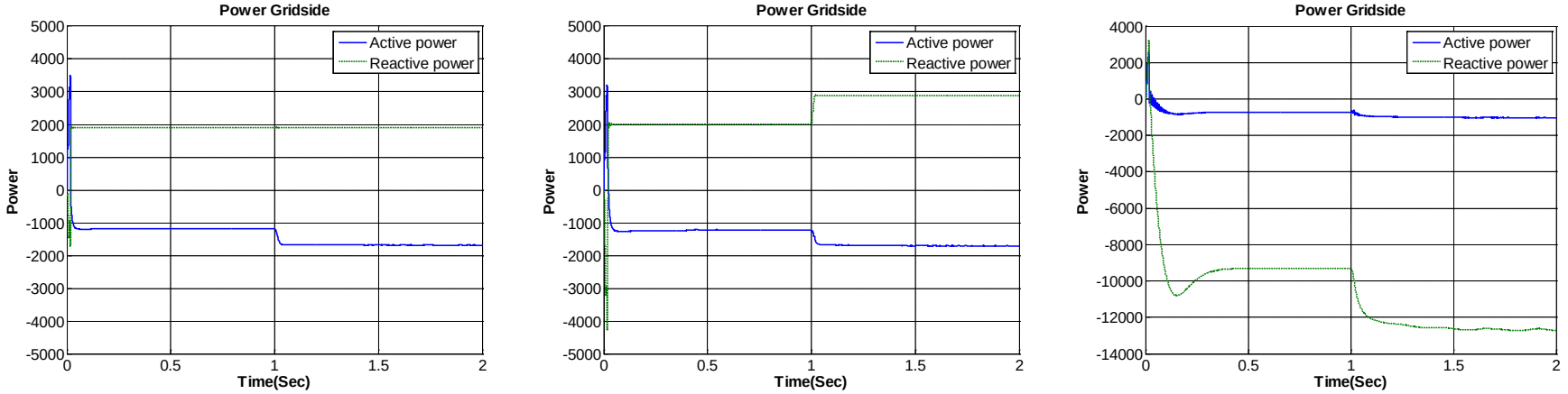


Figure 3. 48: Average output active and reactive power of Case5

(a) Proposed control; (b) Standard d-q method; (c) Standard indirect current method

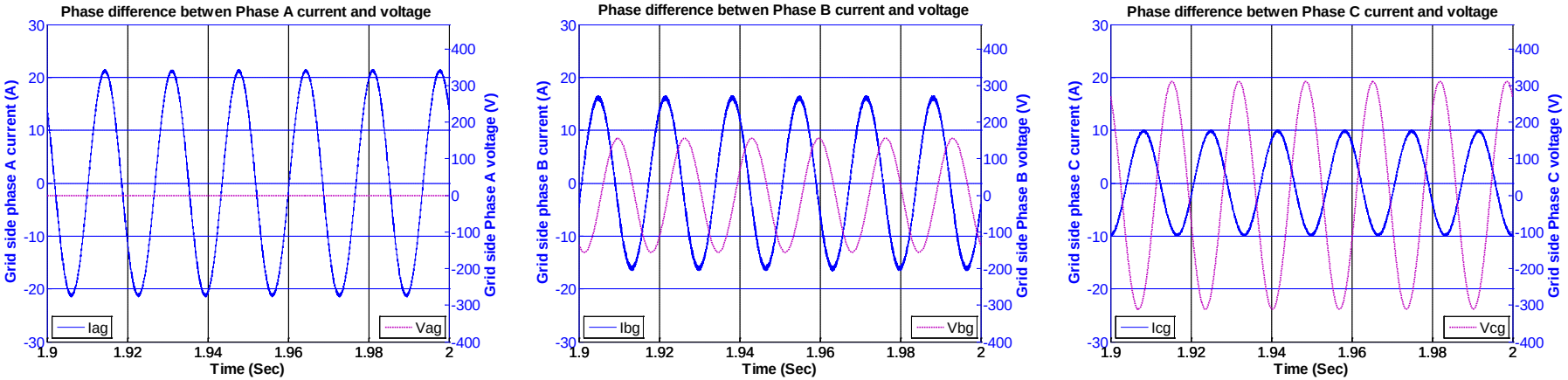


Figure 3. 49: Phase-currents with voltages for Case 5 with proposed method
(a) Phase A ; (b) Phase B; (c) Phase C



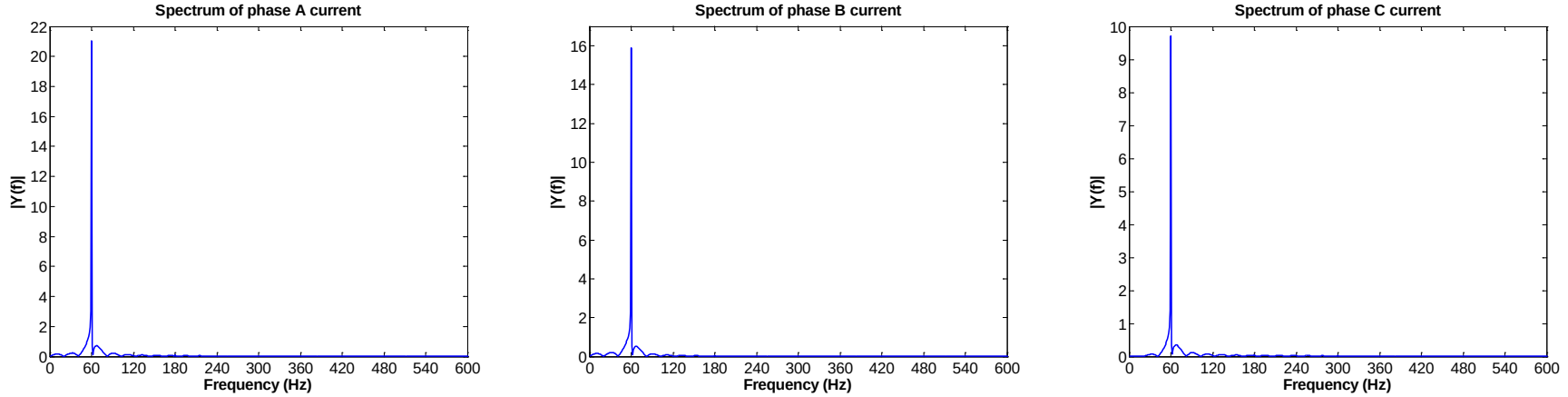


Figure 3. 50: Spectrums of grid currents for Case 5 with proposed method
(a) Phase A; (b) Phase B; (c) Phase C

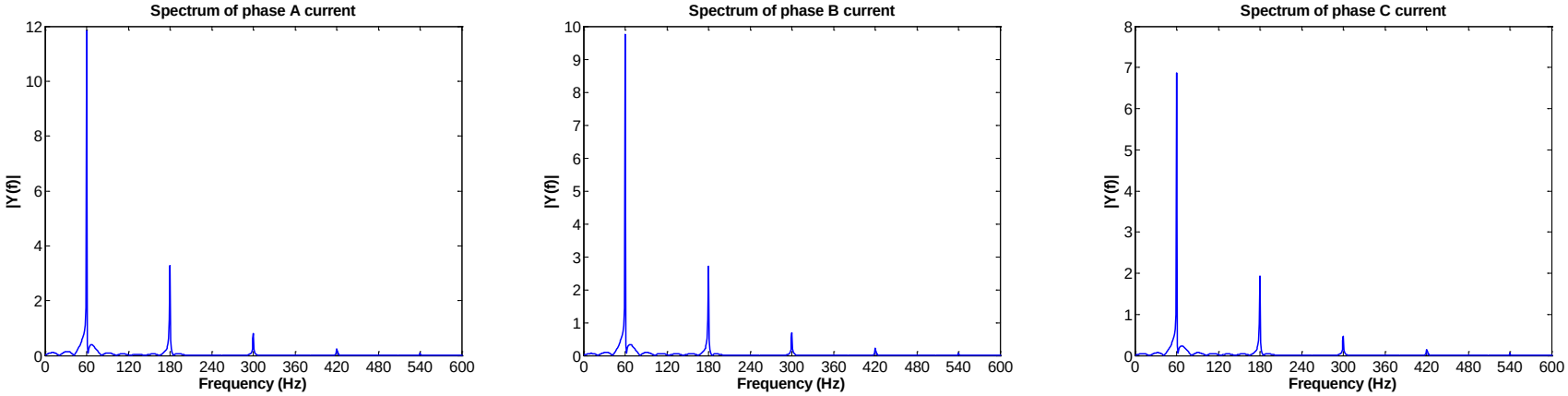


Figure 3. 51: Spectrums of grid currents for Case 5 with traditional d-q method
(a) Phase A; (b) Phase B; (c) Phase C



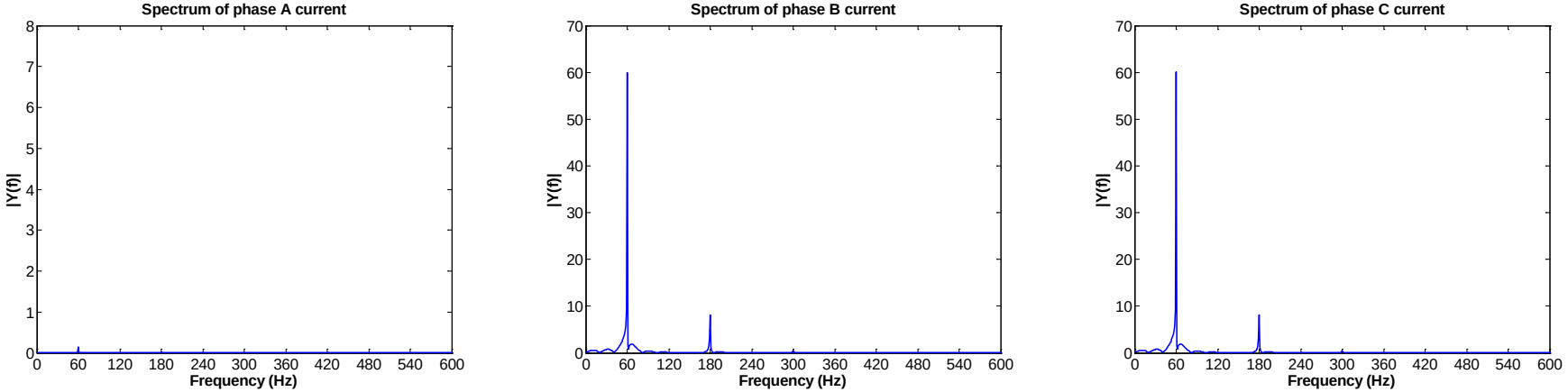


Figure 3. 52: Spectrums of grid currents for Case 5 with traditional d-q method
(a) Phase A; (b) Phase B; (c) Phase C

### 3.3 Control Strategy for the wind power system connected with a self-excited squirrel cage induction generator

The operation of the proposed wind power system with a self-excited squirrel cage induction generator with the schemes of wind power optimal acquisition and harmonic elimination control is simulated using the MATLAB Simulink SimPowerSystem tool box.

The overall systems circuit diagram is show in figure 3.65

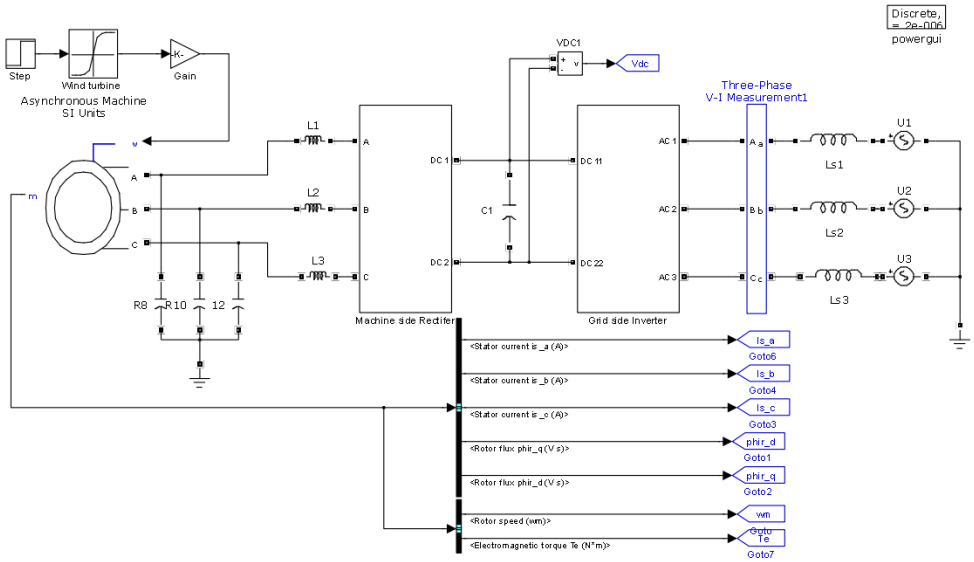


Figure 3. 53: Diagram of a squirrel cage induction generator connected by two PWM converters to the grid for variable wind speed application

#### 3.3.1 Control of the machine side rectifier for a squirrel-cage induction generator

Similar to the purpose of the control of a permanent magnet generator, the control of the squirrel-cage induction generator is to achieve the optimal performance. The optimal desired torque is stored in a look-up table with the wind speed and generator rotor speed as the indexes. A control system with a close loop torque and a

close loop of flux is shown in Figure 3.66.

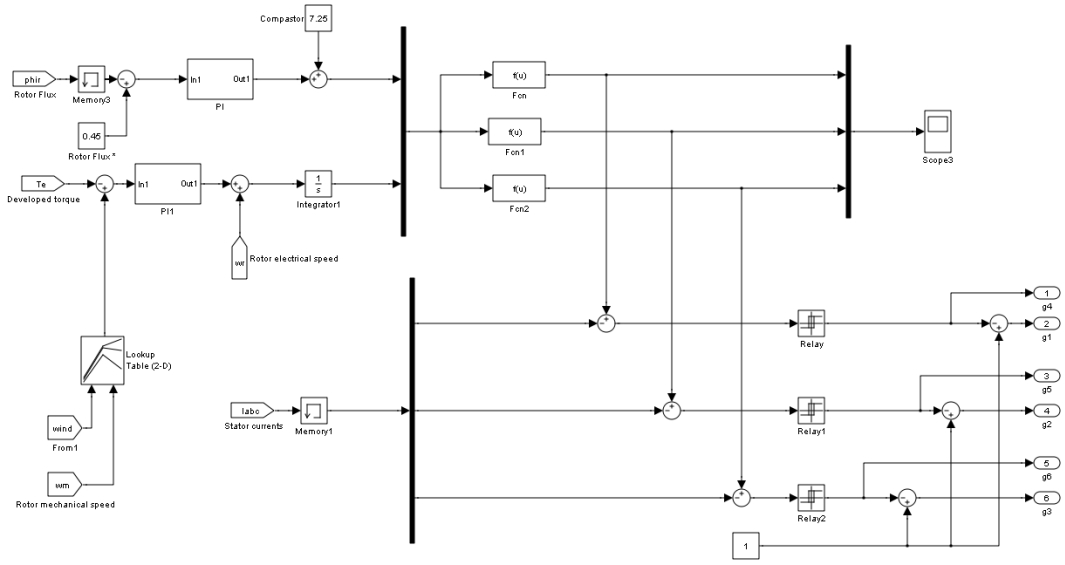


Figure 3. 54: The control system of the machine side rectifier for the squirrel cage induction generator

Instead of controlling the rectifier input voltage, three phase stator currents are controlled, since the torque and flux of the machine are directly proportional to the currents. In figure 3.66, the flux control loop generates the stator current magnitude and the torque control loop generates the stator current frequency. A hysteresis controller is used to make the machine stator currents track the reference currents so the torque can be controlled to follow the optimal value when the wind speed changes and the rotor flux is kept constant.

Since the induction machine can work as an induction generator only in a certain slip range, the generator rotor is coupled with the turbine via a gearbox. In the simulation, the rotor speed of the generator is 200 rad/s and is changed to 190 rad/s at 1.3 second.

In the simulation, the torque is controlled to be -10N.m and changed to -8N.m at 1.3 sec corresponding to the rotor speed. The rotor flux is always controlled at 0.46H.

In the circuit, three capacitors with a capacitance value of 60 μF are connected at the three-phase stator to excite the induction generator with the magnetizing current.

### 3.3.2 Control of the grid side voltage-fed inverter for the wind power system connected with an induction generator

The control of the grid side inverter for the wind power system connected with an induction generator is similar to the one with permanent-magnet generator. But during the time when the voltage is building up, the DC link is connected to a pure resistive load rather than the grid. Once the DC link voltage reaches 600 V, it is connected to the grid via the grid side inverter and the resistive load is disconnected. Two controllable switches are used in the simulation shown in figure 3.67. The DC link voltage is controlled constantly at 625 V.

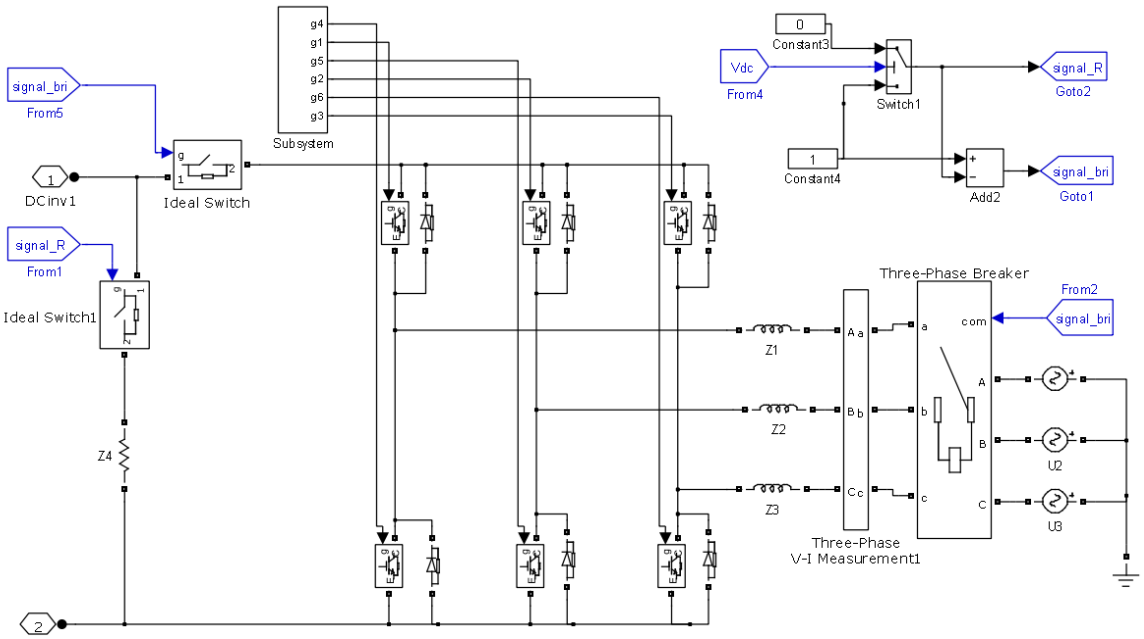


Figure 3. 55: Grid side inverter for the wind power system with a squirrel cage IG.

Five different simulation cases are selected to verify the optimal power acquisition in the machine side and the harmonic elimination in the gird side under unbalanced grid voltage operation. Comparison cases are provided with standard indirect current control in a-b-c frame and power control in d-q rotating frame. Table 3.4 lists the parameters of the squirrel cage induction generator used in the simulation; Table 3.5 lists the parameters of the DC link and the converters. Table 3.6 lists the simulation cases.

Table 3. 4: Parameters used for the squirrel cage induction generator used in the simulation

| | |
|---|---|
| **Stator phase resistance Rs** | 1.115 ohm |
| **Stator inductance** | 0.005974 H |
| **Rotor resitance Rr** | 1.083 ohm |
| **Rotor inductance** | 0.005974 H |
| **Poles** | 4 |
| **Mutual inductanc Lm** | 0.2037 H |
| **Power Rating** | 3730 W |
| **Rated Voltage** | 460 V |
| **Rated Speed** | 1750 rpm |
| **Self excited capacitance C3** | 60 μF×3 |

Table 3. 5: Parameters of the DC link and converters for the wind power system with squirrel cage induction generator

| **Parameter** | **Value** | **Parameter** | **Value** |
|---|---|---|---|
| f | 60Hz | Hysteresis band | 0.02A |
| C | 300 μF | Switch on resistance | 0.5 Ω |
| Ls | 1mL | Sampling time | 0.02ms |
| IGBT forward voltage | 1V | Diode forward voltage | 1.5V |

Table 3. 6: Simulation cases for the wind power system with squirrel cage induction generator

| **Case** | **Grid side voltage** | **Line impedance** | **Power factor** |
|---|---|---|---|
| 6 | $U_a$=220∠0, $U_b$ =220∠-120, $U_c$ =220∠120. | $L_1 = L_2 = L_3 =$ 5mL | 1 |
| 7 | $U_a$=110∠0, $U_b$ =160∠-120, $U_c$ =220∠120. | $L_1 = L_2 = L_3 =$ 5mL | 1 |
| 8 | $U_a$=0∠0, $U_b$ =110∠-120, $U_c$ =220∠120. | $L_1 = L_2 = L_3 =$ 5mL | 1 |
| 9 | $U_a$=0∠0, $U_b$ =110∠-120, $U_c$ =220∠120. | $L_1 = L_3$ = 5mL ; $L_2$ =2mL | 1 |
| 10 | $U_a$=0∠0, $U_b$ =110∠-120, $U_c$ =220∠120. | $L_1 = L_3$ = 5mL ; $L_2$ =2mL | 0.7 lagging |

### 3.4 Simulation results of the wind power system with the squirrel cage induction generator

At about 0.34s, the voltage from the induction generator is built up and the rectifier output voltage reaches 600V. The DC link is connected to the grid and begins to transfer the power from the generator to the grid. At 1.3s, the wind speed changes and the power from the generator decreases; so does the power absorbed by the grid. Figure 3.68 shows generator rotor speed and electromagnetic torque. Figure 3.69 shows the generator rotor flux. Figure 3.70 shows the grid side phase A current. Figure 3.71 shows the DC link voltage. Figure 3.72 shows the average power of the grid.

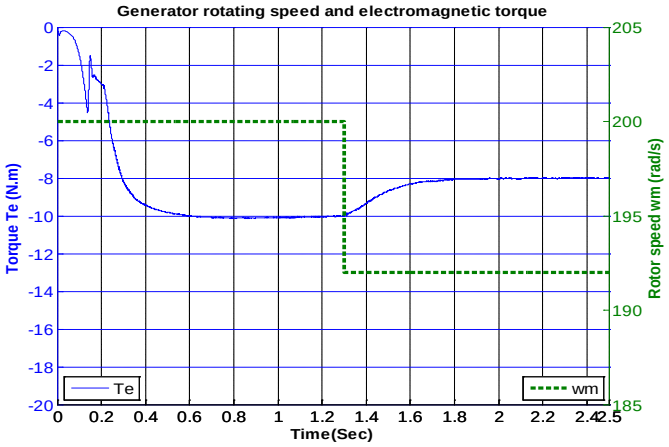


Figure 3. 56: The rotor speed and electromagnetic torque of Case 6 from 0.0s-2.5s

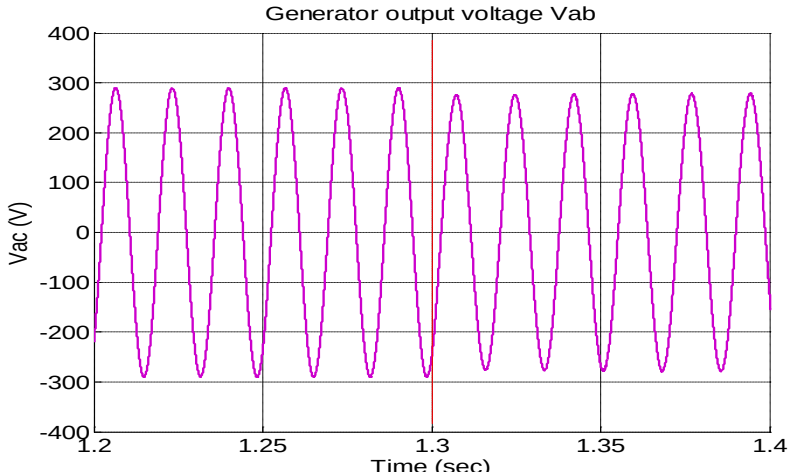


Figure 3. 57: The generator output voltage Vab of Case 6 from 1.2s-1.4s

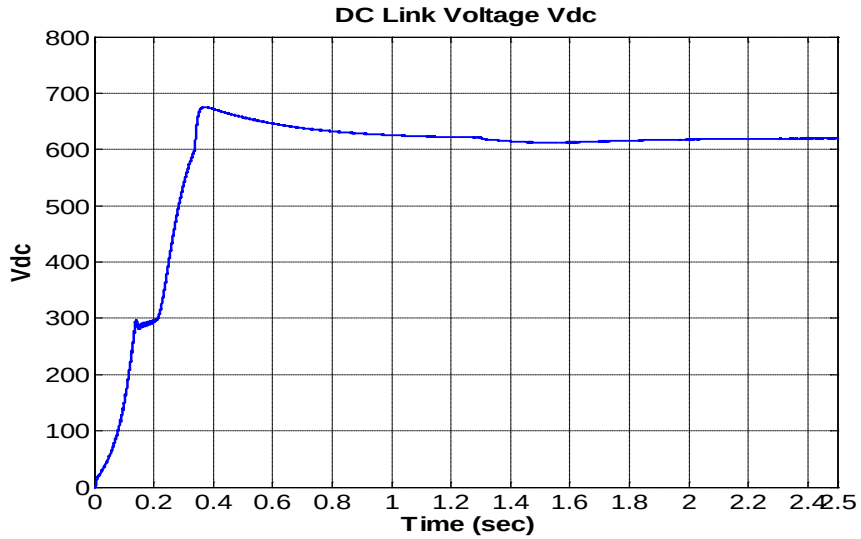

Figure 3. 58: The DC link voltage of Case 6 from 0.0s-2.5s

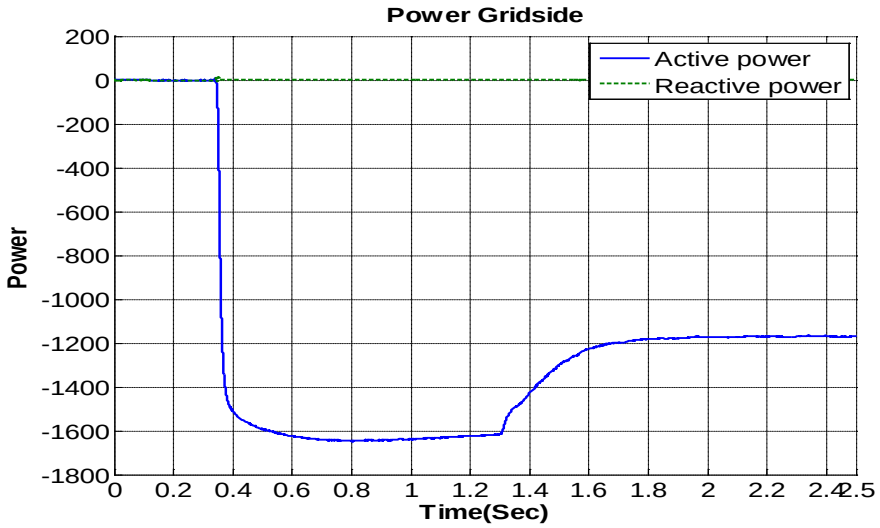

Figure 3. 59: The average power of grid of Case 6 from 0.0s-2.5s

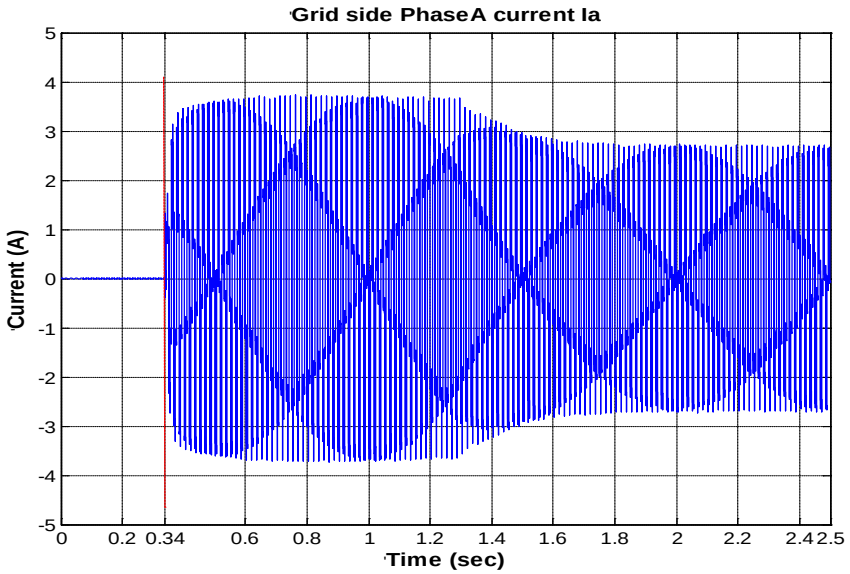

Figure 3. 60: The grid phase A current of Case 6 from 0.0s-2.5s

The simulation results of the grid side voltage, the grid side currents, the DC link voltage, the transfer active and reactive power, the torque and rotor speed of the generator, the rotor flux of the IG and the spectrum of the grid side currents using the three methods are shown below.

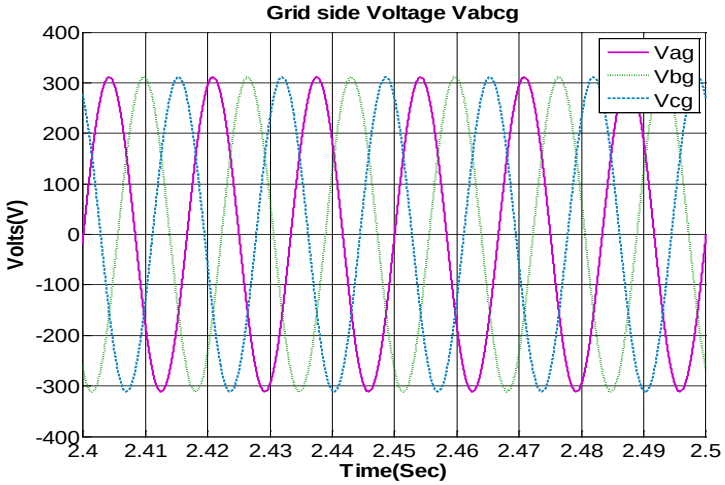


Figure 3. 61: Three-phase balanced grid voltage (phase to ground) of Case 6

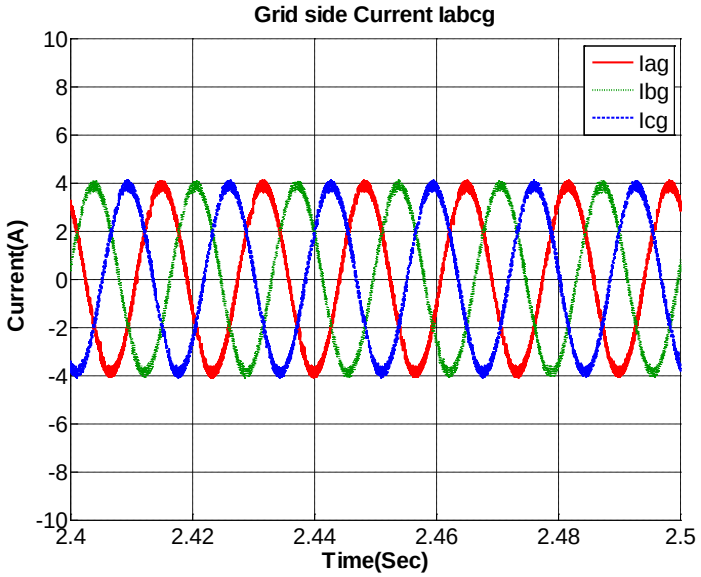


Figure 3. 62: Three-phase balanced grid currents of Case 6 with proposed method

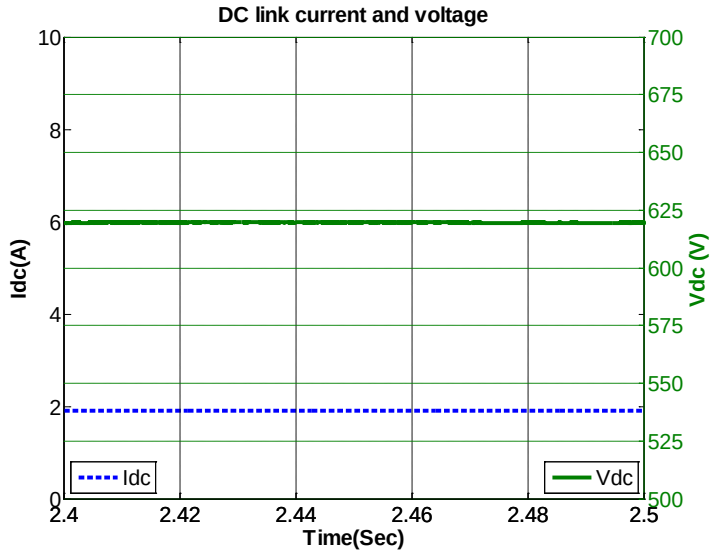


Figure 3. 63: DC link current and voltage of Case 6 with proposed method.

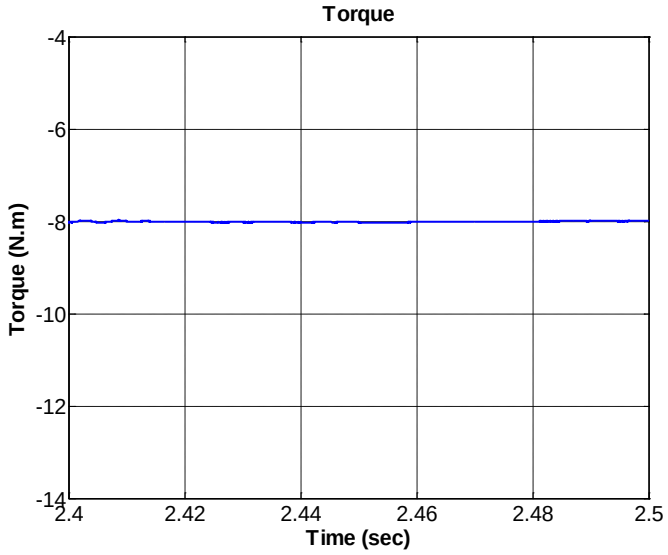


Figure 3. 64: Electromagnetic torque of induction generator of Case 6 with proposed method.

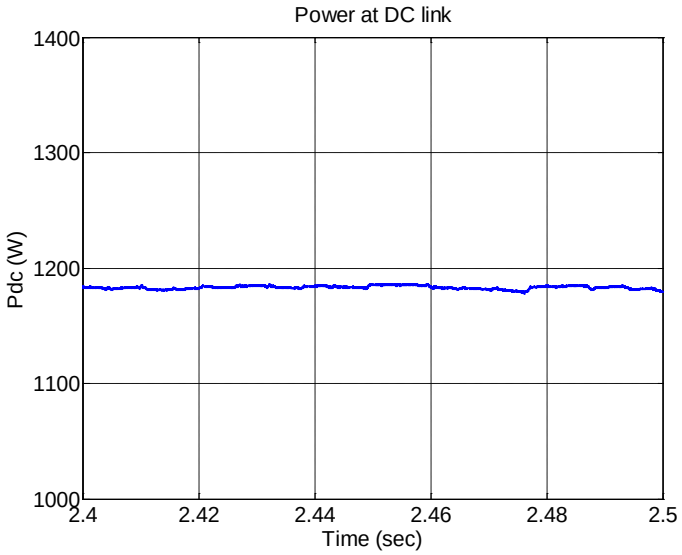


Figure 3. 65: DC link power of Case 6 with proposed method.

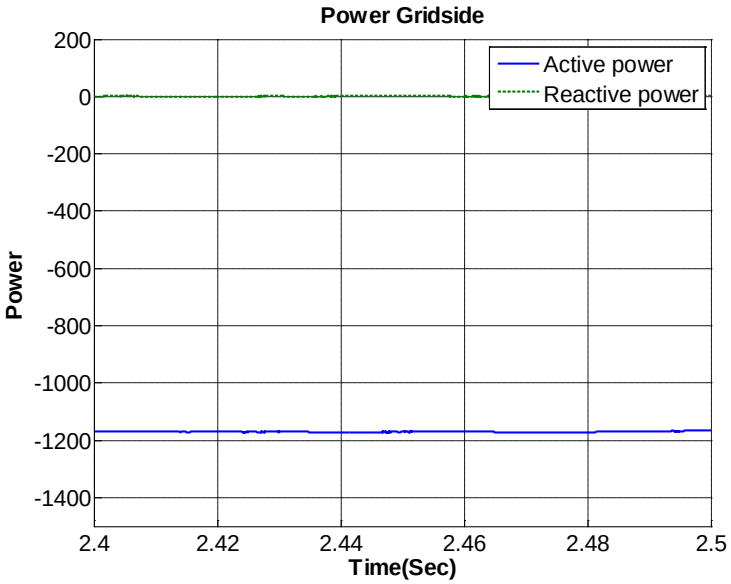

Figure 3. 66: Average grid side power of Case 6 with proposed method.

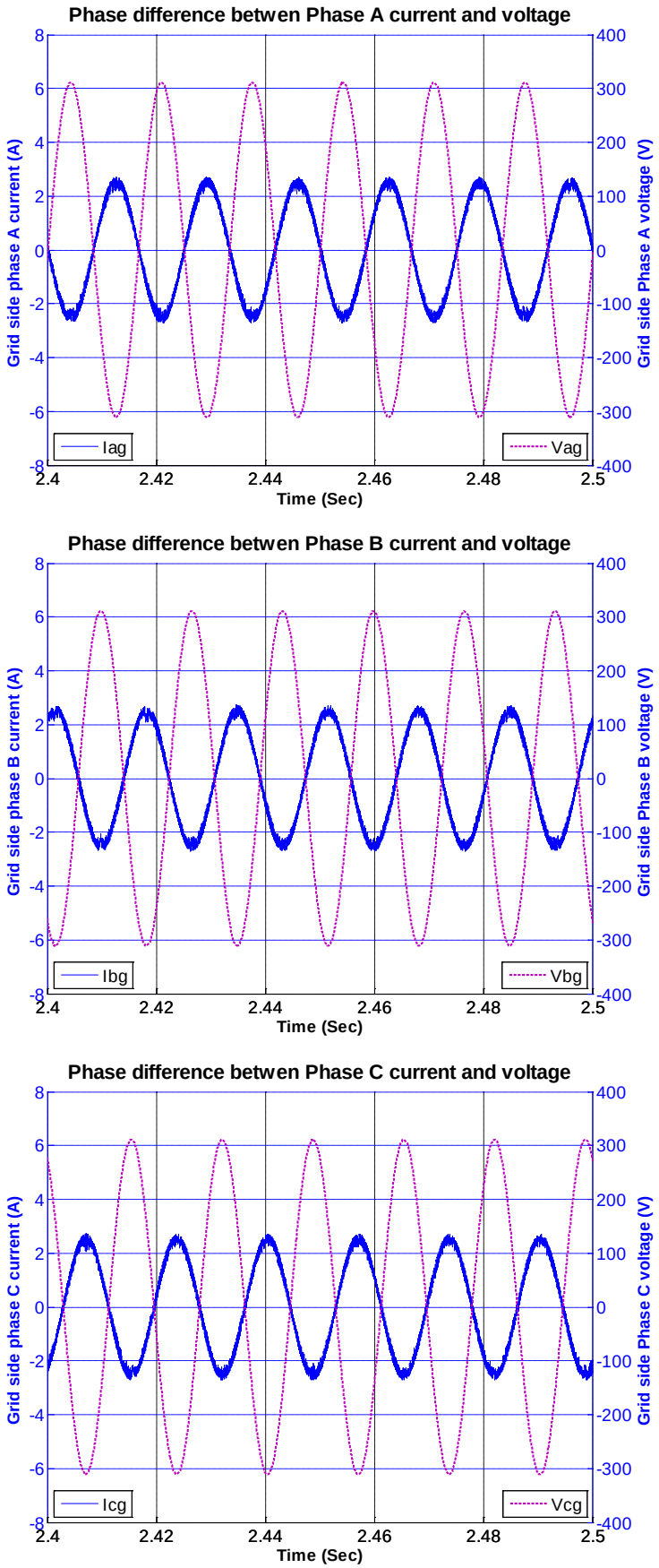


Figure 3. 67: Phase currents with voltages of Case 6 with proposed method.

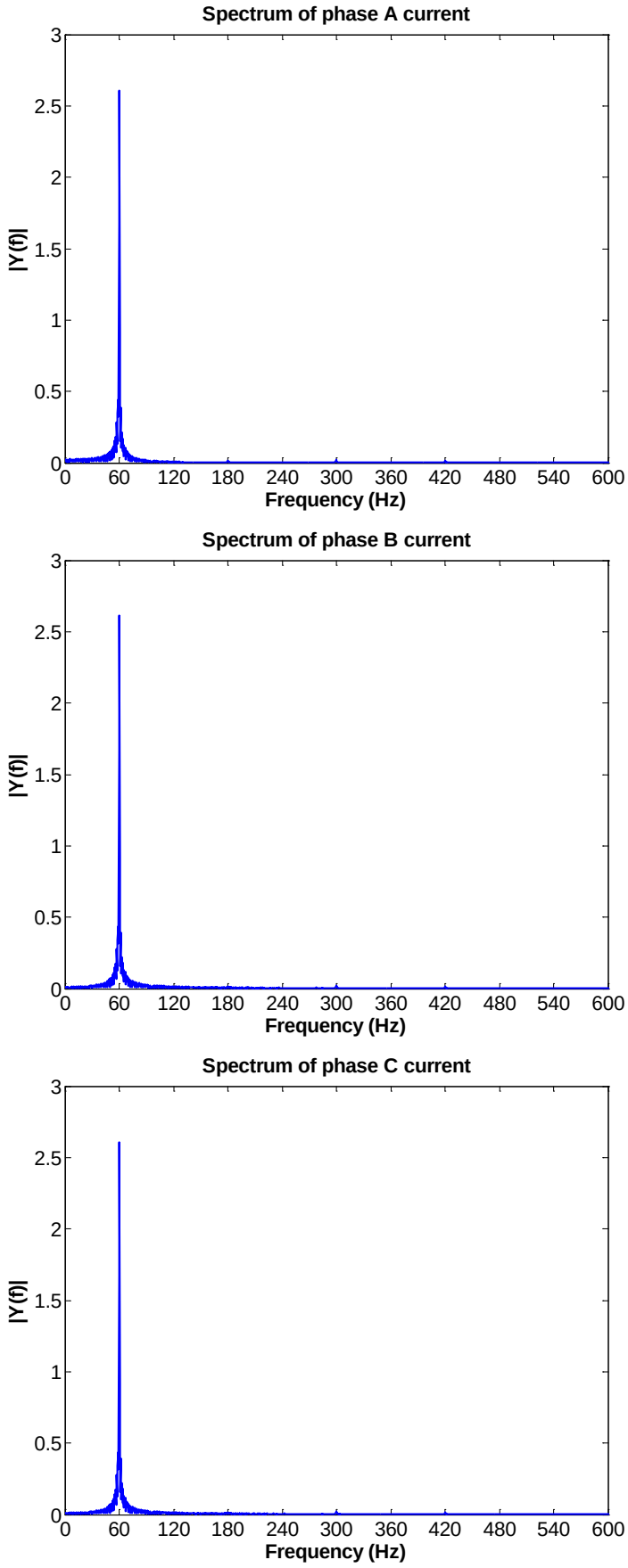


Figure 3. 68: Spectrums of Phase currents of Case 6 with proposed method.

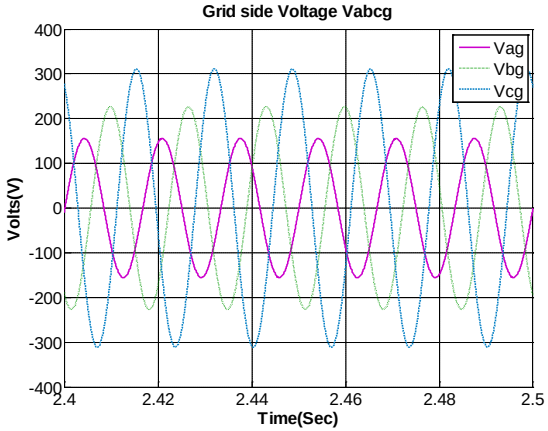


Figure 3. 69: Three-phase grid voltage (phase to ground) for Case 7



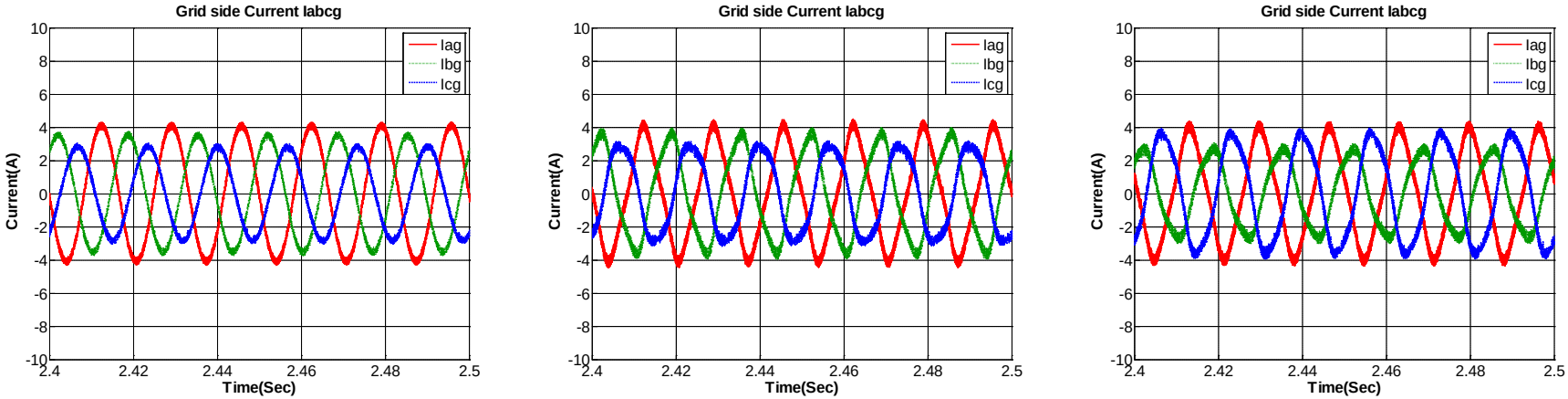


(a) (b) (c)

Figure 3. 70: Three-phase grid currents Case 7

(a) with proposed control; (b) with standard d-q method; (c) with standard indirect current method

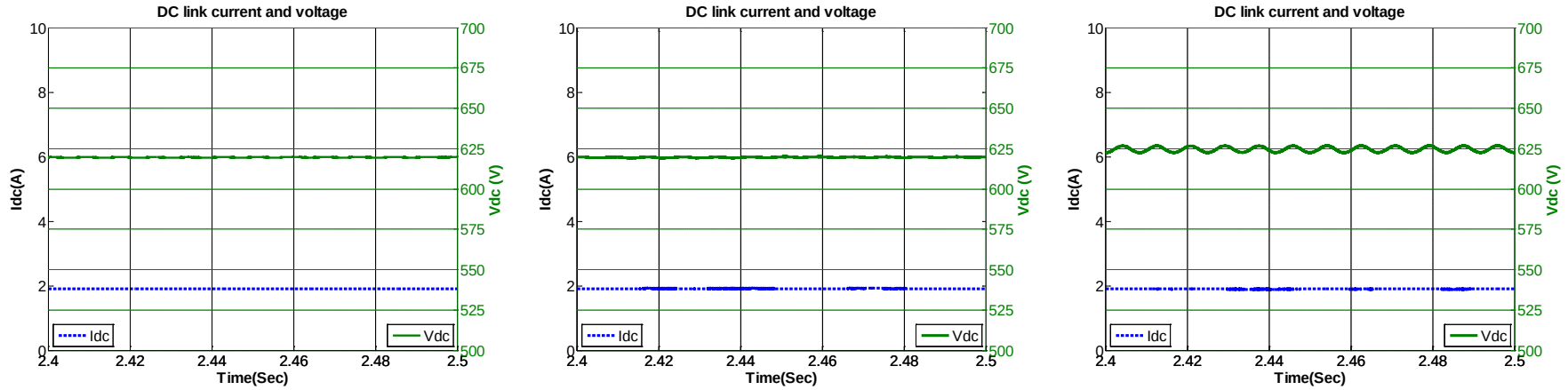


(a) (b) (c)

Figure 3. 71: DC link current and voltage of Case 7

(a) with proposed control; (b) with standard d-q method; (c) with standard indirect current method.

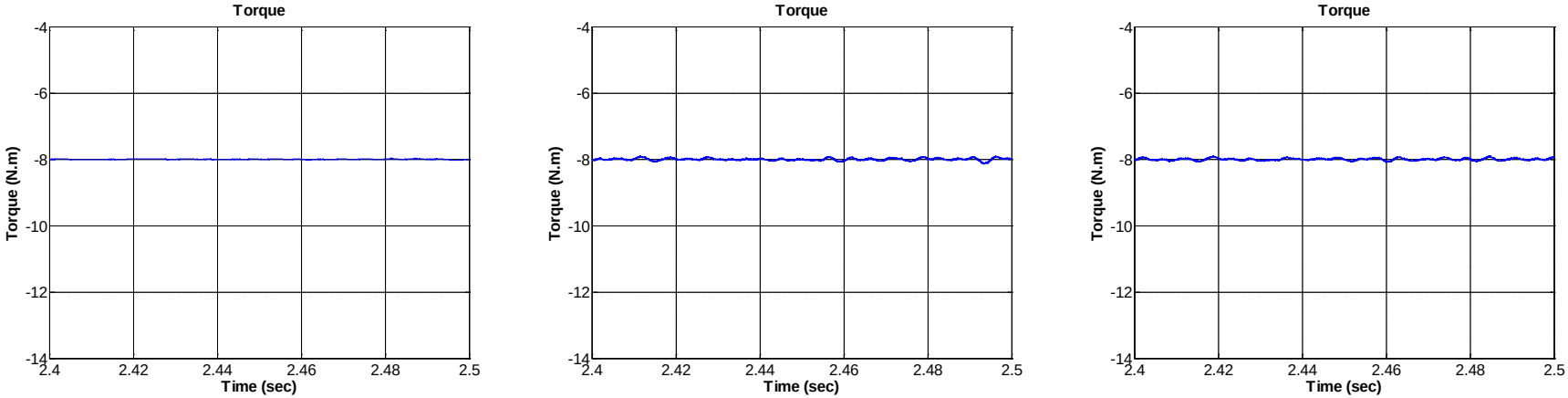


(a) (b) (c)

Figure 3. 72: Electromagnetic torque of induction generator of Case 7

(a) with proposed control ; (b) with standard d-q method; (c) with standard indirect current method.

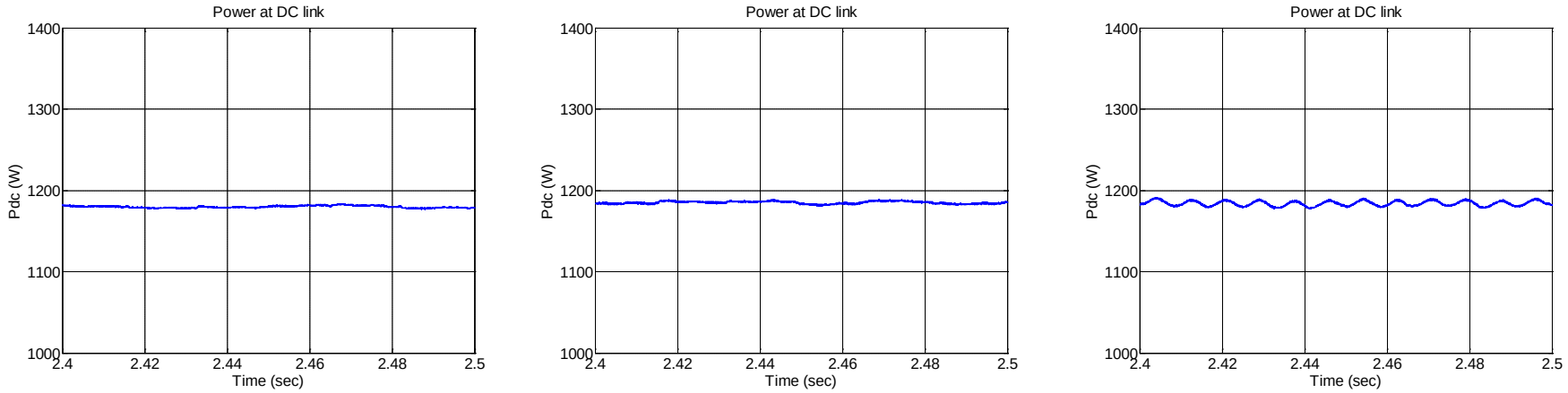


(a) (b) (c)

Figure 3. 73: DC link power of Case 7
(a) with proposed control; (b) with standard d-q method; (c) with standard indirect current method.

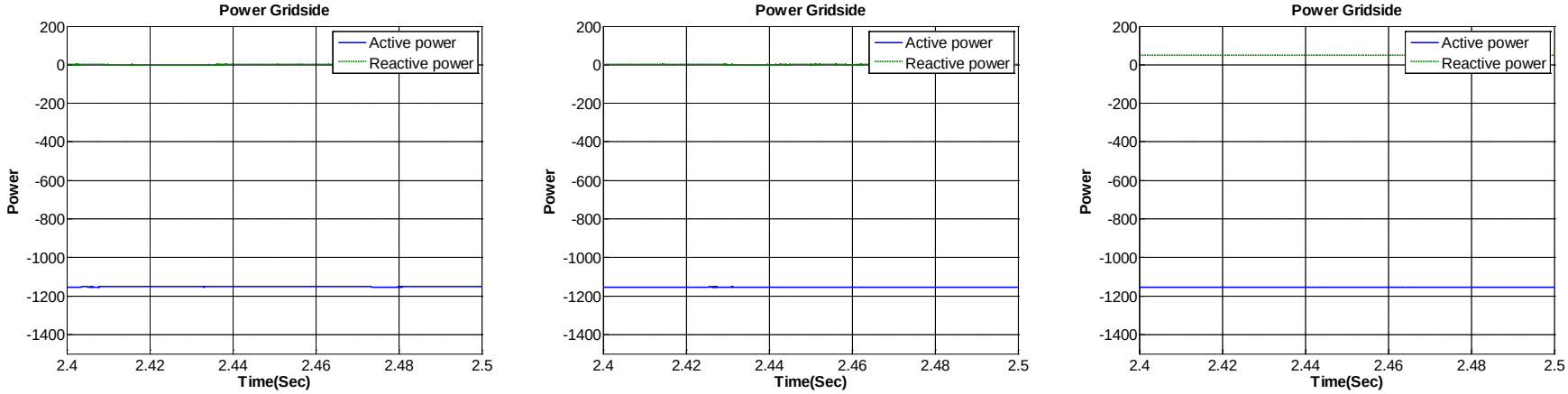


(a) (b) (c)

Figure 3. 74: Average output active and reactive power of Case 7:
(a) with proposed control; (b) with standard d-q method; (c) with standard indirect current method.

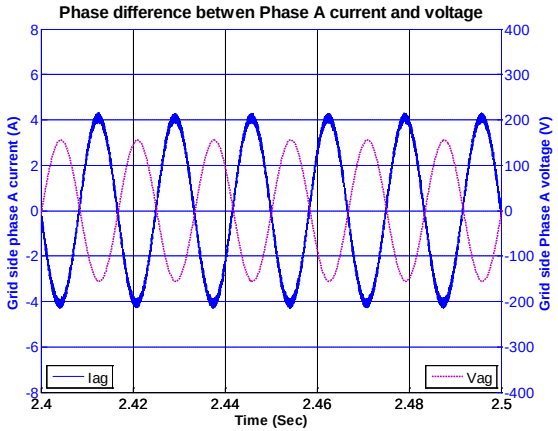


(a)

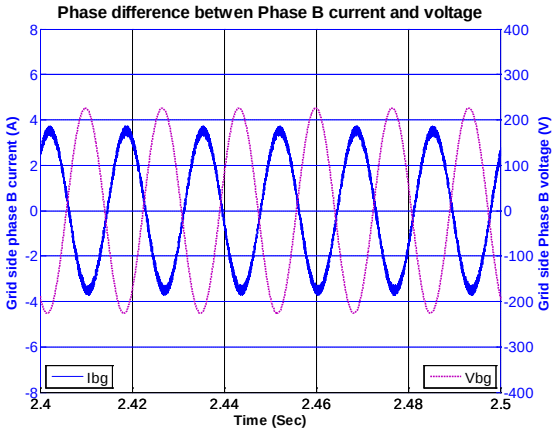


(b)

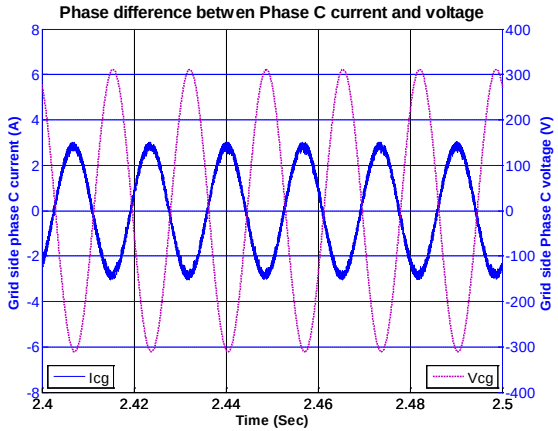


(c)

Figure 3. 75: Phase-currents with voltages for Case 7 with proposed method
(a) Phase A; (b) Phase B; (c) Phase C

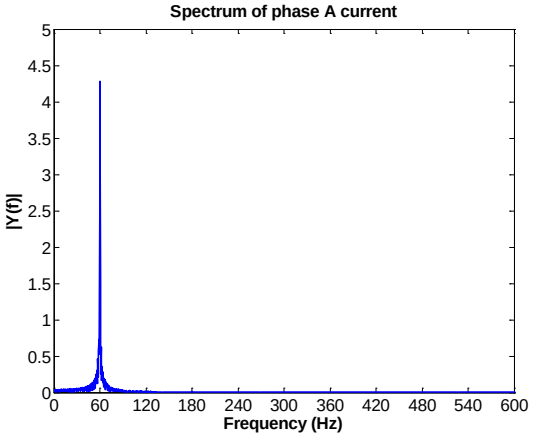


(a)

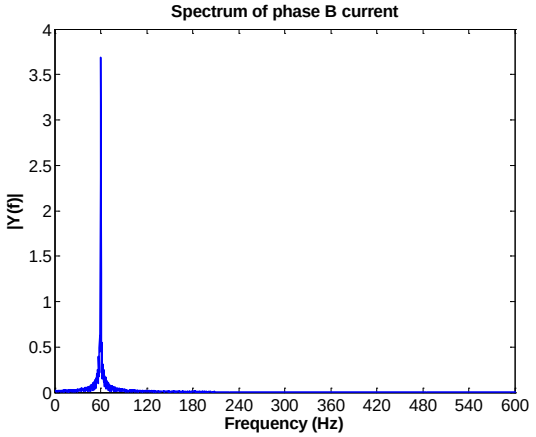


(b)

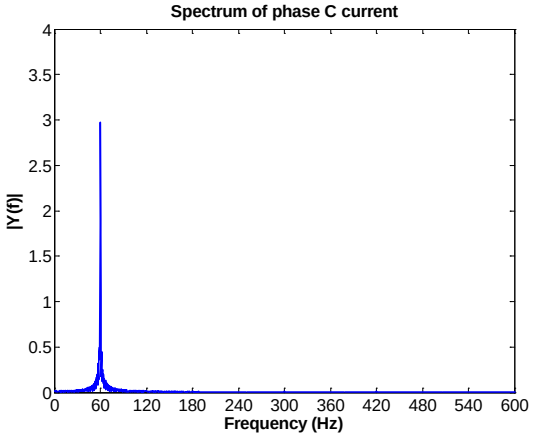


(c)

Figure 3. 76: Spectrums of grid currents for Case 7 with proposed method
(a) Phase A; (b) Phase B; (c) Phase C

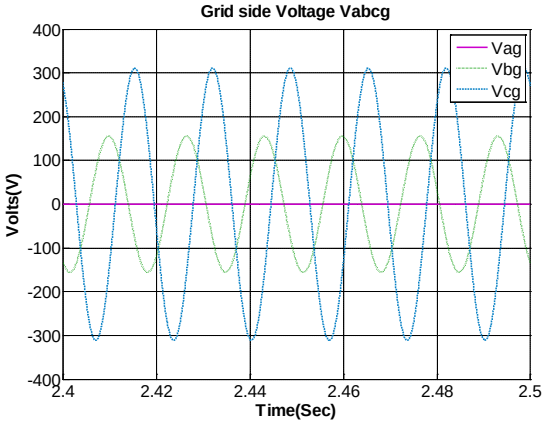


Figure 3. 77: Three-phase grid voltage (phase to ground) for Case 8



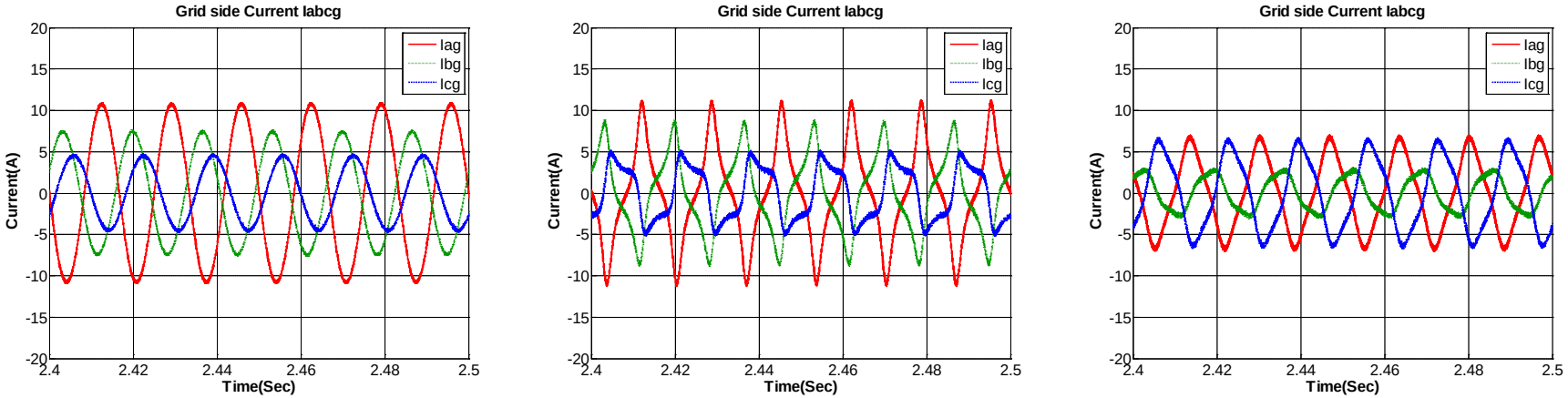


(a) (b) (c)

Figure 3. 78: Three-phase grid currents Case 8

(a) with proposed control; (b) with standard d-q method; (c) with standard indirect current method

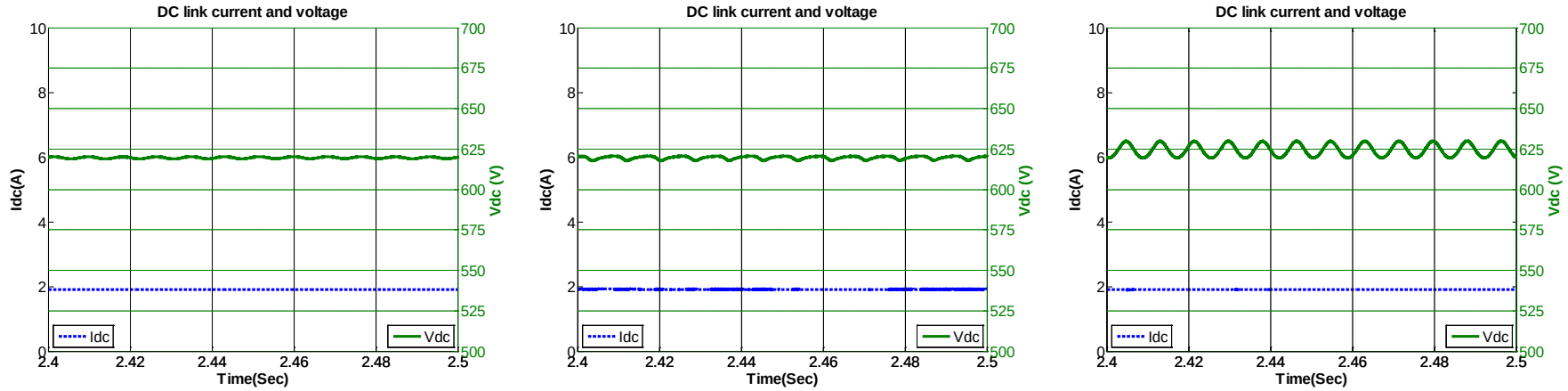


(a) (b) (c)

Figure 3. 79: DC link current and voltage of Case 8

(a) with proposed control; (b) with standard d-q method; (c) with standard indirect current method.

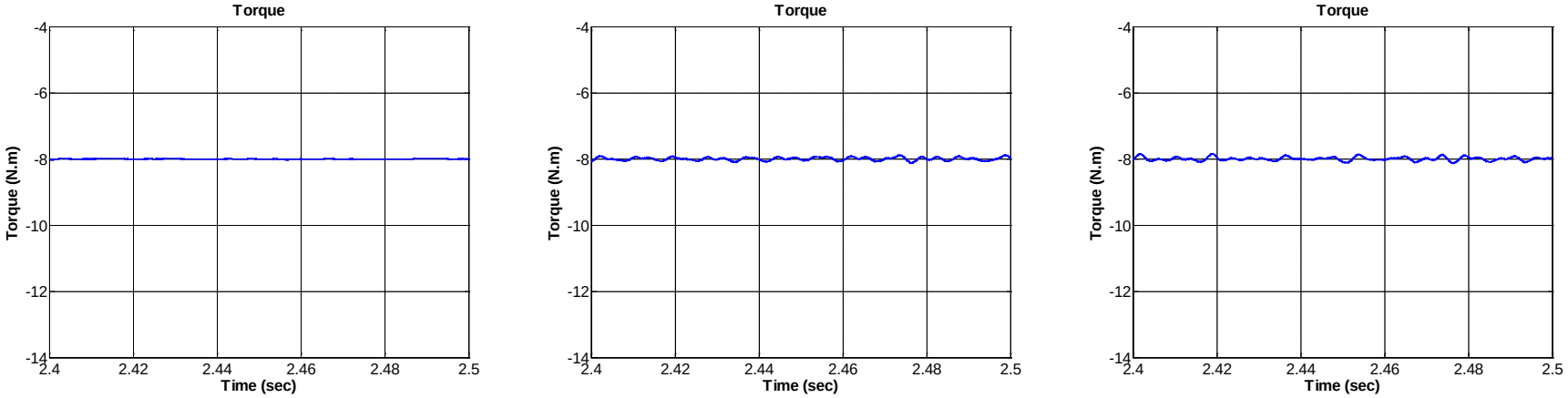


(a) (b) (c)

Figure 3. 80: Electromagnetic torque of induction generator of Case 8

(a) with proposed control ; (b) with standard d-q method; (c) with standard indirect current method.

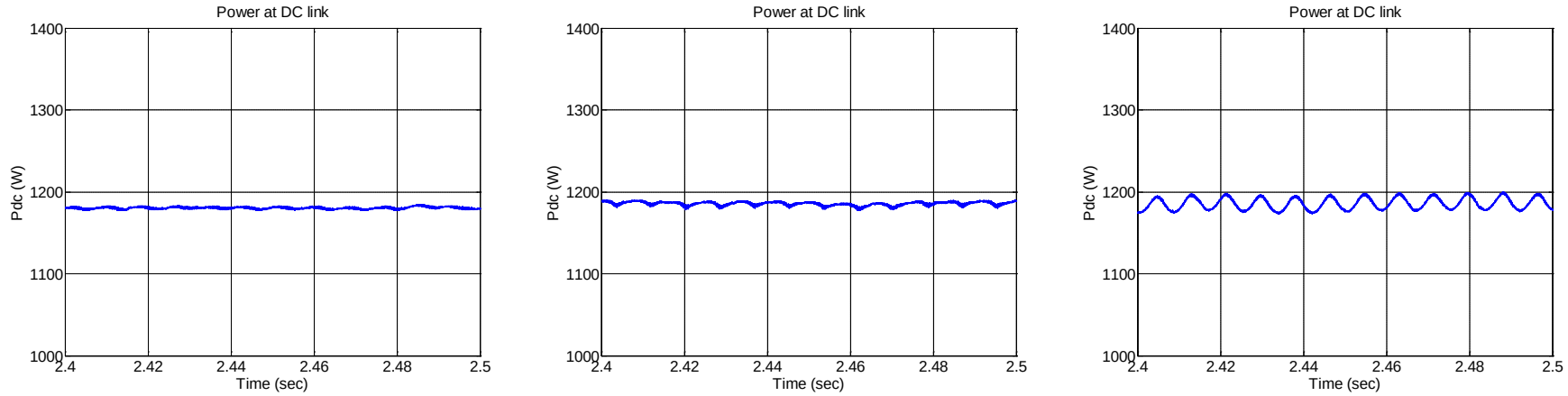


(a) (b) (c)

Figure 3. 81: DC link power of Case 8
(a) with proposed control; (b) with standard d-q method; (c) with standard indirect current method.

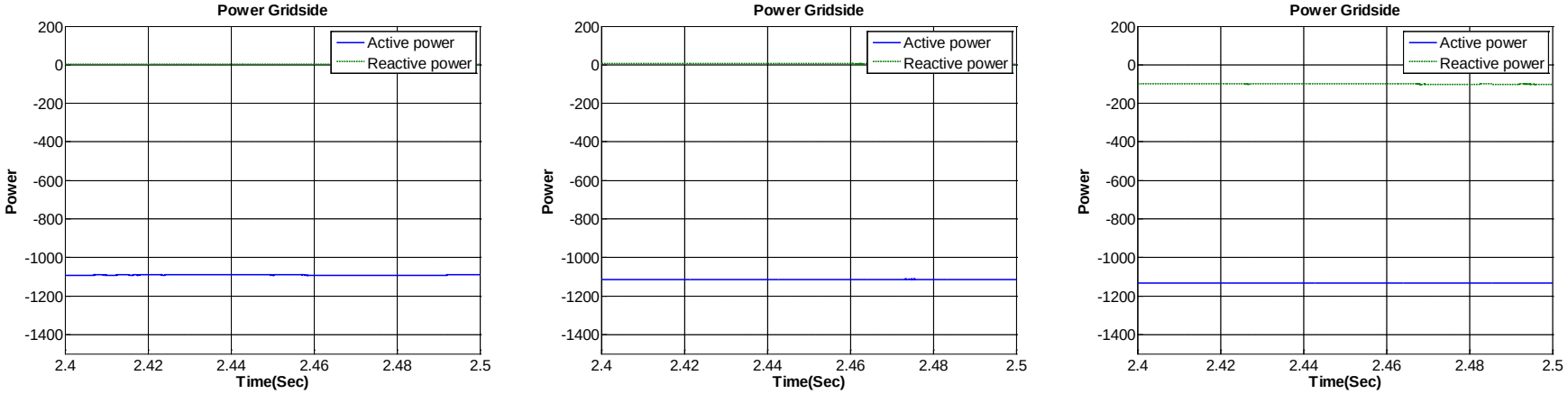


(a) (b) (c)

Figure 3. 82: Average output active and reactive power of Case 8:
(a) with proposed control; (b) with standard d-q method; (c) with standard indirect current method.

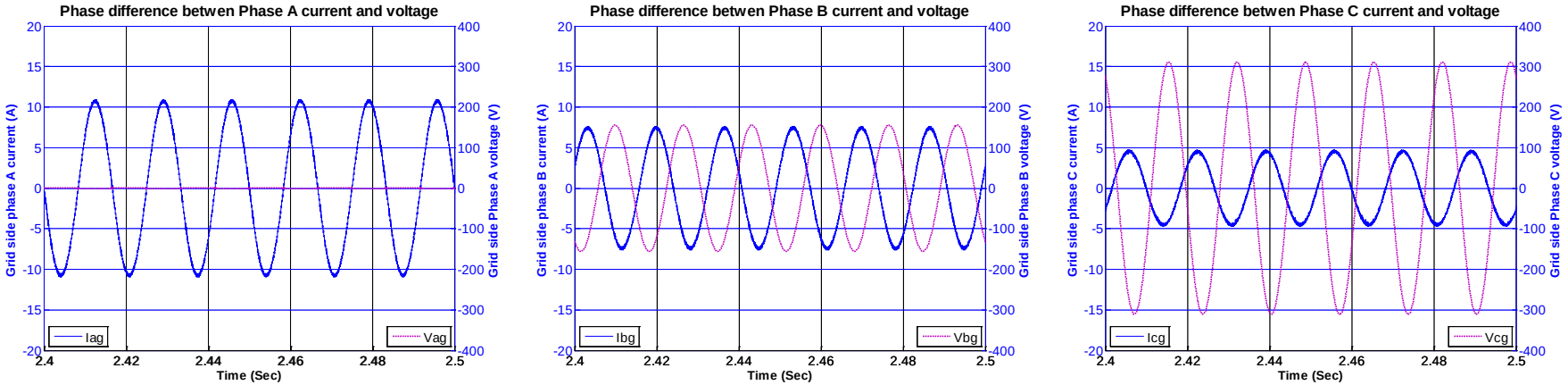


(a) (b) (c)

Figure 3. 83: Phase-currents with voltages for Case 8 with proposed method
(a) Phase A; (b) Phase B; (c) Phase C



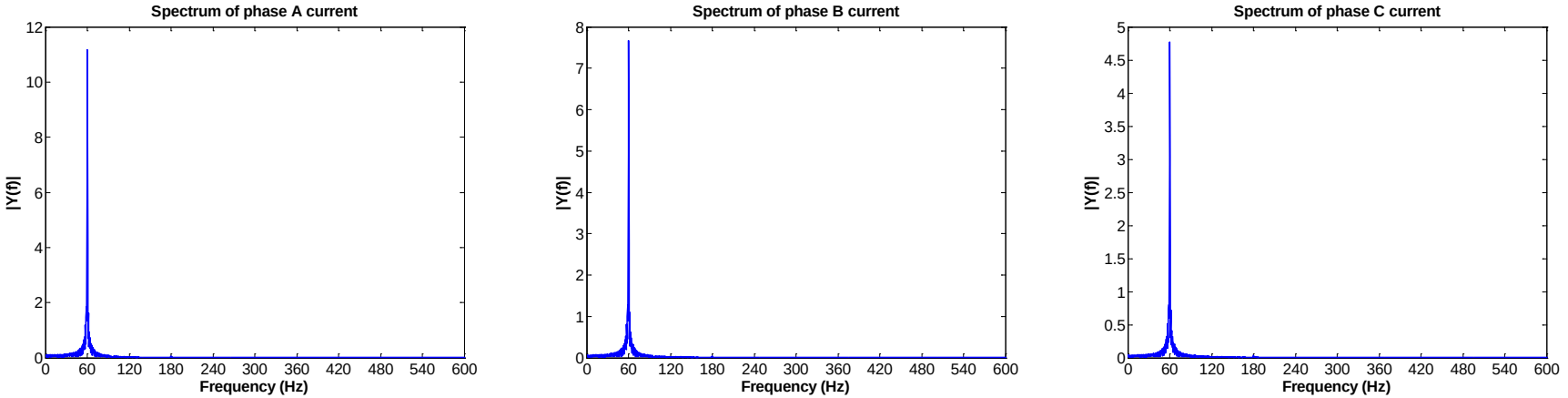


(a) (b) (c)

Figure 3. 84: Spectrums of grid currents for Case 8 with proposed method
(a) Phase A; (b) Phase B; (c) Phase C

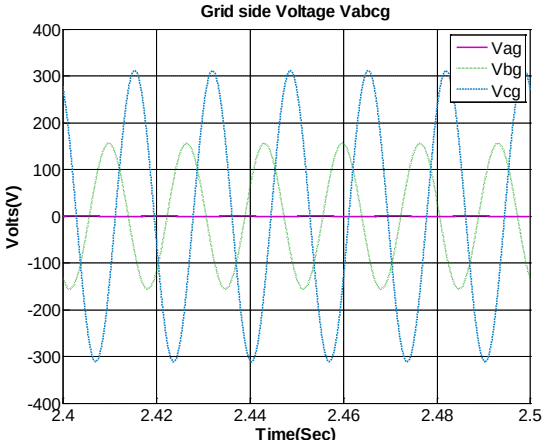


Figure 3. 85: Three-phase grid voltage (phase to ground) for Case 9

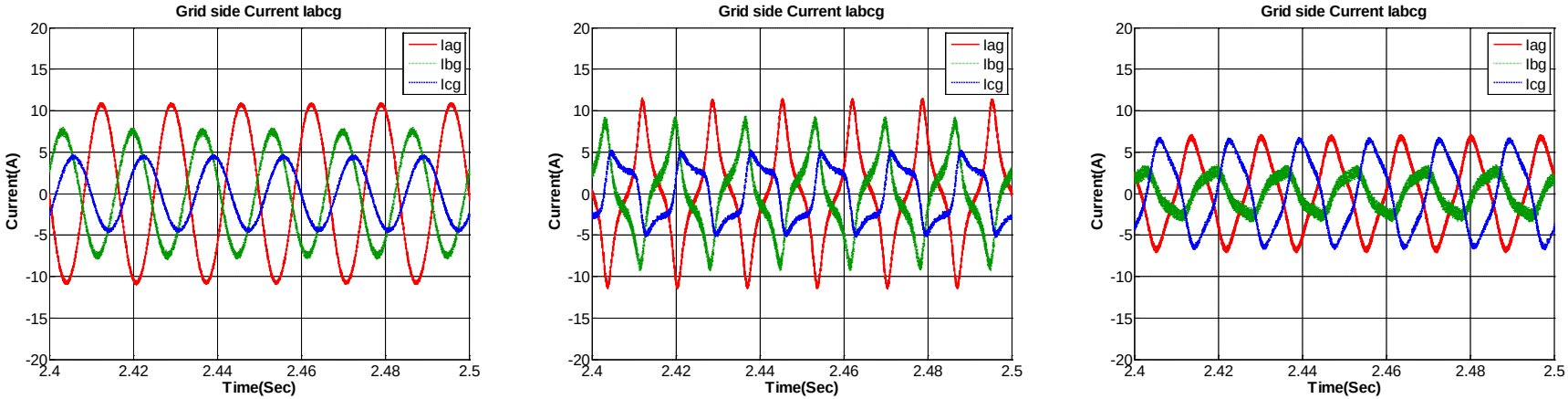


(a) (b) (c)

Figure 3. 86: Three-phase grid currents Case 9
(a) with proposed control; (b) with standard d-q method; (c) with standard indirect current method

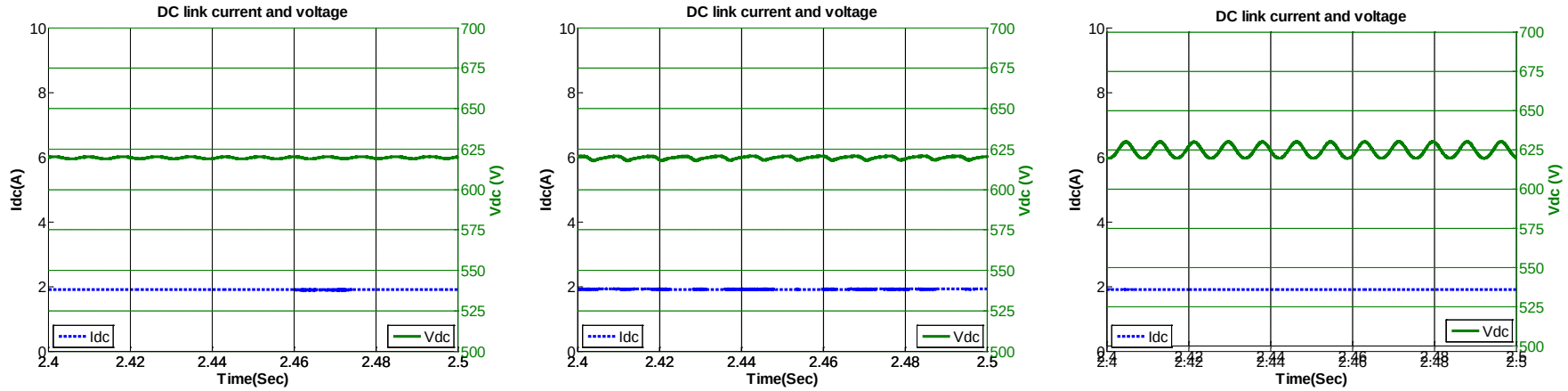


(a) (b) (c)

Figure 3. 87: DC link current and voltage of Case 9

(a) with proposed control; (b) with standard d-q method; (c) with standard indirect current method.



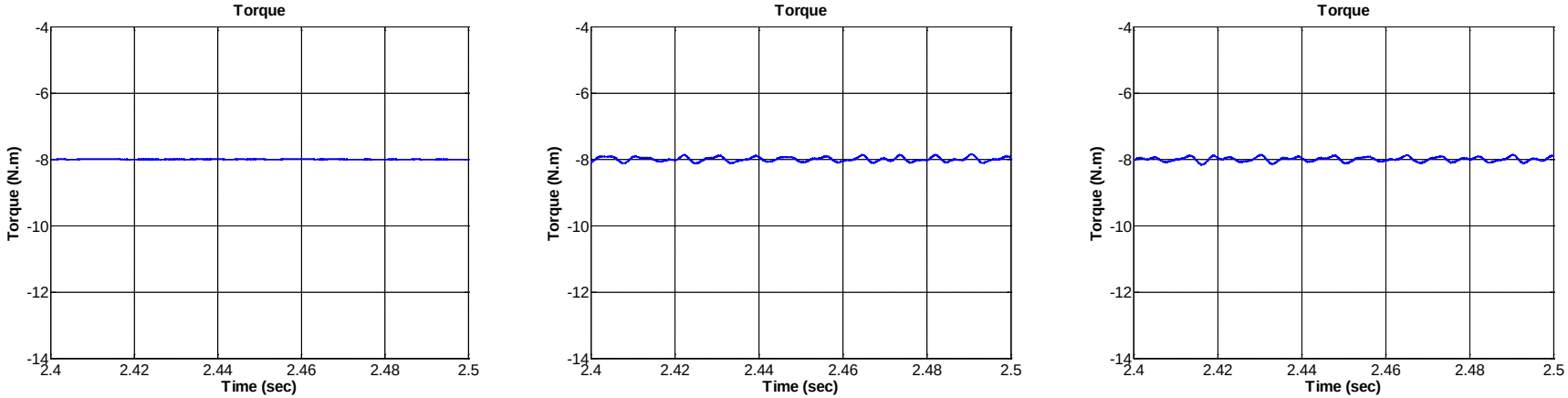


(a) (b) (c)

Figure 3. 88: Electromagnetic torque of induction generator of Case 9

(a) with proposed control ; (b) with standard d-q method; (c) with standard indirect current method.

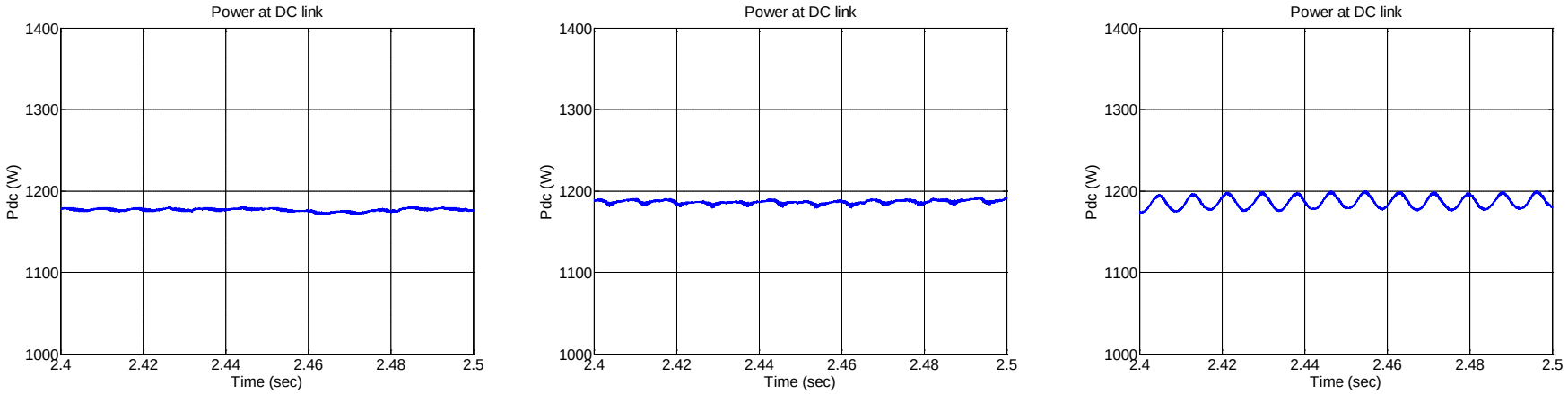


(a) (b) (c)

Figure 3. 89: DC link power of Case 9:
(a) with proposed control; (b) with standard d-q method; (c) with standard indirect current method.



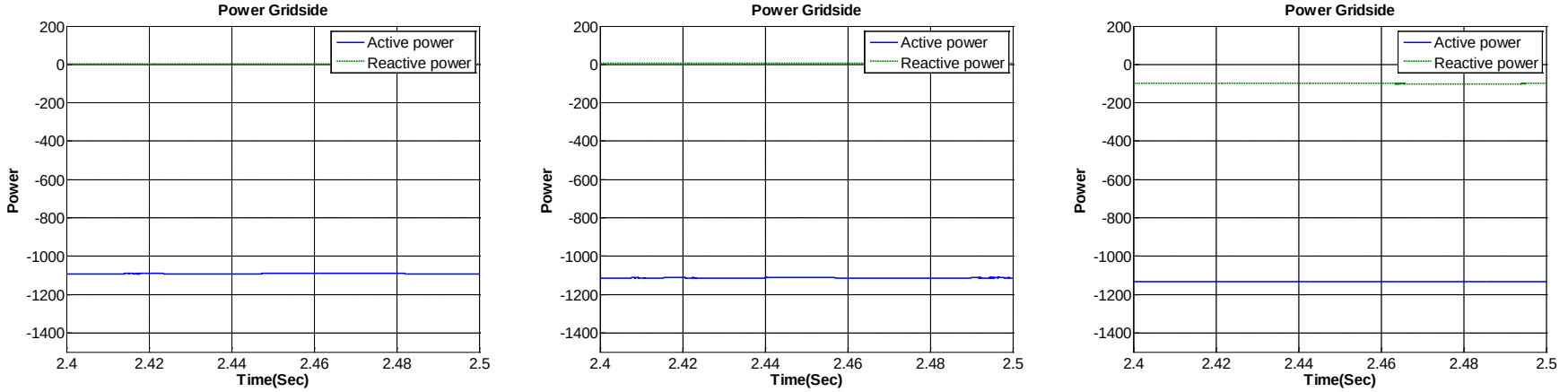


(a) (b) (c)

Figure 3. 90: Average output active and reactive power of Case 9:
(a) with proposed control; (b) with standard d-q method; (c) with standard indirect current method.

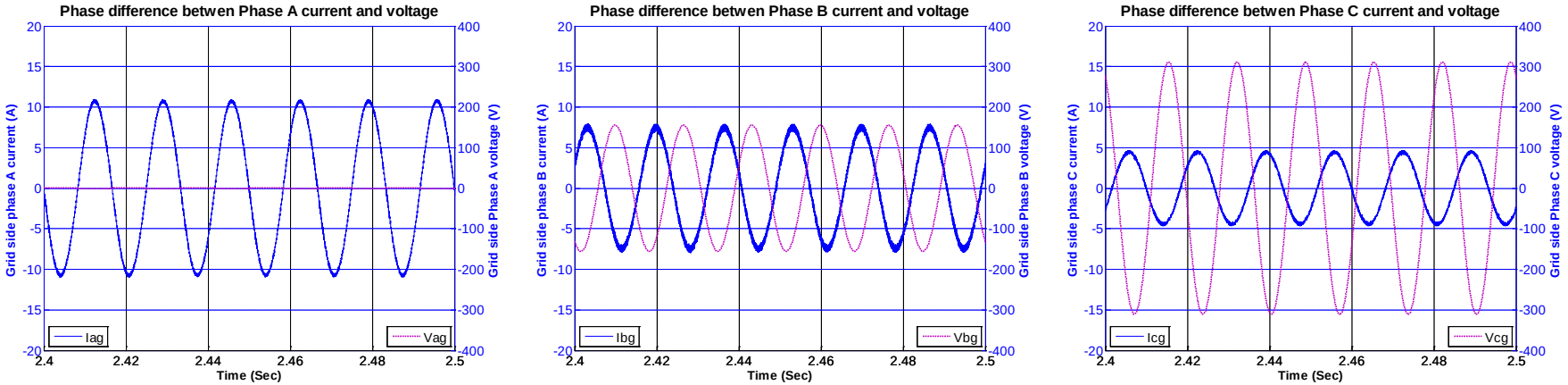


(a) (b) (c)

Figure 3. 91: Phase-currents with voltages for Case 9 with proposed method
(a) Phase A; (b) Phase B; (c) Phase C

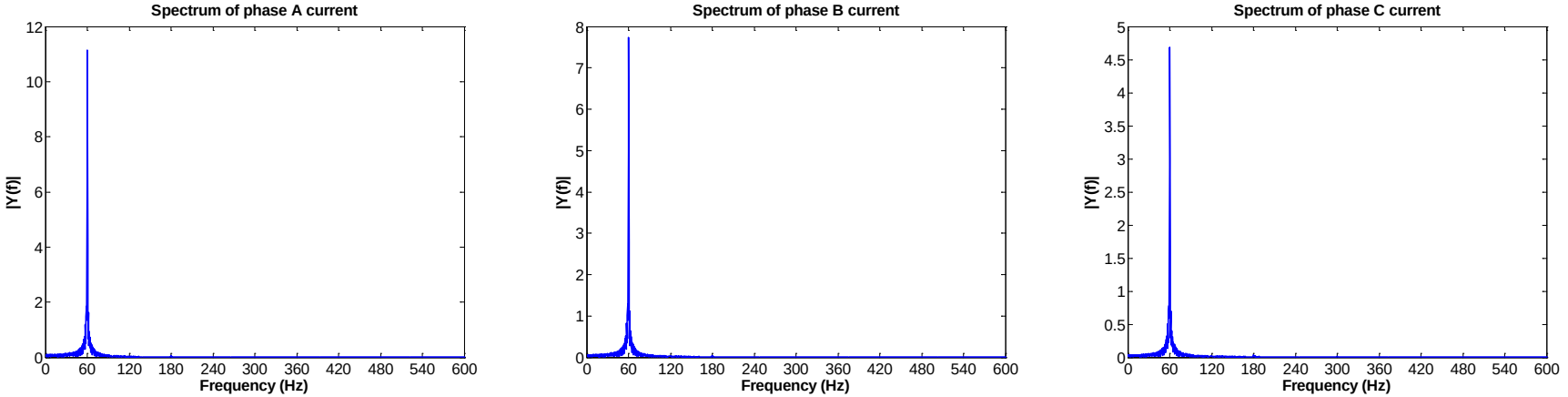


(a) (b) (c)

Figure 3. 92: Spectrums of grid currents for Case 9 with proposed method
(a) Phase A; (b) Phase B; (c) Phase C

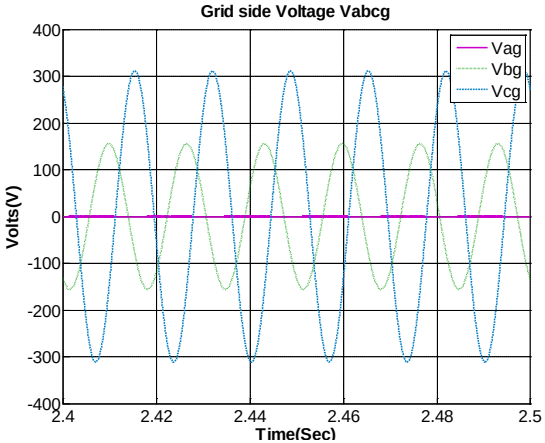


Figure 3. 93: Three-phase grid voltage (phase to ground) for Case 10

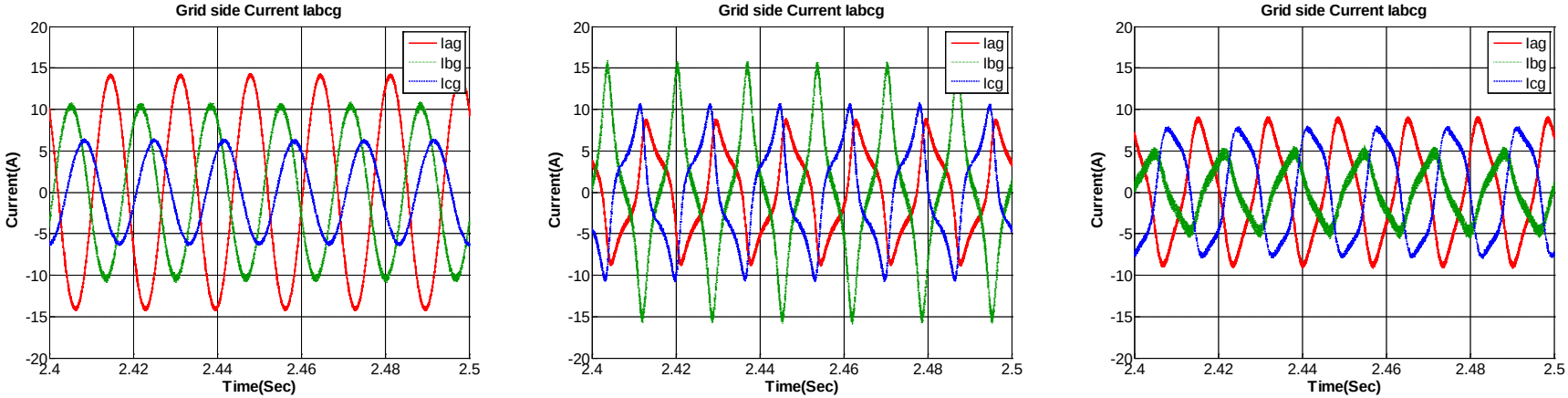


(a) (b) (c)

Figure 3. 94: Three-phase grid currents Case 10
(a) with proposed control; (b) with standard d-q method; (c) with standard indirect current method

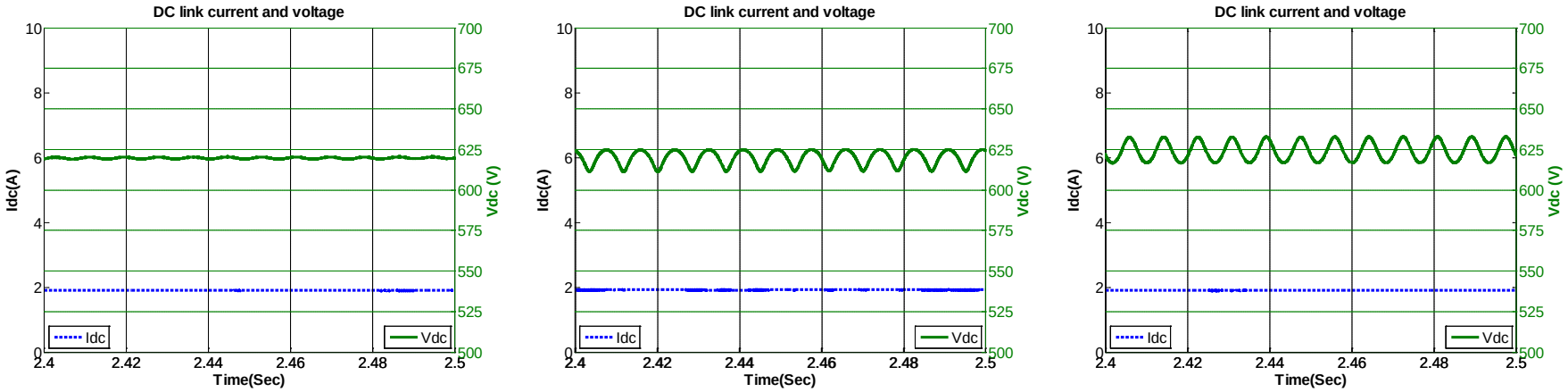


(a) (b) (c)

Figure 3. 95: DC link current and voltage of Case 10
(a) with proposed control; (b) with standard d-q method; (c) with standard indirect current method.

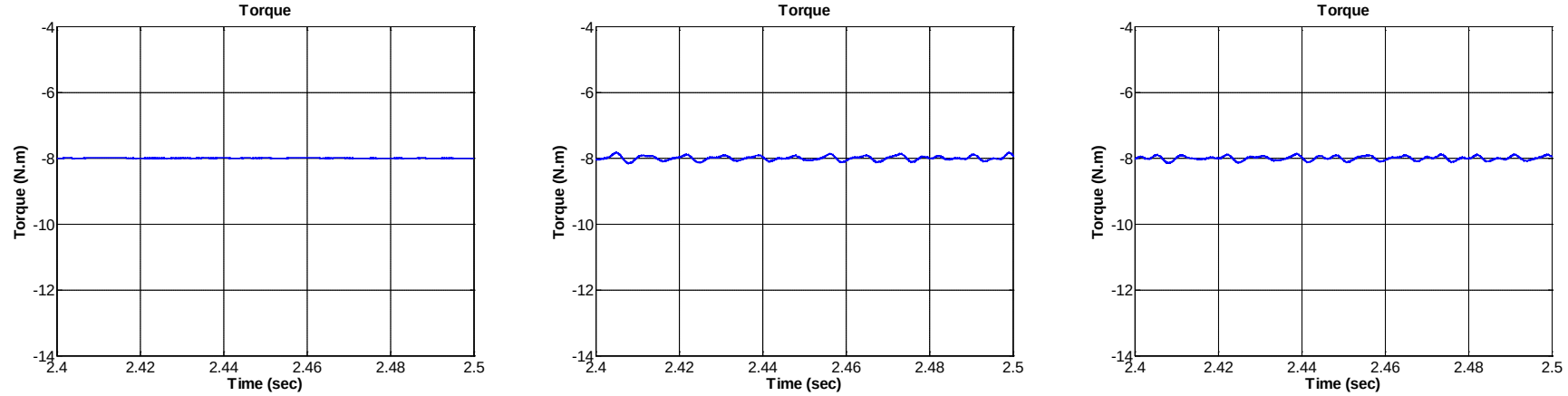


(a) (b) (c)

Figure 3. 96: Electromagnetic torque of induction generator of Case 10
(a) with proposed control ; (b) with standard d-q method; (c) with standard indirect current method

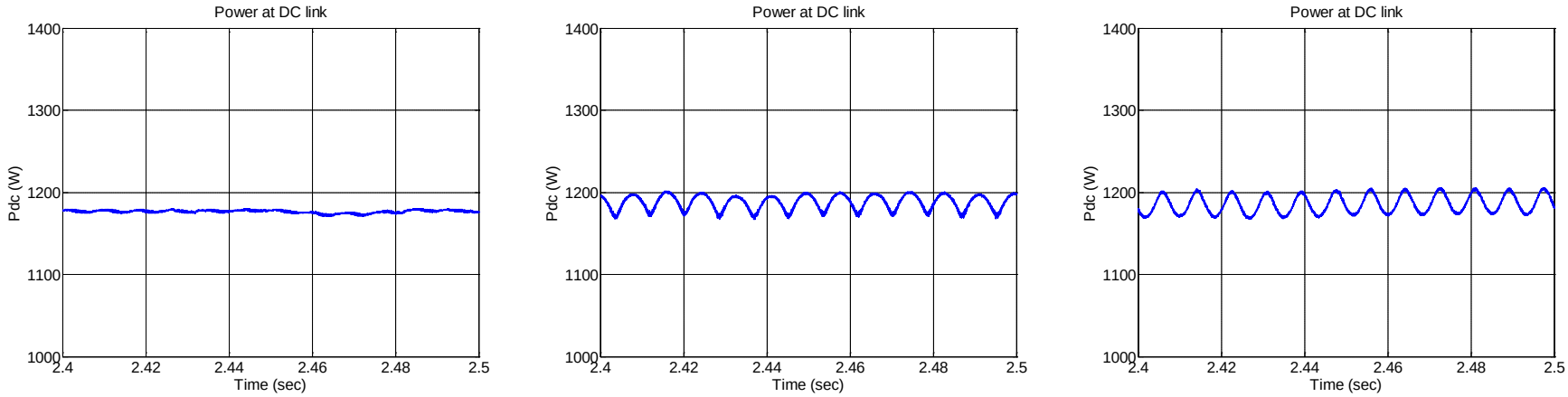


(a) (b) (c)

Figure 3. 97: DC link power of Case 10
(a) with proposed control; (b) with standard d-q method; (c) with standard indirect current method.

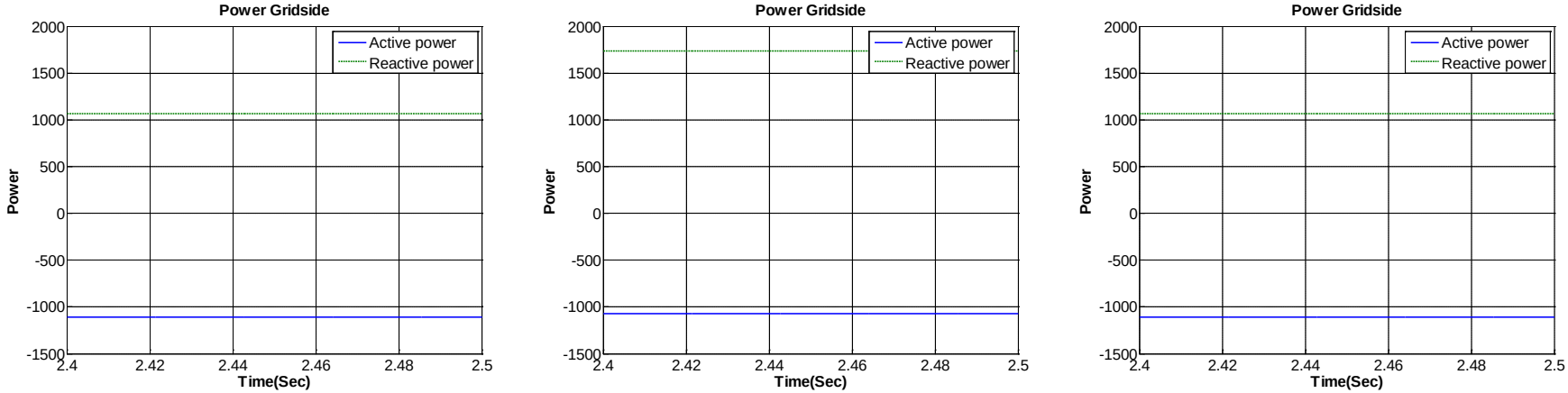


(a) (b) (c)

Figure 3. 98: Average output active and reactive power of Case 10:
(a) with proposed control; (b) with standard d-q method; (c) with standard indirect current method.

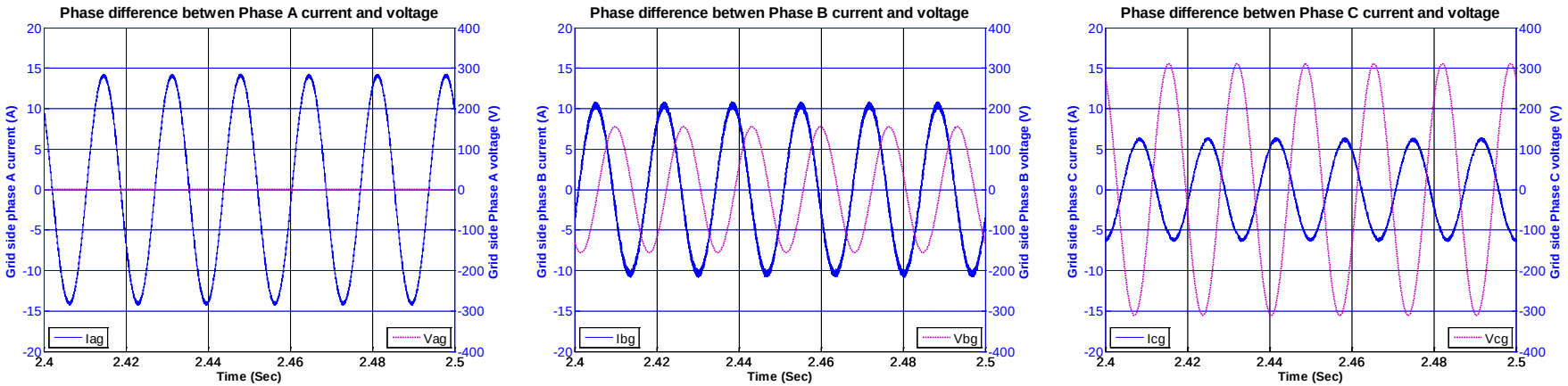


(a) (b) (c)

Figure 3. 99: Phase-currents with voltages for Case 10 with proposed method
(a) Phase A; (b) Phase B; (c) Phase C

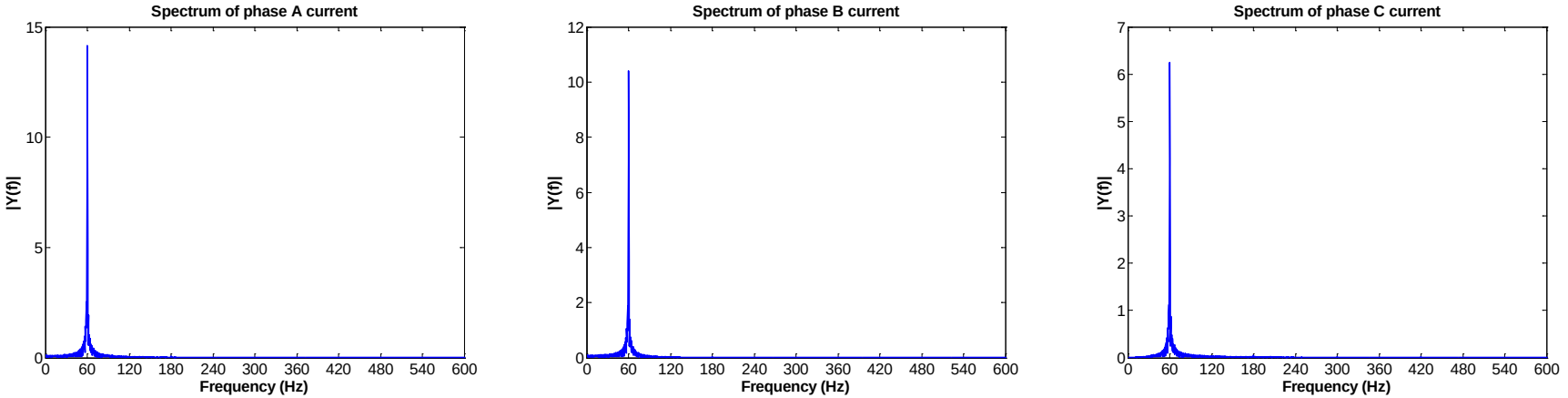


(a) (b) (c)

Figure 3. 100: Spectrums of grid currents for Case 10 with proposed method
(a) Phase A; (b) Phase B; (c) Phase C

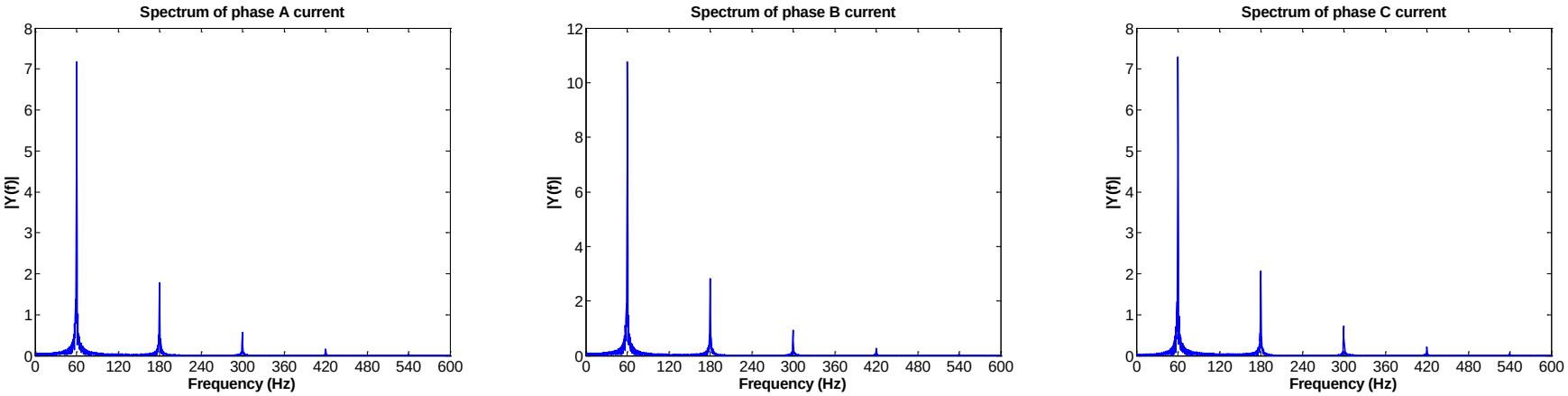


(a) (b) (c)

Figure 3. 101: Spectrums of grid currents for Case 10 with standard d-q method
(a) Phase A; (b) Phase B; (c) Phase C

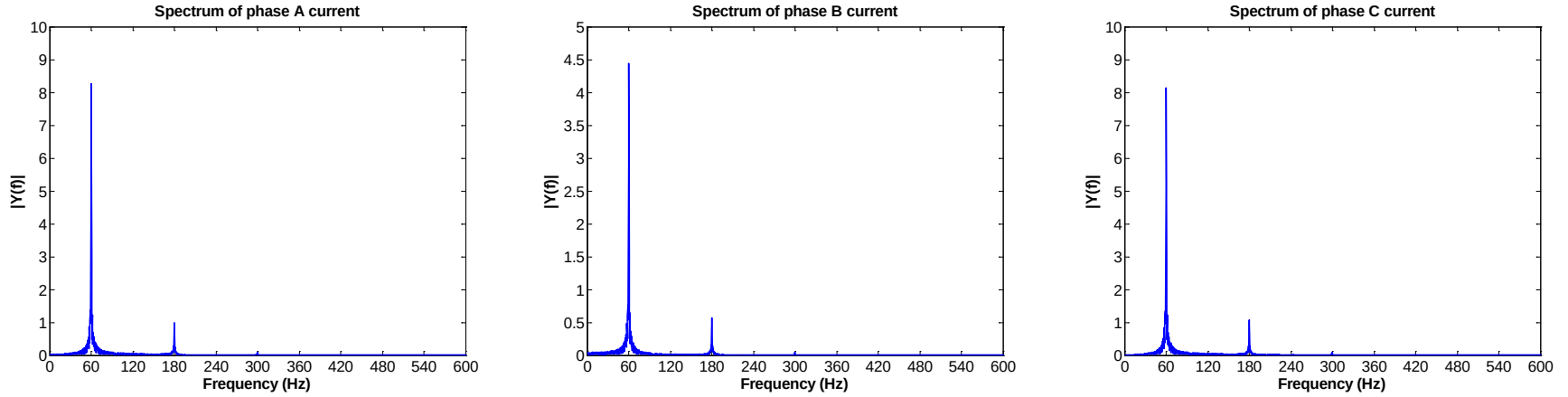


(a) (b) (c)

Figure 3. 102: Spectrums of grid currents for Case 10 with indirect current method
(a) Phase A; (b) Phase B; (c) Phase C

### 3.5 Simulation results of the grid-fault ride-through

The proposed method is also tested under the grid-fault ride-through scenario. Table lists the simulation case 11 and case 12.

In case 11, the wind system with a permanent-magnet generator is simulated. At 1.0 s, phase A and phase B voltage decrease to 80% of the rated valued and phase C voltage decrease to 50% of the rated value. At 1.2 s, the voltages recover to the original rated values. At the same time, the line impedance is unbalanced. The simulation results with proposed method and the traditional indirect current control without the harmonic elimination control are provided.

In case 12, the wind system with a squirrel-case induction generator is simulated. At 1.2 s, phase A and phase B voltage decrease to 80% of the rated valued and phase C voltage decrease to 50% of the rated value. At 1.2 s, the voltages recover to the rated values. At the same time, the line impedance is unbalanced.

Optimal power tracking of the turbine is used to increase the power conversion efficiency.

However, during grid-fault ride-through, the unbalanced can cause current stress in the inverter.

So the power tracking should include the power limit when the grid-fault occurs so to limit the currents.

Table 3. 7: The grid-fault case

| Case | Grid side voltage | Line impedance | Power factor |
|---|---|---|---|
| **11** | $U_a$=176∠0, $U_b$ =176∠-120, $U_c$ =110∠120. | $L_1 = L_3 = 5mL$; $L_2 = 2mL$ | 1 |

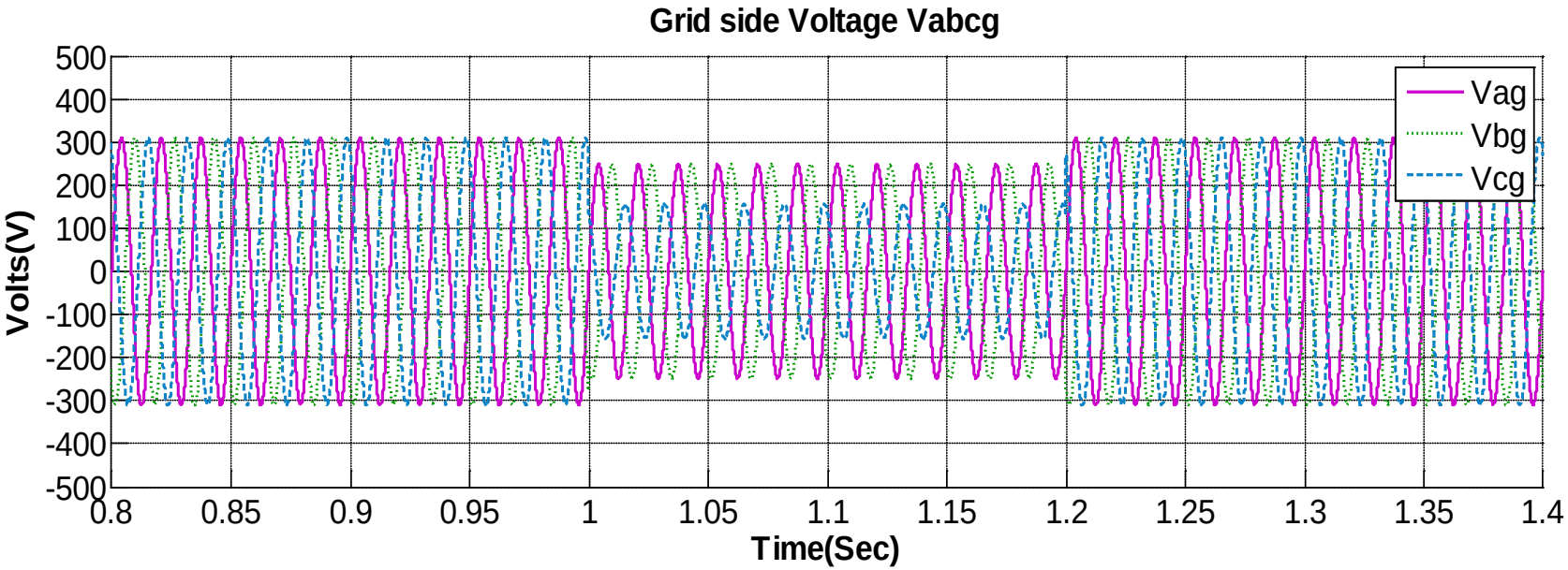


Figure 3. 103: Three-phase grid voltage of Case 11

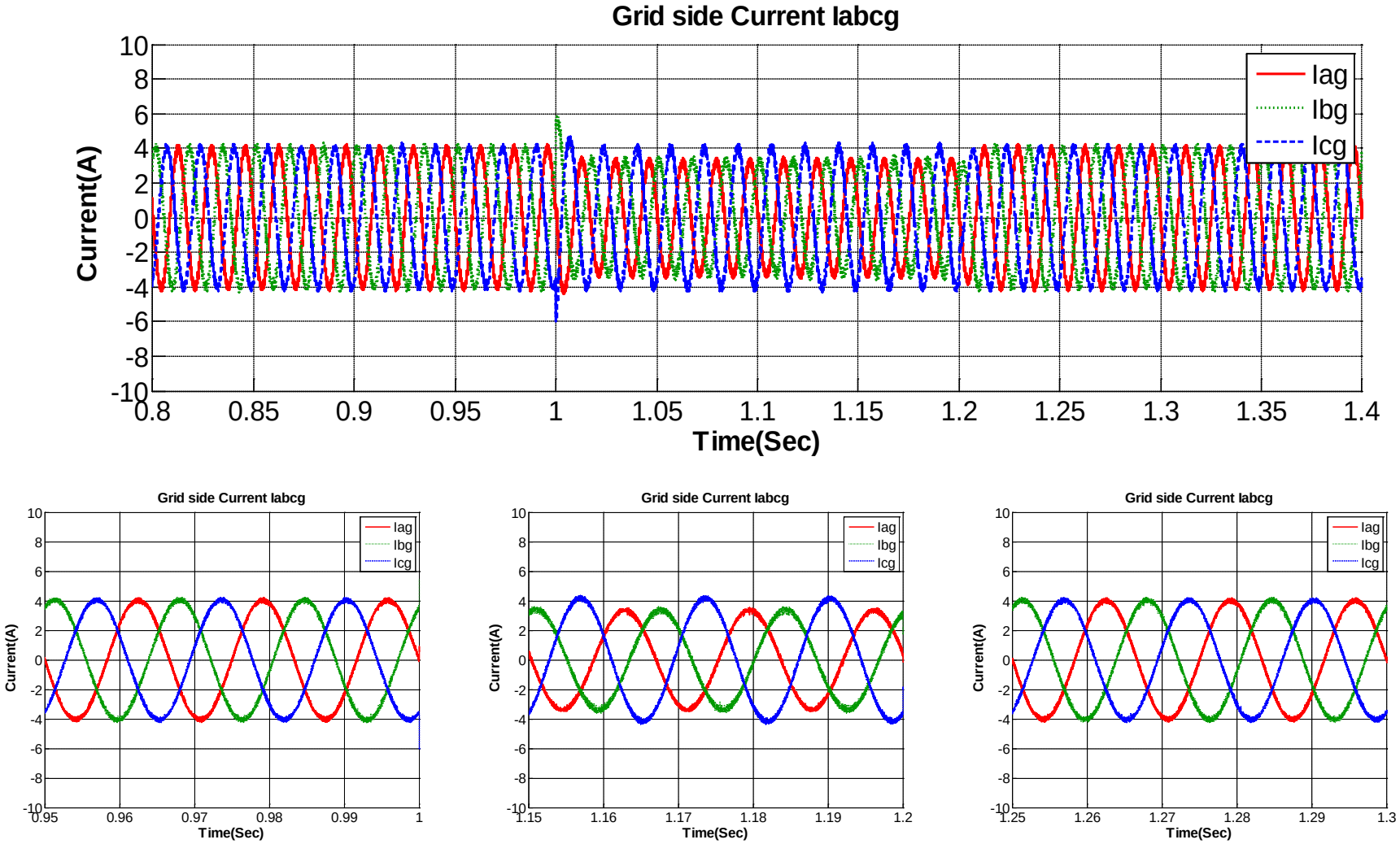


Figure 3. 104: Three-phase grid currents of Case 11 with proposed method

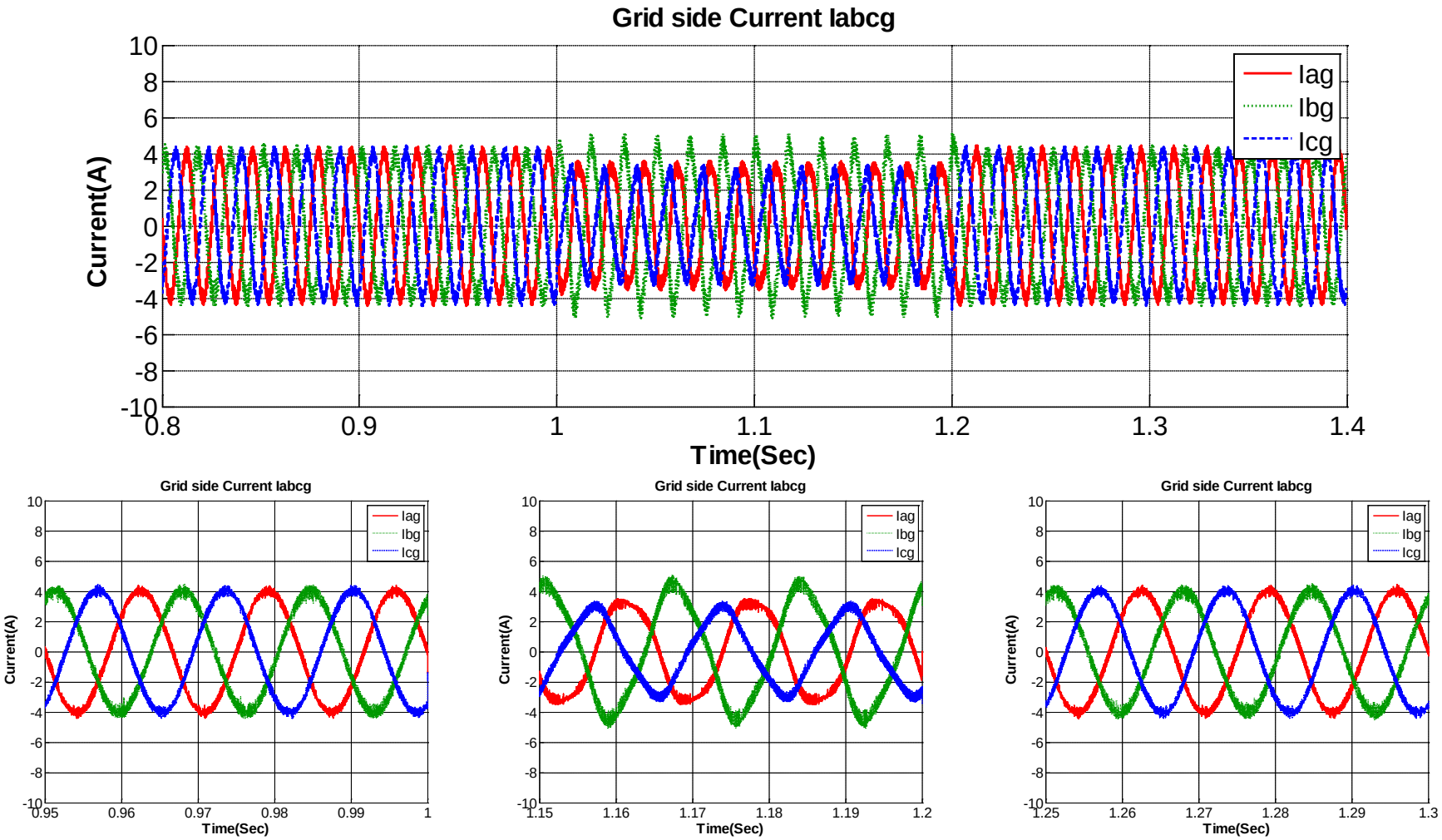


Figure 3. 105: Three-phase grid currents of Case 11 with indirect current control

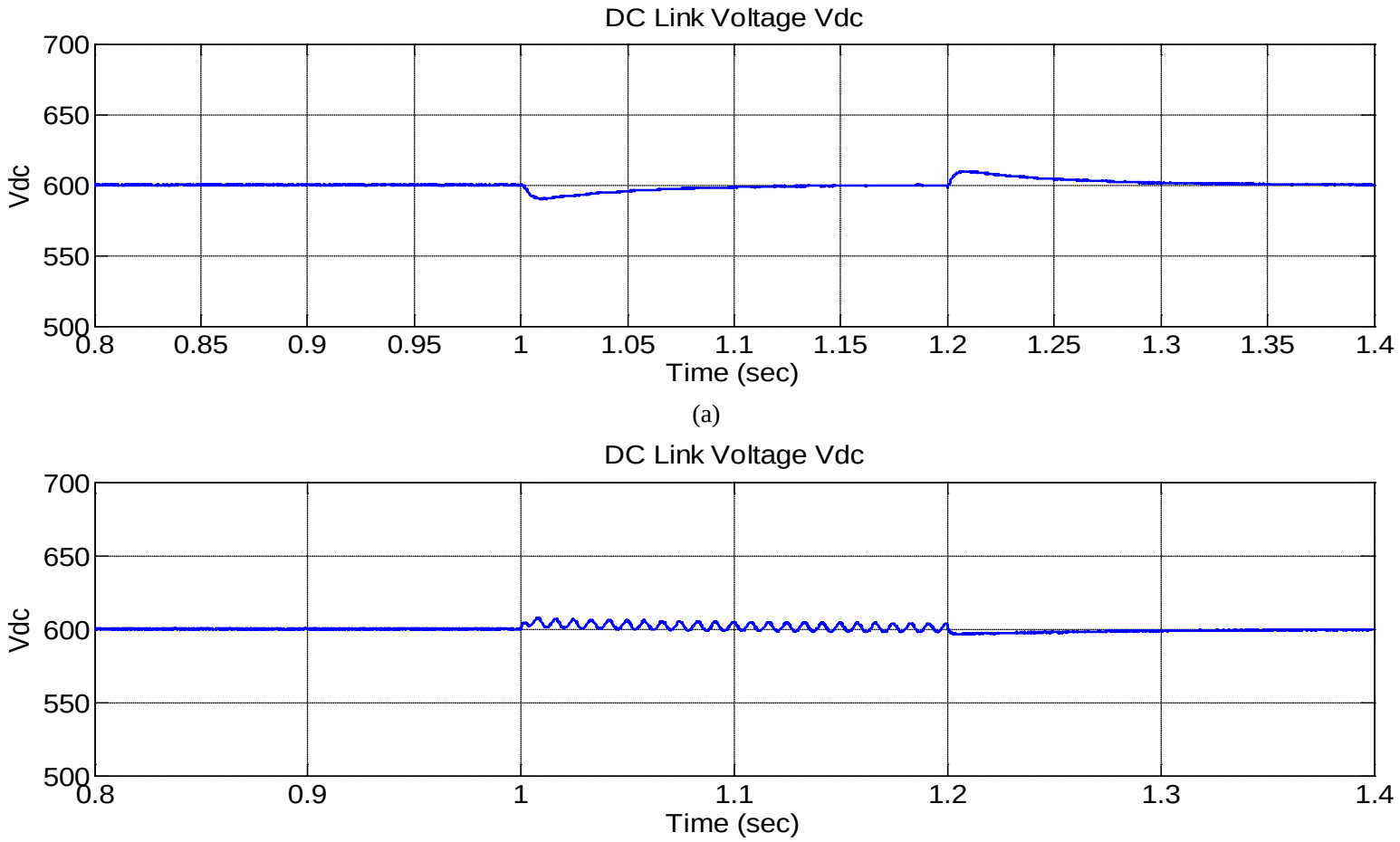


Figure 3. 106: DC link voltage of Case 11
(a) Proposed control; (b) Standard indirect current method

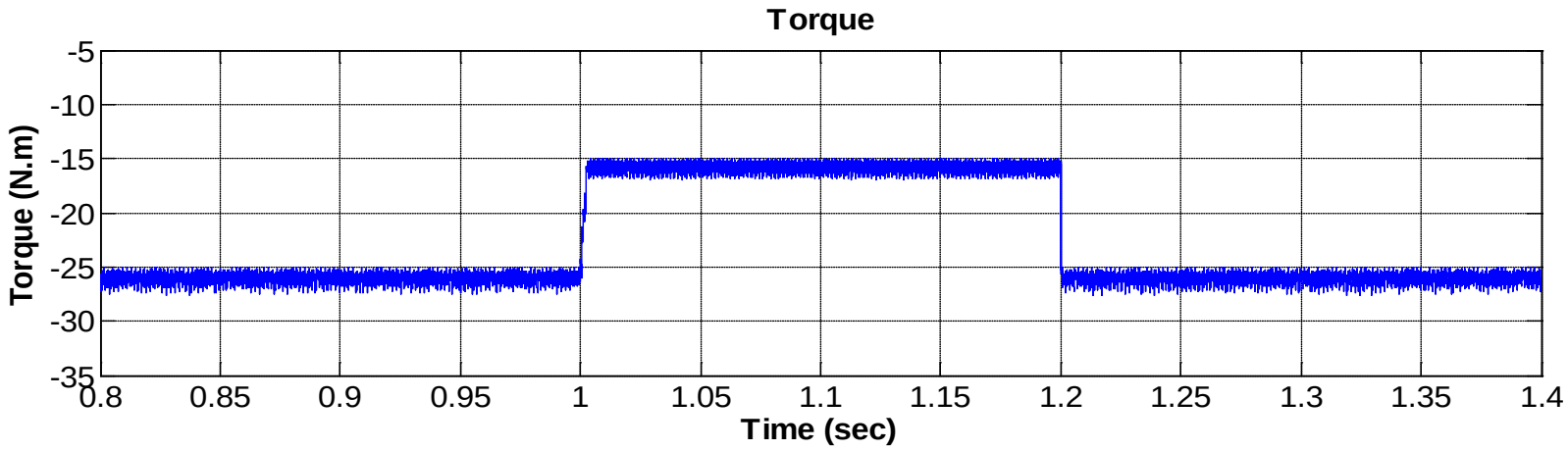


(a)

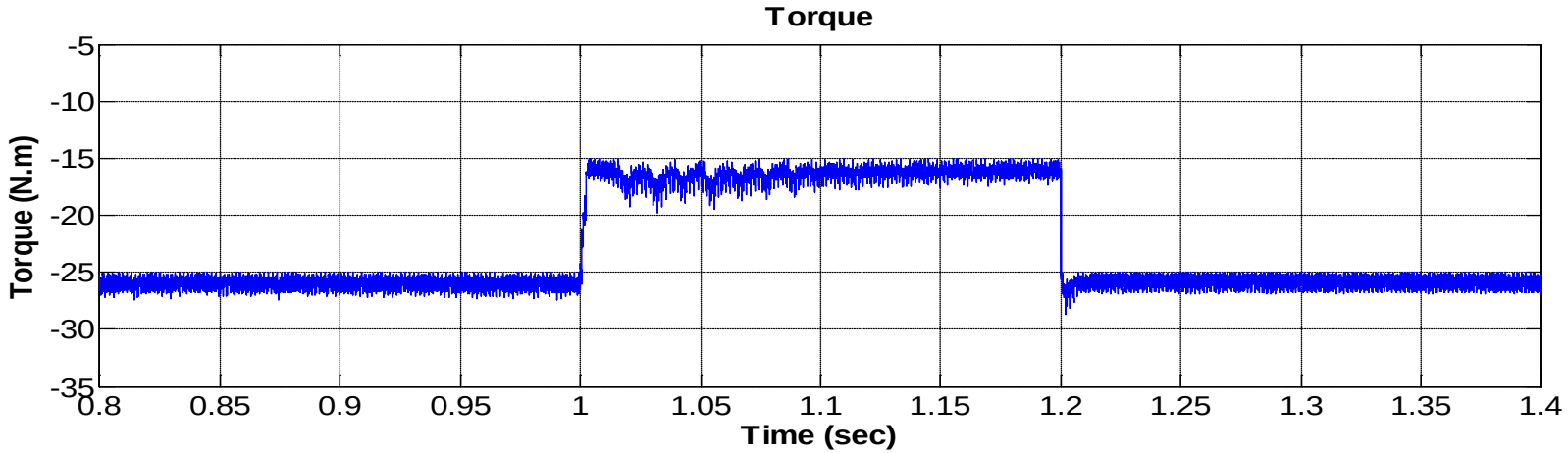


(b)

Figure 3. 107: Electromagnetic torque of Case 11
(a) Proposed control; (b) Standard indirect current method

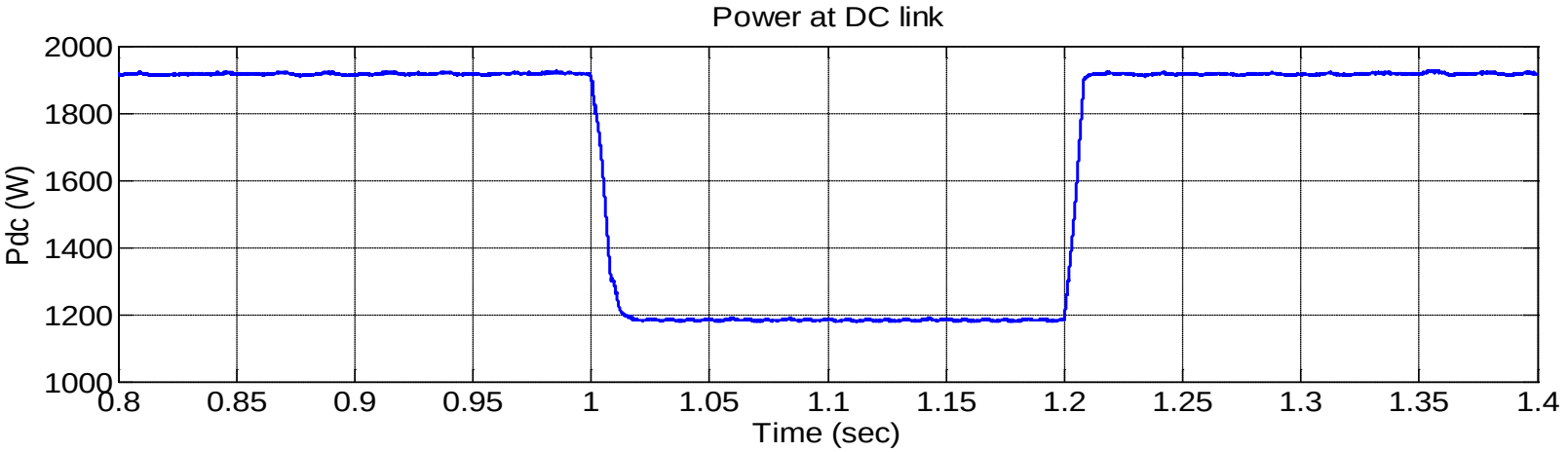


(a)

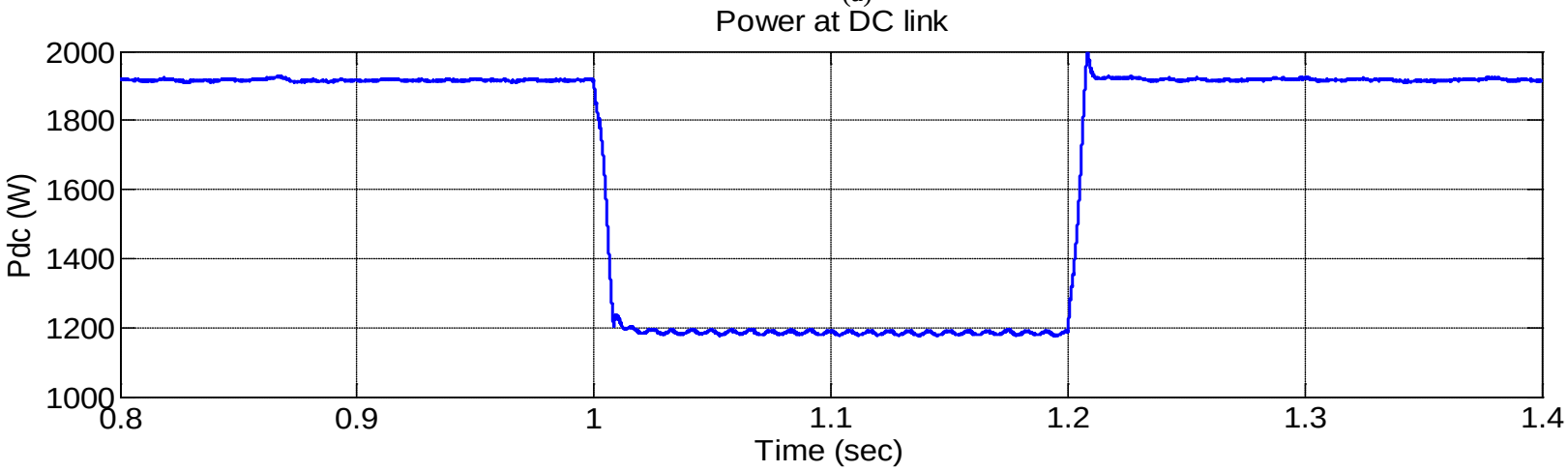


(b)

Figure 3. 108: DC link power of Case 11
(a) Proposed control; (b) Standard indirect current method

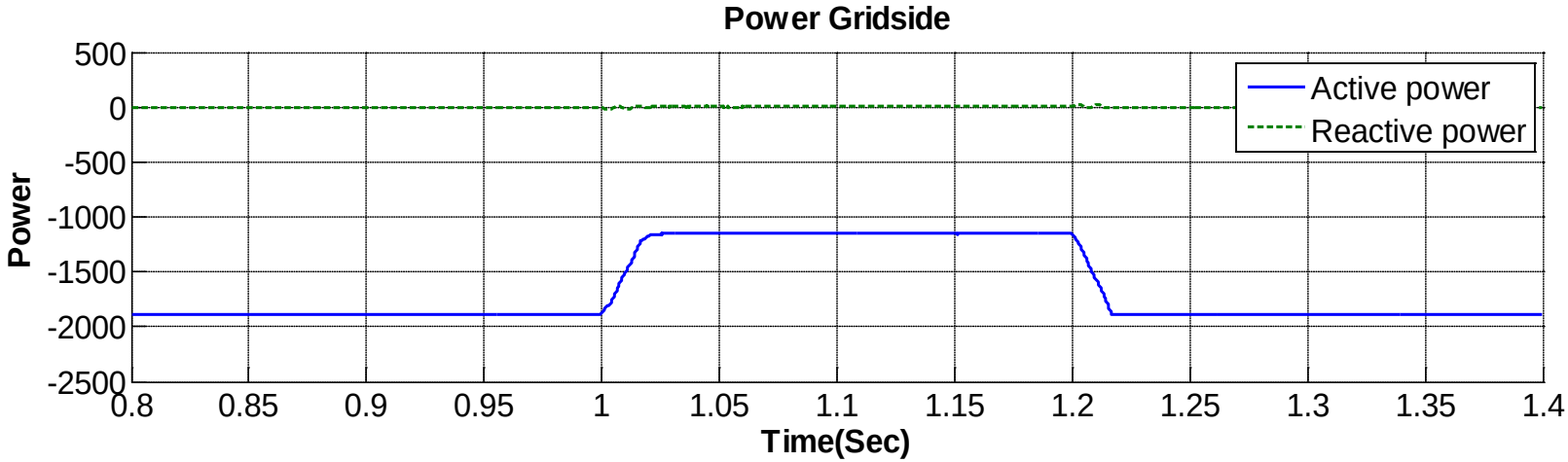


(a)

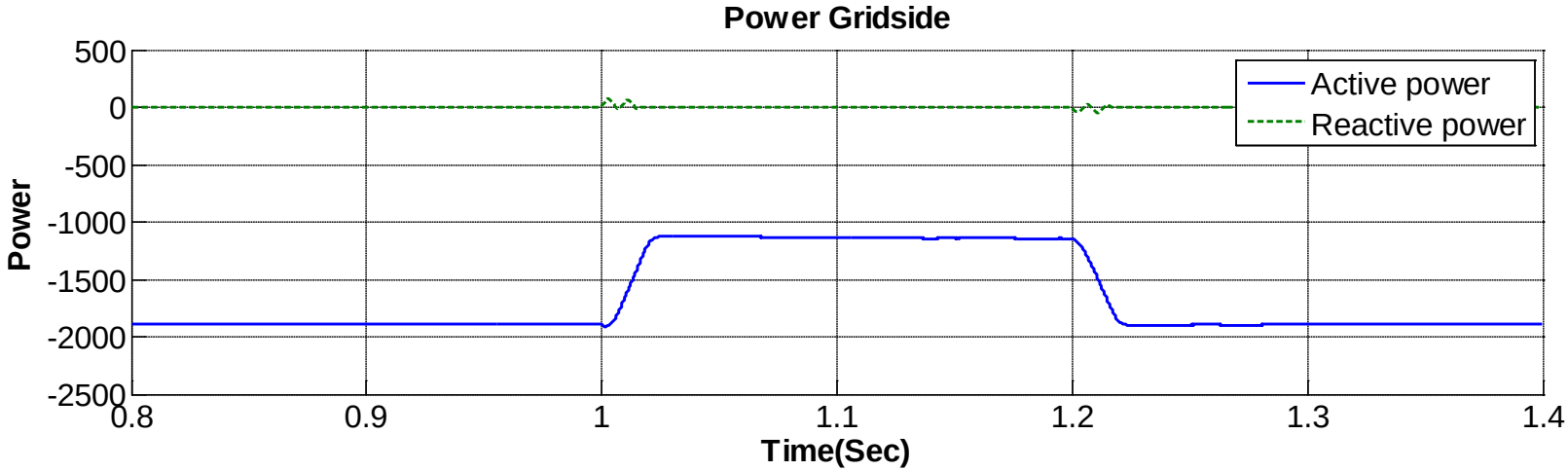


(b)

Figure 3. 109: Average output power of Case 11
(a) Proposed control; (b) Standard indirect current method

### 3.6 Analysis of simulation results

From the simulation results of Case 6, it can be seen that in the wind power system, the unbalanced grid operation will cause the torque pulsation of the generator, if the grid side inverter is without the harmonic elimination control, figure 3.60 (c). This is because the unbalanced voltage operation will cause the third-order harmonics in the grid side current, and this will cause the second order harmonic in the DC link, figure 3.59 (c), and this finally causes the second order pulsation of the electromagnetic torque of the generator. Moreover, the torque pulsation leads to the three-phase unbalanced currents in the generator stator winding, figure 3.61(c). The unbalanced currents in the stators can result in the uneven heating of the winding and this may short the lifetime of the machine.

The grid side inverter achieves input-output harmonic elimination by using the proposed control method. It can be seen from figure 3.59 (a) that there is no low order DC voltage ripples and no second order torque pulsation figure 3.60 (a). The Fourier analysis, figure 3.64, also shows that, by using the proposed method, there is no low-order harmonics in the grid side currents under the unbalanced grid voltage operation. At the same time, with the close-loop operation, DC link voltage is controlled at constant value for 600 V and this will ensure that the power is transferred from the DC link to the grid.

It is also shown in the figure 3.62 and figure 3.63 that, with the proposed method, the grid side inverter can change the power factor even under the unbalanced case while the tradition method in d-q frame and the traditional indirect current control can not.

At last, the proposed control of the grid side inverter is tested for its application

for its grid fault ride-through ability in Case 11. In figure 3.118, at 1.0s, the phase A and phase B voltages drop to 80% and the phase C voltage dropped to half of its rated value. After 0.2s, the voltage goes back to the rated value. The line impedances are unbalanced for $L_1$=$L_3$=5mL $L_2$=2mL. It shows in figure 3.86 (b) and figure 3.87 (b) that with the traditional indirect current control, there is a large amount of ripple content for the DC voltage. Compared to the traditional method, it can be seen from figure 3.86 (a) and figure 3.87 (a) that the currents are without obvious low-order harmonics and the amount of DC ripple content is decreasing by applying the proposed method. By observing the simulation results, it can be concluded that the inverter can ride through the grid fault by applying the proposed method.

# CHAPTER IV

# CONCLUSION AND FUTURE WORK

## 4.1 Conclusion

This thesis applied the generalized harmonic elimination control method for the grid side inverter in a wind power system under unbalanced grid operation. The analytical method is presented for harmonic elimination in grid currents and DC link voltage with variable power factor under unbalanced voltage and line impedance. Based on the analytical solution, the closed loop control method is proposed and verified on a wind power systems model in SIMULINK ®. The system can either be connected to a variable-speed permanent-magnet synchronous generator or a variable-speed squirrel cage induction generator by two back-to-back PWM converters. The simulation results obtained by applying the generalized control method of harmonic elimination are compared with the simulation results obtained by using the traditional grid inverter control methods. The results show that under extreme unbalanced operating conditions, high quality line currents and DC link voltage are obtained by using the proposed control technique. While the results obtained by using the same wind power system with the traditional methods show that

huge low order harmonics exist in line currents and DC link voltage causing torque pulsations.

In addition, from the simulation results it can be seen that the proposed method can be used for the grid fault ride-through control of wind turbine inverters.

## 4.2 Suggestions for Future Work

(1) The system under balanced and unbalanced cases is simulated. The experiment is expected to be conducted in the future to verify the method.

(2) The good steady state results are obtained and compared to the traditional methods. Furthermore, the grid faults ride-though ability of the inverter by using the proposed method is tested. In the future, the dynamic performance can be studied further.

(3) The permanent-magnet synchronous generator and squirrel cage induction generator are used for low or medium wind power system. For the large-scale wind power system, the doubly-fed induction generator with the two back-to-back PWM converters should be used. But it is also known that the DFIG experiences inherent difficulties to ride through a grid fault [32], [33]. The proposed control of the grid side inverter could coordinate with the control of the machine side rectifier to limit the power pulsation and to eliminate the harmonics in line currents under unbalanced grid voltage.

## REFERENCES


[1] U.S Department of Energy, 20% Wind Energy by 2030 Report, July 2008. http://www1.eere.energy.gov/windandhydro/pdfs/41869.pdf

[2] Zhang, C., "Analysis of the interaction between voltages unbalanced and wind power plant operation," *Wind Engineering*, vol.20, no.5, pp. 307-18, 1996.

[3] Carrasco, J. M., M., Franquelo, L. G., Bialasiewicz, J. T., Galvan, E., Guisado, R. C., Angeles, M., Prats, A. M., Leon, J. I., Moreno-Alfonso, N., "Power-Electronic Systems for the Grid Integration of Renewable Energy Source: A Survey," *IEEE Transaction on Industrial Electronics*, vol. 53, no. 4, pp. 1002-1016, August 2006.

[4] Muljadi, E., Yildirim, D., Batan, T., Butterfield, C.P., "Understanding the unbalanced-voltage problems in wind turbine generation," *in Proc. of 34th Annual Meeting of the IEEE Industry Applications,* vol.2, pp. 1359-65, Phoenix, USA,1999.

[5] Mohan, N., Undeland, T., Robbins, W., Power Electronics: Converters, Application, and Design, J John Wiley & Sons, Inc., p.30, 2003.

[6]. Moran, L.; Ziogas, P. D.; Joos, G., "Design aspects of synchronous PWM rectifier-inverter systems under unbalanced input voltage conditions," *IEEE Transactions on Industry Applications* vol.28, no.6, pp.1286-93, 1992.

[7] Ng, C. H., Li, R., Bumby, J., "Unbalanced-grid-fault ride-through control for a wind turbine inverter," *IEEE Transactions on Industrial Electronics*, vol.44, no.3, pp. 845-56, 2008.

[8] Stankovic, A. V., Chen, K., "A new control method for input-output harmonic elimination of the PWM boost-type rectifier under extreme unbalanced operating conditions," *IEEE Transactions on Industry Applications*, vol.56, no.7, p 2420-30, July 2009.

[9] Ackerman, T., Wind power in power system, John Wiley & Sons, Inc., 2005.

[10] Pillay, P., Krishnan, R., "Modeling, simulation, and analysis of permanent-magnet motor drives, Part I: the permanent-magnet synchronous motor drive," *IEEE Transactions on Industry Applications*, vol.25, no.2, pp.265-73, 1989.

[11] Grauers, A., "Efficiency of three wind energy generator systems" IEEE *Transactions on Energy Conversion*, vol. 11, no. 3, pp. 650–657, Sep. 1996.

[12] Chinchilla, M., Arnaltes, S., Burgos, J.C, "Control of permanent-magnet generator applied to variable-speed wind-energy systems connected to the grid," *IEEE Transactions on Energy Conversion*, vol. 21, no. 1, pp. 130-135, 2006.

[13] Bassett, E.D. and Potter F.M., “Capacitive excitation for induction generator It1Capacitive Excitation for Induction Generators", *AIEE Transactions. (Electrical Engineering)*, vol.54, pp. 540-45, 1935.

[14] Medri, K.E., Wu, B., “A variable frequency PWM rectifier for wind driven induction generator,” *in Proc. of 32nd Annual Conference on IEEE Industrial Electronics*, pp. 1417-22, Paris, France, 2006.

[15] Bose, B. K, Modern power electronics and AC drives, Person Education, 2002.

[16] Wang, Q., Chang, L., “PWM control strategies for wind turbine inverters,” *Wind Engineering*, vol.25, no.1, pp. 33-40(8), 2001.

[17] Pena, R., Clare, J.C, Asher, G.M “Doubly fed induction generator using back-to-back PWM converters and its application to variable-speed wind-energy generation,” *IEE Proceedings-Electric Power Applications*. vol.143, no.3, pp. 231-41, 1996.

[18] Dixon, J.W., Boon-Teck Ooi, “Indirect Current control of a unity power factor sinusoidal current boost type three-phase rectifier,” *IEEE Transactions on Industrial Electronics*, vol. 35, pp. 508-15, 1988.

[19] Muljadi, E., Yildirim,D. , Batan,T. , Butterfield,C.P. , “Understanding the unbalanced-voltage problem in wind turbine generation,” *IEEE Industry Applications Conference*, vol.2, pp.1359-1365, Phoenix, USA, 1999

[20] Hansen, A. D., Michalke, G., “Multi-pole permanent magnet synchronous generator wind turbines' grid support capability in uninterrupted operation during grid faults,” *IET Renewable Power Generation*, vol.3, no.3, pp. 333-48, 2009.

[21] Abedini, A., Nasiri, A., “PMSG wind turbine performance analysis during short circuit faults,” *2007 IEEE Canada Electrical Power Conference*, pp. 160-65, Canada, 2007.

[22] Zhang,Y., Gong, J., Xie, D. J ,“Inverter control strategy for direct-drive permanent magnet wind generator under unbalance of three-phase source voltage,” *in proc. of 2008 11th International Conference on Electrical Machines and Systems*, pp. 2497-501. Wuhan, China, 2008.

[23] Lazarov, V., Apostolov, D., “PWM inverter power transfer under unbalanced voltage condition,” *ISEIMA '06. First international Symposium on Environment Identities and Mediterranean Area*, pp. 254-259, 2006

[24] Song, H. S., Nam, V., “Dual current control scheme for PWM converter under unbalanced input voltage conditions,” *IEEE Transactions on Industrial Electronics*, vol.46, no.5, pp. 953-9, Oct. 1999.

[25] Yazdani, A., Iravani , R. , “A unified dynamic model and control for the voltage-source converter under unbalanced grid conditions,” *IEEE Transactions on Power Delivery*, vol.21, issue. 3, pp. 1620-1629, July 2006.

[26] Suh, Y., Tijeras, V., Lipo, T. A., “A control method in dq synchronous frame for PWM boost rectifier under generalized unbalance condition,” *in proc. 2002 Power Electronics Specialists Conference*, vol. 3, pp. 1425-1430, 2002.

[27] Suh, Y., Tijeras, V. , Lipo, T. A., “A nonlinear control of the instantaneous power in dq synchronous frame for PWM ac dc converter under generalized unbalanced operating conditions,” *in proc of 2002 IEEE Industry Applications Conference*, vol.2, pp. 1189-96, 2002.

[28] Hu, J., He, Y., “Modeling and control of grid-connected voltage-source converters under generalized unbalanced operation conditions,” *IEEE Transaction on Energy Conversion*, vol.23, pp.903 – 913, 2008.

[29] Rodriguez, P., Timbus, A., Teodorescu, R., Liserre, M., Blaabjerg, F., “Reactive power control for improving wind turbine system behavior under grid faults,” *IEEE Transactions on Power Electronics*. vol.24, no.7, pp. 1798-801, July 2009

[30] Rodriguez, P., Timbus, A.V., Teodorescu, R., Liserre, M., Blaabjerg, F., “Flexible active power control of distributed power generation systems during grid faults,” *IEEE Transactions on Industrial Electronics*, vol. 54, pp. 2583-2592, 2007.

[31] Chen, K., DSPACE Implementation of a generalized method of harmonic elimination for PWM boost type rectifier under unbalanced operation conditions, Master’s dissertation, Cleveland State University, 2008.

[32] Zhou, Y., Bauer, P., Ferreira, J. A., Pierik, J., “Control of DFIG under unsymmetrical voltage dip,” *in proc. of IEEE 38th Annual Power Electronics Specialists Conference*, pp. 933-8, 2007.

[33] Lie, X., “Coordinated control of DFIG's rotor and grid side converters during network unbalance,” *IEEE Transactions on Power Electronics*, vol.23, no.3, pp.1041-9, 2008.

# APPENDICES

## Simulink model of online calculation of the reference currents

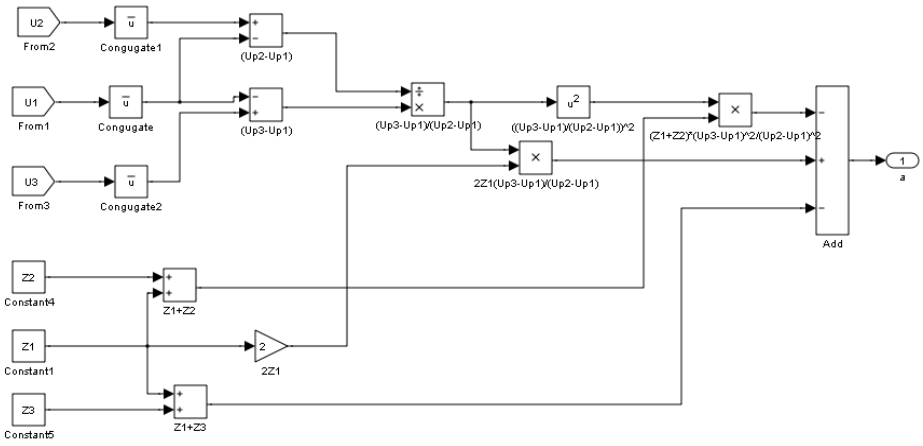


Figure I: Simulink model of online calculation for “a”

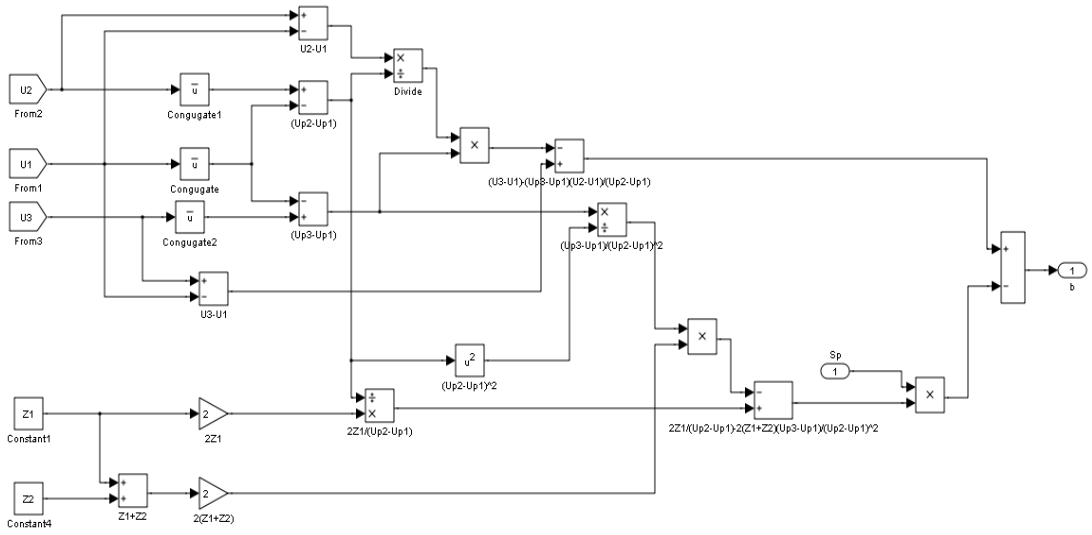


Figure II: Simulink model of online calculation for “b”

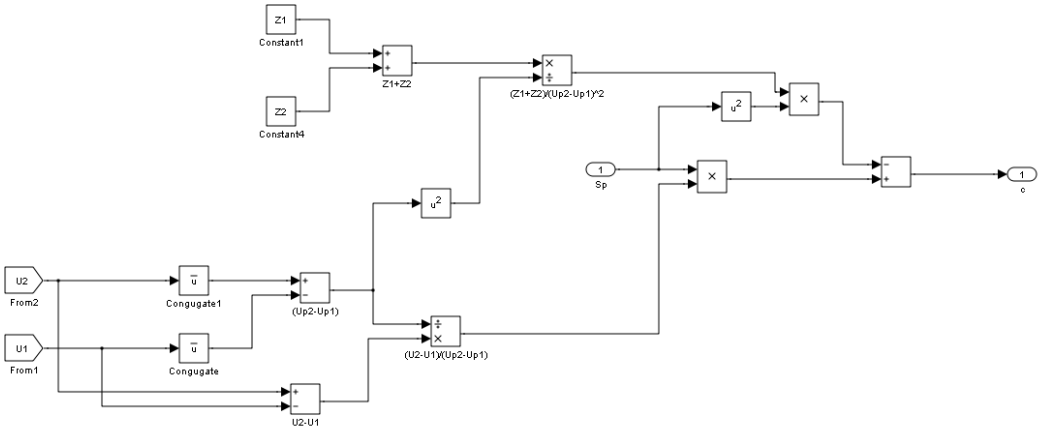


Figure III: Simulink model of online calculation for “c”

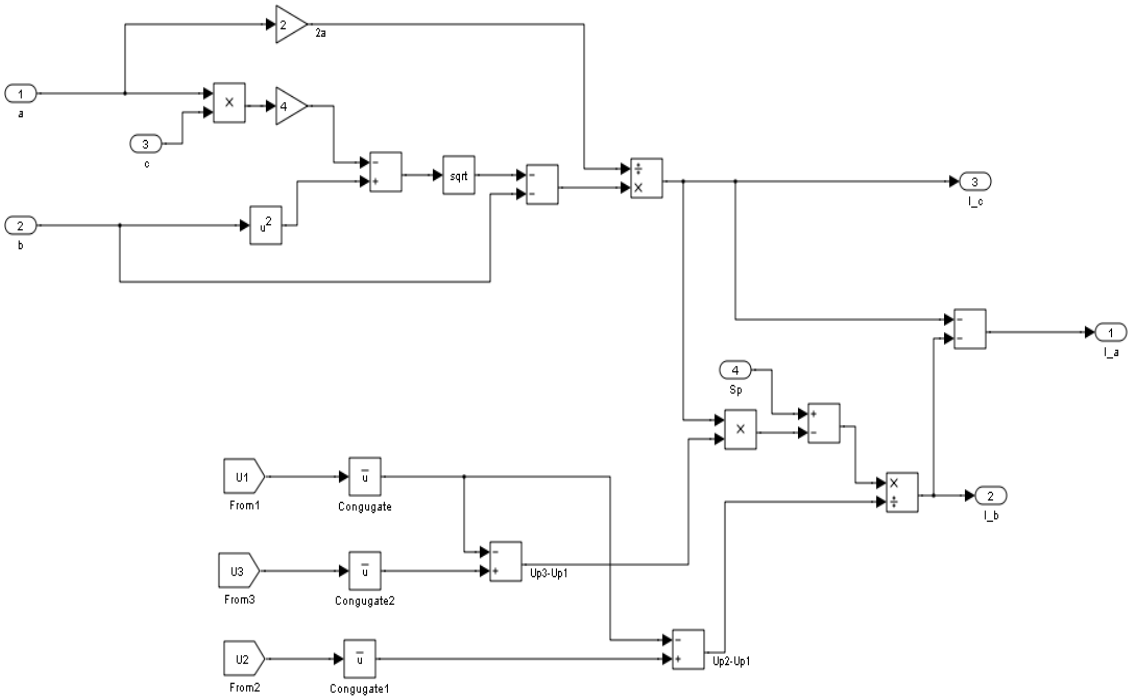


Figure IV: Simulink model of online calculation for reference currents